OPTIMIZATION OF HEAT TRANSFER SYSTEMS AND USE OF THE ENVIRONMENTAL EXERGY POTENTIAL

APPLICATION TO COMPACT HEAT EXCHANGERS AND HEAT PUMPS

Paulo Manuel Ferrão Canhoto

Tese apresentada à Universidade de Évora
para obtenção do Grau de Doutor em Engenharia Mecatrónica e Energia
Especialidade: Energia e Ambiente

ORIENTADOR: *Professor Doutor António Domingos Heitor da Silva Reis*

ÉVORA, MAIO 2012

INSTITUTO DE INVESTIGAÇÃO E FORMAÇÃO AVANÇADA

Co-financiamento POPH / FSE

To Elisa, Joana and Sara

Summary

In this thesis, the optimization of forced convection heat sinks and groundwater--source heat pumps is addressed with the purpose of improving energy efficiency. Parallel ducts heat sinks are considered under constrained (fixed) pressure drop, pumping power and heat transfer rate. The intersection-of-asymptotes method is employed together with numerical simulations and relationships for determining optimum hydraulic diameter are put forward. An optimal design emerges under fixed heat transfer rate, which matches that found through the joint minimization of pressure drop and pumping power. With regard to heat pumps optimization, the relation between coefficient-of-performance and air-to-ground exergy potential is established, showing that energy saving as compared to air-to-air systems depends on the square root of that potential. The exergy potential in the Évora region is estimated, and exergy analysis of groundwater-source systems helps identifying distinct conditions of operation: maximum/null net exergy output and best trade-off between environmental exergy utilization and power input.

Resumo

Optimização de sistemas de transferência de calor e aproveitamento do potencial de exergia ambiental – Aplicação a permutadores de calor compactos e a bombas de calor

Esta tese apresenta a optimização de dissipadores de calor e de bombas de calor geotérmicas para melhoramento da eficiência energética. São estudados dissipadores de passagens paralelas sujeitos a constrangimentos de queda de pressão, potência de bombeamento e taxa de transferência de calor. Utiliza-se o método da intersecção-das-assimptotas juntamente com simulações numéricas, e apresentam-se expressões do diâmetro hidráulico óptimo. Um design ideal emerge no caso de transferência de calor fixa, o qual se aproxima da minimização conjunta de queda de pressão e potência de bombeamento. Relativamente às bombas de calor, estabelece-se uma relação entre coeficiente-de-performance e potencial de exergia ar-solo, e mostra-se que a redução de consumo energético comparado com sistemas ar-ar depende da raiz quadrada desse potencial. O potencial de exergia em Évora é avaliado, e identificam-se várias condições de funcionamento usando análise exergética: máxima/nula saída líquida de exergia e compromisso óptimo entre utilização de exergia ambiental e potência fornecida.

Acknowledgments

This thesis has only been possible with the support and contribution of many people.

Firstly, I would like to thank my supervisor Professor António Heitor Reis for his endless support and for providing me the opportunity to progress with this work. His suggestions and recommendations were crucial.

I thank Professor António Miguel for his comments and suggestions which contributed to the development of this work.

I am deeply grateful to Professors Rui Namorado Rosa, Augusto Fitas, Ana Maria Silva and João Monteiro Marques for their support since my time as graduation student and for their encouragement to accomplish this thesis. I thank Professors Mourad Bezzeghoud and Isabel Malico for their support and constant encouragement. I thank Professors Rui Salgado and Mouhaydine Tlemçani for their support and companionship. I thank Eng. José Pombinho for his technical computer assistance.

I acknowledge the support of the Geophysics Centre of Évora and of the Physics Department of the University of Évora, including all the technical staff, for providing me the conditions to develop this work. I also acknowledge the support of the Portuguese National Science and Technology Foundation – FCT (Fundação para a Ciência e Tecnologia) through the Grant No. SFRH/BD/36840/2007.

I thank my family, especially Elisa and my daughters Joana and Sara, to whom I dedicate this thesis. I owe great gratitude to my mother and to the memory of my father. This work would not have been possible without their extraordinary support.

Contents

List of Papers

This thesis includes the following papers:

I. Paulo Canhoto, A. Heitor Reis, Optimization of fluid flow and internal geometric structure of volumes cooled by forced convection in an array of parallel tubes, International Journal of Heat and Mass Transfer 54 (2011) 4288–4299. [Chapter 3]

II. Paulo Canhoto, A. Heitor Reis, Optimization of forced convection heat sinks with pumping power requirements, International Journal of Heat and Mass Transfer 54 (2011) 1441–1447. [Chapter 2]

III. Paulo Canhoto, A. Heitor Reis, A.F. Miguel, Performance analysis of an endoreversible heat pump system for optimal air-ground or water environmental exergy potential utilization, International Journal of Energy Research 33 (2009) 205–210. [Chapter 5]

IV. Paulo Canhoto, A. Heitor Reis, A.F. Miguel, R. Rosa, Utilisation of air--groundwater exergy potential for improvement of the performance of heat pump systems, International Journal of Exergy 3 (2006) 1–15. [Chapter 4]

Other publications related with the subject of the present thesis, but not included, are:

i. Paulo Canhoto, A. Heitor Reis, Heat transfer in the thermal entry region of singly-connected tubes with uniform wall temperature, *in* Jornadas de Física por ocasião da Jubilação do Professor Rui Namorado Rosa, University of Évora, Portugal, 2010, pp. 231–239.

ii. A.F. Miguel, Paulo Canhoto, A. Heitor Reis, Optimization of geometry and performance of cooling bundles of parallel tubes with pumping fluid requirements, *in* Proceedings of HT2007 ASME-JSME Thermal Engineering Summer Heat Transfer Conference, paper HT2007-32078, Vancouver, Canada, 2007.

iii. Paulo Canhoto, A. Heitor Reis, A.F. Miguel, Exergy analysis and optimisation of a ground or water source heat pump system for maximum environmental

exergy potential utilisation, *in* Proceedings of The 3rd International Energy, Exergy and Environment Symposium, Évora, Portugal, 2007.

iv. Paulo Canhoto, A. Heitor Reis, A.F. Miguel, Análise exergética e optimização de uma bomba de calor com fonte no solo/água para a máxima utilização de exergia ambiental, *in* Resumos do 3^o Encontro de Pós-Graduação em Investigação e Ensino das Ciências Físicas e da Terra da Universidade de Évora, Évora, Portugal, 2007.

v. A. Heitor Reis, Paulo Canhoto, A.F. Miguel, R. Rosa, Non-flow exergy potential of the near-ground atmosphere with respect to soil in the Évora region (Portugal), *in* Proceedings of the First International Exergy, Energy and Environment Symposium, Izmir, Turkey, 2003.

List of Figures

List of Tables

Chapter 1

Introduction

1.1 Preliminary remarks

The optimization of heat transfer systems is an important issue in science and technology due to environmental impacts and energy consumption concerns. The main objective is to maximize performance and decrease energy demand, thus contributing to the rational use of energy and to the reduction of carbon dioxide emissions. Heat transfer systems are used in a wide variety of engineering applications and technologic apparatus (e.g. cooling devices in computers, air conditioning in inhabitation houses, industrial processes, and many others). Although they can have diverse working principles and designs, their main purpose is either to transfer heat between two fluids or from a solid device to a coolant. In certain applications, heat transfer is also associated with mass transfer processes and/or with chemical reactions.

The fundamental theory that describes the heat transfer modes – conduction, convection and radiation – is quite well known and established [1 – 3], as well as the numerical solution methods of the mass, momentum and energy conservation equations (e.g. see Refs. [4, 5]). These numerical methods have been often used in optimization procedures based on energy analysis, while other methods have been developed based on the entropy generation minimization [6] and, more recently, on the constructal theory [7, 8]. In this last case, we must refer the method of intersecting the asymptotes, which is a straightforward but powerful tool for predicting the optimal internal geometric structure of volumes cooled either by forced or natural convection [9].

Exergy analysis [10 – 14] is also a useful tool for the optimization of heat transfer systems, because it takes into account the internal irreversibilities and allows comparing the maximum useful work that can be obtained from different energy fluxes in relation to a reference environment. As an example, this analysis is useful in dealing with systems that require an external power source (e.g. shaft work) and that exchange heat with the atmosphere, which is the case of heat pumps used in air conditioning.

In general, most heat transfer systems require an external energy input to operate, as for example are forced convection heat sinks, heat exchangers and heat pumps, in which power must be supplied either to a fan, pump or compressor. These systems are usually optimized in order to maximize the heat transfer rate while the amount of heat that is transferred per unit of energy that is supplied is a measure of its performance. Moreover, a thermal efficiency defined as the ratio of actual to maximum heat transfer rate is often used in heat exchangers analysis. In the same manner, exergy efficiency is defined as the ratio of the useful output of exergy to exergy input, and rational efficiency is defined as the ratio of total exergy output to total exergy input. There are other systems that do not require an external energy input, as for example are free convection heat sinks and heat pipes, which must be optimally designed to promote and maximize heat transfer rate.

This thesis is focused on the optimization of forced convection heat sinks and of groundwater or water source heat pumps. Both systems require external power input to operate although they have different configuration and different working principles. In the first case, power is supplied to a fan or pump which drives the fluid flow through the heat sink channels in order to extract heat from the device to be cooled. In the second case, power is supplied to the compressor, fans and fluid pumps in a vapour compression heat pump system with the purpose of transferring heat from a cold reservoir onto a hot reservoir. The selection of the two systems studied and the development of this work were based on the following ideas and criteria:

1. *Energy analysis* and *exergy analysis* – These are the two broad approaches on which the optimization procedures are based;

2. *Component optimization* and *system operation optimization* – We look onto the component optimization procedure as the improvement of existing devices or with the purpose of design of new and specific devices, which are part of a heat transfer system. Conversely, we look onto the system optimization procedure as the improvement of the operation of a thermal system composed of generic components or devices;

3. *Energy efficiency* and *rational use of energy* – The search for new and renewable energy sources for reducing fossil fuels demand must be carried out together with two complementary actions: improvement of energy efficiency and rational use of energy. It means that it is crucial to built up more efficient equipments but it is also essential to use those equipments properly because the capacity of installation of renewable energy systems is finite in a long term perspective, even though this kind of resource is inexhaustible at the human time scale (e.g. solar energy).

Accordingly, the issues studied in the present work are addressed and organized as follows:

(i) Optimization of forced convection heat sinks

♢ *energy analysis* – optimization is based on energy analysis taking into account the relation between heat transfer rate, pressure drop and pumping power;

♢ *component optimization* – the internal geometric structure of a compact heat sink is optimized using both the intersection-of-asymptotes and numerical methods;

♢ *improvement of energy efficiency* – the objective pursued is maximization of heat transfer rate and/or minimization of pumping power to achieve a better energy efficiency;

(ii) Optimization of groundwater or water source heat pumps

♢ *exergy analysis* – optimization is based on exergy analysis taking into account irreversibilities and input and output exergy fluxes;

♢ *system operation optimization* – heat pump operation is optimized in order to obtain the ideal relation between heat transfer rate and coefficient of performance;

♢ *rational use of energy* – the objective is to maximize the use of the environmental exergy potential, i.e. the non-flow exergy potential that exists between the groundwater or water from lakes and rivers and the atmospheric air due to the natural temperature differences. This corresponds to optimization of the system operation with the purposes of performance improvement and the rational use of energy in comparison with the conventional air-to-air systems.

1.2 Aim

The work presented in this thesis has the purpose of contributing to advances in the optimization of forced convection heat sinks and groundwater or water source heat pumps, for achieving maximum performance together with minimum energy consumption. Two distinct approaches and methods are used: (i) in the first case, the objective is the optimization of fluid flow and internal geometric structure of parallel ducts heat sinks (component optimization) based on energy analysis and using both the intersection-of-asymptotes and numerical methods; and (ii) in the second case, the objective is the optimization of a vapour compression heat pump system connected to a groundwater or water heat reservoir (system optimization) based on exergy analysis and aiming at optimal utilization of environmental air-to--ground exergy potential.

1.3 Optimization of forced convection heat sinks and the method of intersecting the asymptotes

In general, the objective of heat sink optimization is to maximize heat transfer rate under global constraints. Geometric constraints exist which depend on the available space and construction requirements (e.g. fixed volume and fixed porosity), while fluid flow constraints (e.g. fixed pressure drop and fixed pumping power) depend on the fluid flow arrangement in which the heat sink is connected.

Optimization can be carried out through numerical simulations or using the method of intersecting the asymptotes. Numerical techniques use either simulations of entire temperature and flow fields [4] or correlations for Nusselt number and friction factor [2, 3]. In the first case, computational simulations for each set of free parameters values are required, which can be coupled to numerical optimization procedures [15 – 17] in order to determine the optimal design. A recent example of this technique can be found in Ref. [18]. Similar numerical optimization procedures can also be employed in the case of using correlations for modelling heat transfer and fluid flow as functions of free parameters. An example of this approach can be found in Ref. [19], in which optimization of heat transfer in a bundle of parallel tubes in a solid matrix is carried out for pumping power minimization either with laminar or turbulent flow regimes. Although these methods are quite exact they often require non-negligible computational and time resources. On the other hand, the method of intersecting the asymptotes is a simple and straightforward analytical tool for predicting the scale or order-of-magnitude of optimum values.

The method of intersecting the asymptotes was first reported by Bejan [20] for the optimization of a natural convection heat sink composed of parallel plates, and thereafter applied to the optimization of a heat sink of similar geometry under forced convection and subjected to fixed pressure drop and uniform wall temperature [21]. This method was further extended for the cases of fixed pumping power and fixed mass flow rate [22] and, more recently, generalized for a heat sink composed of parallel circular or non-circular ducts under fixed pressure drop [23]. The case of parallel plates with uniform heat flux was also addressed using this method [24].

The method of asymptotes is based on the intersection of two dissimilar trends or limits: (i) for increasing large hydraulic diameters of the heat sink passages the flow approaches to the hydrodynamic and thermal developing flow limit, while (ii) for vanishing small hydraulic diameters the flow approaches to the fully developed limit. In the developing flow limit the fluid in the core flow participates very inefficiently in the heat transfer process as the local temperature tends to the value of temperature at the inlet. Conversely, in the fully developed limit the fluid bulk temperature tends to the surface temperature (fluid 'overheating') with the consequent decreasing on

heat transfer coefficient. Both limits must be avoided in heat sink design. In fact, the maximum heat transfer rate under global constraints is achieved with the optimal hydraulic diameter that is close to that obtained by intersecting these two limits. If fixed pressure drop is considered, this optimal design corresponds to the case in which boundary layers merge just at the exit of flow channels [21].

This simple geometric criterion was also invoked in the optimization of other channel configurations and flow conditions either with natural or forced convection, as in the following examples: stacks of equidistant and non-equidistant plates [25]; stacks of parallel plates shielded by porous screens [26]; parallel plates cooled by turbulent forced convection [27, 28]; staggered plates [29, 30]; pin fins arrays with impinging flow [31]; parallel cylinders in crossflow [32 – 34]; heat-generating strips inside ducts [35]; vertical diverging or converging channels with natural convection [36]; and compact heat exchangers composed of metal honeycombs [37]. A review on the cooling optimization of electronic packages using this method is presented in Refs. [7] and [38], in which some of the geometries referred above are addressed. The same criterion together with the scale of optimal hydraulic diameter predicted by intersecting the asymptotes have been used to optimize stacks of parallel plates with multiple lengths under forced [39 – 41] and natural convection [42], and to design multi-scale heat exchangers for maximum heat transfer density [43].

The method of intersecting the asymptotes was also used in the design of porous media with decreasing flow lengths, in which limit the large spacing asymptote is modelled based on heat transfer by conduction between the surface of solid substrate and a stationary fluid [44], and in the design of compact heat sinks composed of multi-scale tubes [45]. Rogiers and Baelmans [46] addressed the problem of heat transfer maximization at decreasing lengths of parallel plates counterflow heat exchangers and obtained the optimal internal geometry based on the intersection of the asymptotic relationships for the cases of large and small channels, and taking into account the axial heat conduction in the plates. Additionally, this method was used to find the optimal geometry of L and C-shaped ducts with natural convection [47], and to optimize the aspect ratio and volume fraction of flow passages in micro--channels heat sinks [48, 49] and vascularized materials [50] under forced convection with the purpose of minimizing the peak temperature. Sadeghipour and Razi [51] used the intersection of asymptotes to find out the optimum confining wall-to-wall distance for maximum heat transfer rate from a confined horizontal cylinder with isothermal surface under laminar natural convection.

Hollow sandwich cylinders with prismatic cores were designed by using this method together with a structural model for maximum heat transfer rate and mechanical performance at minimum mass [52]. A structural optimization of two--dimensional cellular metals cooled by forced convection at fixed pumping power

was also reported [53]. In another recent work, the optimal thickness of a metal foam layer wrapped around a cylinder in crossflow was obtained through both numerical and asymptotes methods [54]. Dallaire et al. [55] carried out a numerical optimization of rotary heat exchangers with porous core and used scale analysis and the method of asymptotes to predict the optimum longitudinal length and porosity.

Hegazy [56] has found the optimum channel depth in flat-plate solar air heaters by intersecting the fully developed and developing turbulent flow asymptotes, while Miguel [57] addressed the optimum design that arises from intersecting the laminar and turbulent flow limits in an array of pipes of a solar energy system that is used to warm a room. In this last case, optimum design emerge also as the balance between heat transfer rate augmentation and flow resistance reduction.

The fully developed and developing flow asymptotes have also been combined through the correlation method outlined by Churchill and Usagi [58] to develop models for predicting the heat transfer rate in plate fin heat sinks, as in e.g. Ref. [59] in which the non-uniformity of temperature at fins surface was taken into account. The work by Yilmaz et al. [60] reports an asymptotic analysis for large and small hydraulic diameter ducts of different shapes with forced convection at fixed pressure drop. In that work, the maximum heat transfer rate and the optimal duct geometry are obtained through an exact method based on correlations for Nusselt number.

Other optimization problems have also been solved using the method of intersecting the asymptotes. The work by Lewins [61] provides a mathematical basis for this method and demonstrates that optimal design is achieved through an equi--potential division between the two competing trends. The method is illustrated through optimization of an electric circuit composed of high and low conductivity materials at fixed current and volume, for minimum voltage difference. In this case, in which voltage relates to current by Ohm's Law, the equi-potential division it is also an equi-partition of resistances [8].

Another application is the prediction of natural crack pattern formation in shrinking solids [7, 62], as it occurs in wet soil exposed to the sun and wind. Here, the scale of cracks width is estimated by intersecting the 'many cracks' and 'few cracks' asymptotes for minimum overall drying time or, equivalently, for maximum mass transfer rate from the wet soil to the ambient. In the same manner, the natural flow pattern that appears in fluid layers heated from below can be predicted by intersecting the 'many cells' and 'few cells' asymptotic limits so that maximum upward heat flux is obtained [7, 63]. As result, the optimum number of convective cells, or the optimal cell slenderness ratio, is estimated as a function of layer height, vertical temperature gradient and fluid properties. Similarly, the flow pattern in porous layers saturated with fluid and heated from below is predicted by intersecting two distinct limits: increasing large number of slender cells of vertical counterflow

and decreasing small number of slender cells of horizontal counterflow in which the upward thermal conductance (convective) is dominated by two horizontal boundary layers [7, 63, 64].

Reis et al. [65] have made use of the method of intersecting the asymptotes to design air-cleaning devices composed of either parallel channels (tubes or parallel plates) or porous material (filter), for maximum particle transfer rate from air to cleaning surfaces. This maximum is achieved when concentration boundary layers merge just close to the exit plane, which is in agreement with the result for heat sink optimization if we consider the analogy between heat and mass transfer.

Regarding again the optimization of forced convection heat sinks, it must be noted that the thermally developed and developing flow limits can always be reached if diverse constraints are considered, and thus the method of the intersection of asymptotes as enounced above constitutes a general rule for heat sink optimization. Accordingly, one can foresee that this method can also be useful for predicting the optimal fluid flow conditions if a fixed heat transfer rate is considered. This is relevant because in certain applications the heat transfer rate and the maximum or nominal temperature of operation are known, and the objective is to reduce pumping power and/or pressure drop.

These aspects were not explicitly addressed in previous works using this method and a comparison between the results for different constraints was not carried out. Furthermore, the analysis of results has been focused mainly in the hydraulic diameter or aspect ratio of ducts while the analysis of the optimal dimensionless thermal length, which is a measure of the thermal development of the flow, was not sufficiently addressed for all the cases. Additionally, the optimal internal geometric structure of heat sinks composed of circular or non-circular ducts under fixed pumping power was not reported yet.

This thesis reports the following new advances in the optimization of forced convection heat sinks and in the method of intersecting the asymptotes:

(i) the optimal internal design of heat sinks composed of circular or non-circular ducts is obtained either for maximization of heat transfer density at fixed pumping power as well as for pumping power minimization with specified heat transfer rate;

(ii) a broad scale analysis of heat sink optimization is carried out together with numerical simulations by considering three different constraints – fixed pressure drop, fixed pumping power and fixed heat transfer density – and the method of intersecting the asymptotes is derived using dimensionless thermal length as the primary optimization variable and hydraulic diameter as the design variable. The optimal internal design of heat sinks composed of parallel

tubes is obtained for these three cases;

(iii) the concept on which the method of asymptotes is based on is further explored by deriving and intersecting both the fully developed and developing flow limits with specified heat transfer density and without imposing any fluid flow condition. New results are found that clarify the meaning of optimal design that emerges from this method, by showing its relation to optimal fluid flow conditions;

(iv) a new relation for Nusselt number of thermally developing flows in ducts is deduced based on the assumptions assumed in the developing flow asymptote. This relation is similar to the well known Lévêque solution [1] but presents a better agreement with data in practical ranges of dimensionless thermal length. This outcome proves the correctness of the assumptions used in this work and constitutes also a new result.

1.4 Optimization of groundwater or water source heat pumps and the use of environmental exergy potential

The incoming solar radiation is the major source of energy that generates and sustains transfer processes and life on Earth. On the other hand, the same amount of energy that is absorbed has to be radiated by the Earth back into the space, according to a global energy balance. While the energy balance of the Earth's surface and atmosphere allows quantifying the different forms of energy in which absorbed solar radiation is converted to, the exergy balance gives us additional information about the capacity of that energy flows to produce useful work [66 – 68]. That is, exergy analysis provides information on the 'quantity' and 'quality' of energy and on the exergy losses associated with the transfer processes. Such exergy fluxes occur as the result of the non-uniform heating of the Earth's surface and atmosphere, and constitute some of the most used renewable energy resources (e.g. wind energy). A review on exergy analysis of renewable energy and conversion technologies can be found in Refs. [69, 70].

The non-uniform heating of the Earth generates time dependent temperature gradients between distinct masses of air in the atmosphere and also between the atmospheric air and the ground and water of rivers and oceans. In that sense, we can identify and define an exergy potential that is associated to the natural air-to--ground temperature difference, which may be used for improving the performance of heat pump systems in buildings by reducing its energy consumption in comparison to air-to-air systems. This is due to the lower average temperature difference between ground (or either groundwater or water from lakes and rivers) and the

air in the acclimatized space as compared to the temperature difference between outside air and acclimatized space. Moreover, ground display rather more moderate temperature changes than the overlaying air.

One reason for expressing the natural air-to-ground temperature difference as exergy potential is that it allows establishing connection between two similar quantities while related to the external exergy input (shaft power) of heat pumps. Although this is a low exergy potential as compared to the conventional geothermal resources [71], it may replace a real environmental exergy source in the sense that this potential contributes for reducing energy consumptions instead of being used to generate power directly. The use of low exergy systems for heating and cooling of buildings has been already recognized as a good practice for achieving a sustainable built environment and considerable energy savings [72 – 74]. This approach shows that low exergy resources are advantageous as compared to high valued energy carriers (as e.g. fossil fuels) for producing the low exergy heating and cooling required in buildings. Reis et al. [75] addressed the evaluation of the exergy potential of the near ground atmosphere with respect to the soil and presented an analysis on the use of this potential for improvement of natural ventilation, air conditioning, and passive heating and cooling systems.

Ground source systems comprise pipe coils buried horizontally or vertically in the ground. The working fluid of the heat pump is made to circulate within pipes (or a different fluid, usually brine, in a secondary loop) for exchanging heat with the ground. If brine circulation loop is used an additional heat exchanger and fluid pump are required, thus lowering the global performance of the installation. The ground temperature near the buried coils depends on the local climatic conditions and of heat pump operation mode – it decreases in wintertime while it increases in summertime. As for the rate of heat exchange with the ground is highly dependent on moisture content in the soil. This temperature field has been studied using theoretical models, numerical simulations and experimental techniques [76 – 80]. Groundwater or water source heat pumps can operate either as open or closed systems. In open systems, groundwater is pumped into the heat pump unit and then re-injected in a different well or used for other purpose. In closed systems, pipe coils (or heat exchangers) are placed in a well at a deep below the groundwater table, or placed at the bottom of lakes and rivers.

Several studies show that improvements on the performance of heating and cooling systems can be achieved with heat pumps connected to ground or groundwater heat reservoirs [81 – 90]. The recent work by Kalz et al. [91] reports a detailed energy analysis on the performance of heat pumps using environmental heat sources and sinks – ground, groundwater, rainwater and ambient air – for application in buildings. The use of water from rivers and lakes was addressed in the study by

Buyukalaca et. al. [92]. Hybrid systems such as those combining rainwater and ground heat sources/sinks [93] and solar-assisted ground-source heat pumps [94 – 99] have been also investigated and developed.

Petit and Meyer [100] presented a techno-economic analysis on the performance of horizontal-ground-source air-conditioners in comparison with air-source systems. This study was conducted for the climatic conditions of Pretoria (South Africa) and shows that, although capital cost of an air-source system is cheaper, the lower operation cost of a ground-source system makes it more viable economically. Zogou and Stamatelos [101] addressed the effect of climatic conditions on the performance of ground and groundwater source heat pumps by comparing specific examples in the northern and southern parts of Europe. They concluded that climatic conditions greatly affect the performance of such systems and that high gains of performance can be achieved in the Mediterranean region.

Exergy analysis of heat pumps allows identifying the irreversibility of each process of the thermodynamic cycle [10, 102]. Szargut [103] studied the influence of the internal irreversibilities on the coefficient of performance and expressed this parameter as the product of the thermodynamic efficiencies of each component. Detailed exergy analysis of ground source heat pumps was reported in various studies, as e.g. in Refs. [104 – 106]. Alhazmy [107] used the Second Law of thermodynamics and exergy analysis to estimate the minimum work required for air conditioning process in hot and humid climates. On the other hand, the variation of the environmental conditions affects the performance of such systems (particularly in the case of air-source systems) and influences the exergy balance depending on the selected reference conditions – either standard or actual atmospheric air conditions. Göğüş et al. [108] addressed this issue by deriving the exergy balance of a general system taking into account both the variation of the environmental conditions and the motion of that system with respect to the environment.

Cheng and Chen [109] addressed the optimization of an irreversible heat pump by finding the optimum hot-end temperature of working fluid for maximum performance. In that work, the heat reservoirs temperatures and the thermal conductances are considered to be constants, while considering both internal irreversibilities and external irreversibilities due to finite temperature difference and heat leak between reservoirs. Internally reversible (endoreversible) [110] and irreversible refrigerators [111] were optimized using the same method.

Optimization of heat pumps, refrigerators and air conditioning systems has been also carried out by determining the optimal heat exchanger allocation between hot (condenser) and cold (evaporator) sides [6, 112 – 114]. In this procedure, the total area or the total thermal conductance is constrained (fixed) and its optimal partition between hot and cold sides is obtained for achieving maximum useful heat transfer.

The maximization of coefficient of performance was carried out through a similar procedure [115]. The minimization of total heat transfer area and overall thermal conductance was also conducted either for a given heat transfer load or coefficient of performance [116, 117].

The relations between maximum rate of exergy output and both coefficient of performance and heat transfer load of an endoreversible refrigerator were obtained by Yan and Chen [118]. Another optimization criterion that has been used is the maximization of the so called 'ecological function', which can be defined based on energy or exergy analysis [118 – 120]. This corresponds to the best trade-off between energy (or exergy) output rate and entropy generation rate (or irreversibility).

This thesis reports the following new advances in the assessment of environmental exergy potential and in the optimization of ground/groundwater source heat pumps:

(i) the natural air-to-ground exergy potential is defined as the specific non-flow exergy of atmospheric air with respect to the ground conditions;

(ii) a simple expression relating the air-to-ground exergy potential to the power input of both air-source and ground-source systems is deduced, which allows estimation of the order-of-magnitude of energy savings;

(iii) the air-to-ground exergy potential and the performance of ground-source systems are assessed for the conditions at the Évora region (Portugal) based on the hourly and monthly averaged values of air and ground temperatures;

(iv) the optimization of a groundwater-source heat pump is carried out through exergy analysis for four distinct criteria – maximum net exergy output, null net exergy output, maximum 'ecological function', and optimum compromise between environmental exergy utilization and power input.

1.5 Outline of the thesis

This thesis comprises six chapters. Chapter 1 presents a general introduction to the thesis. Chapters 2 and 3 concern the optimization of forced convection heat sinks. Chapters 4 and 5 concern the optimization of groundwater source heat pumps and the use of environmental exergy potential. Chapter 6 presents the general conclusions.

Chapter 2 addresses the optimization of compact heat sinks composed of parallel ducts for the cases of heat transfer density maximization and pumping power minimization. An asymptotic analysis is carried out together with an exact method based on correlations for circular tubes, parallel plate ducts, rectangular ducts, square ducts and equilateral triangular ducts. Chapter 3 addresses optimization of fluid

flow and internal geometric structure of volumes cooled by forced convection in an array of parallel tubes. A new approach of the intersection-of-asymptotes method is developed and applied to the following cases: (i) heat transfer rate maximization at fixed pressure drop; (ii) heat transfer rate maximization at fixed pumping power; and (iii) fluid flow optimization at fixed heat transfer rate. This optimization is validated and complemented by means of numerical simulations of entire temperature and flow fields.

Chapter 4 addresses the use of the natural air-to-ground exergy potential in the performance improvement of groundwater source heat pumps, and a relation between that potential and both coefficient of performance and power consumption is established. An assessment of the non-flow exergy potential in the region of Évora (Portugal) is also presented and estimates of maximum energy savings in cooling and heating modes are reported. Chapter 5 addresses the optimization based on exergy analysis of an endoreversible heat pump connected to a groundwater or water heat reservoir.

References

[1] R.B. Bird, W.E. Stewart, E.N. Lightfoot, Transport Phenomena, Wiley, New York, 1960.

[2] F.P. Incropera, D.P. DeWitt, Fundamentals of Heat and Mass Transfer, Wiley, New York, 1985.

[3] A. Bejan, Convection Heat Transfer, Wiley, New York, 1995.

[4] H.K. Versteeg, W. Malalasekera, An Introduction to Computational Fluid Dynamics: The Finite Volume Method, Longman Scientific & Technical, England, 1995.

[5] M.F. Modest, Radiative Heat Transfer, McGrawHill, New York, 1993.

[6] A. Bejan, Entropy Generation Minimization – The Method of Thermodynamic Optimization of Finite-Size Systems and Finite-Time Processes, CRC Press, New York, 1996.

[7] A. Bejan, Shape and Structure, from Engineering to Nature, Cambridge University Press, Cambridge, UK, 2000.

[8] A.H. Reis, Constructal Theory: From Engineering to Physics, and How Flow Systems Develop Shape and Structure, Applied Mechanics Reviews 59 (2006) 269–282.

[9] A. Bejan, I. Dincer, S. Lorente, A.F. Miguel, A.H. Reis, Porous and Complex Flow Structures in Modern Technologies, Springer, New York, 2004.

[10] T.J. Kotas, The Exergy Method of Thermal Plant Analysis, Krieger Publishing Company, Malabar, Florida, 1995.

[11] E. Sciubba, G. Wall, A brief commented history of exergy from the beginnings to 2004, Int. J. Thermodynamics 10 (2007) 1–26.

[12] I. Dincer, M.A. Rosen, Exergy: Energy, Environment and Sustainable Development, Elsevier, 2007.

[13] I. Dincer, The role of exergy in energy policy making, Energy Policy 30 (2002) 137–149.

[14] G. Tsatsaronis, Definitions and nomenclature in exergy analysis and exergoeconomics, Energy 32 (2007) 249–253.

[15] W. F. Stoecker, Design of Thermal Systems, third ed., McGrawHill, New York, 1989.

[16] D. G. Luenberger, Linear and Nonlinear Programming, second ed., Addison Wesley Publishing Company, Massachusetts, 1989.

[17] J. S. Arora, Introduction to Optimum Design, McGraw-Hill, New York, 1987.

[18] Z.-H. Wang, X.-D. Wang, W.-M. Yan, Y.-Y. Duan, D.-J. Lee, J.-L. Xu, Multi-parameters optimization for microchannel heatsink using inverse problem method, Int. J. Heat Mass Transfer 54 (2011) 2811–2819.

[19] A.F. Miguel, P. Canhoto, A.H. Reis, Optimization of geometry and performance of cooling bundles of parallel tubes with pumping fluid requirements, *in* Proceedings of HT2007 ASME-JSME Thermal Engineering Summer Heat Transfer Conference, paper HT2007-32078, Vancouver, Canada, 2007.

[20] A. Bejan, Convection Heat Transfer, Wiley, New York, 1984, Problem 11, p. 157; Solutions Manual pp. 93–95.

[21] A. Bejan, E. Sciubba, The optimal spacing of parallel plates cooled by forced convection, Int. J. Heat Mass Transfer 35 (1992) 3259–3264.

[22] S. Mereu, E. Sciubba, A. Bejan, The optimal cooling of a stack of heat generating boards with fixed pressure drop, flowrate or pumping power, Int. J. Heat Mass Transfer 36 (1993) 3677–3686.

[23] Y.S. Muzychka, Constructal design of forced convection cooled microchannel heat sinks and heat exchangers, Int. J. Heat Mass Transfer 48 (2005) 3119–3127.

[24] A. Campo, Bounds for the optimal conditions of forced convective flows inside multiple channels whose plates are heated by uniform flux, Int. Comm. Heat Mass Transfer 26 (1999) 105–114.

[25] A.M. Morega, A. Bejan, S.W. Lee, Free stream cooling of a stack of parallel plates, Int. J. Heat Mass Transfer 38 (1995) 519–531.

[26] A. Bejan, S.J. Kim, A.M. Morega, S.W. Lee, Cooling of stacks of plates shielded by porous screens, Int. J. Heat and Fluid Flow 16 (1995) 16–24.

[27] A. Bejan, A.M. Morega, The optimal spacing of a stack of plates cooled by turbulent forced convection, Int. J. Heat Mass Transfer 37 (1994) 1045–1048.

[28] L. Gosselin, Fitting the flow regime in the internal structure of heat transfer systems, Int. Comm. Heat Mass Transfer 33 (2006) 30–38.

[29] A.J. Fowler, G.A. Ledezma, A. Bejan, Optimal geometric arrangement of staggered plates in forced convection, Int. J. Heat Mass Transfer 40 (1997) 1795–1805.

[30] G.A. Ledezma, A. Bejan, Optimal geometric arrangement of staggered vertical plates in natural convection, J. Heat Transfer 119 (1997) 700–708.

[31] G. Ledezma, A.M. Morega, A. Bejan, Optimal spacings between pin fins with impinging flow, J. Heat Transfer 118 (1996) 570–577.

[32] A. Bejan, A.J. Fowler, G. Stanescu, The optimal spacing between horizontal cylinders in a fixed volume cooled by natural convection, Int. J. Heat Mass Transfer 38 (1995) 2047–2055.

[33] A. Bejan, Optimal spacing for cylinders in crossflow forced convection, J. Heat Transfer 117 (1995) 767–770.

[34] G. Stanescu, A.J. Fowler, A. Bejan, The optimal spacing of cylinders in free-stream cross-flow forced convection, Int. J. Heat Mass Transfer 39 (1996) 311–317.

[35] T. Bello-Ochende, A. Bejan, Fitting the duct to the 'body' of the convective flow, Int. J. Heat Mass Transfer 46 (2003) 1693–1701.

[36] A.K. da Silva, A. Bejan, S. Lorente, Maximal heat transfer density in vertical morphing channels with natural convection, Numerical Heat Transfer–Part A 45 (2004) 135–152.

[37] T.J. Lu, Heat transfer efficiency of metal honeycombs, Int. J. Heat Mass Transfer 42 (1999) 2031–2040.

[38] A. Bejan, Optimal internal structure of volumes cooled by single-phase forced and natural convection, Journal of Electronic Packaging 125 (2003) 200–207.

[39] A. Bejan, Y. Fautrelle, Constructal multi-scale structure for maximal heat transfer density, Acta Mechanica 163 (2003) 39–49.

[40] T. Bello-Ochende, A. Bejan, Maximal heat transfer density: Plates with multiple lengths in forced convection, Int. J. Thermal Sciences 43 (2004) 1181–1186.

[41] A.K. da Silva, S. Lorente, A. Bejan, Constructal multi-scale structures with asymmetric heat sources of finite thickness, Int. J. Heat Mass Transfer 48 (2005) 2662–2672.

[42] A.K. da Silva, A. Bejan, Constructal multi-scale structure for maximal heat transfer density in natural convection, Int. J. Heat and Fluid Flow 26 (2005) 34–44.

[43] A. Bejan, Dendritic constructal heat exchanger with small-scale crossflows and larger-scales counterflows, Int. J. Heat Mass Transfer 45 (2002) 4607–4620.

[44] A. Bejan, Designed porous media: maximal heat transfer density at decreasing length scales, Int. J. Heat Mass Transfer 47 (2004) 3073–3083.

[45] Y.S. Muzychka, Constructal multi-scale design of compact micro-tube heat sinks and heat exchangers, Int. J. Thermal Sciences 46 (2007) 245–252.

[46] F. Rogiers, M. Baelmans, Towards maximal heat transfer rate densities for small-scale high effectiveness parallel-plate heat exchangers, Int. J. Heat Mass Transfer 53 (2010) 605–614.

[47] A.K. da Silva, L. Gosselin, Optimal geometry of L and C-shaped channels for maximum heat transfer rate in natural convection, Int. J. Heat Mass Transfer 48 (2005) 609–620.

[48] T. Bello-Ochende, L. Liebenberg, J.P. Meyer, Constructal cooling channels for micro-channel heat sinks, Int. J. Heat Mass Transfer 50 (2007) 4141–4150.

[49] T. Bello-Ochende, J.P. Meyer, F.U. Ighalo, Combined Numerical Optimization and Constructal Theory for the Design of Microchannel Heat Sinks, Numerical Heat Transfer–Part A 58 (2010) 882–899.

[50] S. Kim, S. Lorente, A. Bejan, Vascularized materials with heating from one side and coolant forced from the other side, Int. J. Heat Mass Transfer 50 (2007) 3498–3506.

[51] M.S. Sadeghipour, Y.P. Razi, Natural convection from a confined horizontal cylinder: the optimum distance between the confining walls, Int. J. Heat Mass Transfer 44 (2001) 367–374.

[52] T. Liu, Z.C. Deng, T.J. Lu, Bi-functional optimization of actively cooled, pressurized hollow sandwich cylinders with prismatic cores, J. Mech. Phys. Solids 55 (2007) 2565–2602.

[53] T. Wen, F. Xu, T.J. Lu, Structural optimization of two-dimensional cellular metals cooled by forced convection, Int. J. Heat Mass Transfer 50 (2007) 2590–2604.

[54] M. Odabaee, K. Hooman, H. Gurgenci, Metal Foam Heat Exchangers for Heat Transfer Augmentation from a Cylinder in Cross-Flow, Transp. Porous Med. 86 (2011) 911–923.

[55] J. Dallaire, L. Gosselin, A.K. da Silva, Conceptual optimization of a rotary heat exchanger with a porous core, Int. J. Thermal Sci. 49 (2010) 454–462.

[56] A.A. Hegazy, Optimization of flow-channel depth for conventional flat-plate solar air heaters, Renewable Energy 7 (1996) 15–21.

[57] A.F. Miguel, Constructal design of solar energy-based systems for buildings, Energy and Buildings 40 (2008) 1020–1030.

[58] S.W. Churchill, R. Usagi, A general expression for the correlation of rates of transfer and other phenomena, Am. Inst. Chem. Eng. 18 (1972) 1121–1128.

[59] P. Teertstra, M.M. Yovanovich, J.R. Culham, Analytical forced convection modelling of plate fin heat sinks, J. Electronics Manufacturing 10 (2000) 253–261.

[60] A. Yilmaz, O. Buyukalaca, T. Yilmaz, Optimum shape and dimensions of ducts for convective heat transfer in laminar flow at constant wall temperature, Int. J. Heat Mass Transfer 43 (2000) 767–775.

[61] J. Lewins, Bejan's constructal theory of equal potential distribution, Int. J. Heat Mass Transfer 46 (2003) 1541–1543.

[62] A. Bejan, Y. Ikegami, G. Ledezma, Constructal theory of natural crack pattern formation for fastest cooling, Int. J. Heat Mass Transfer 41 (1998) 1945–1954.

[63] R.A. Nelson, Jr., A. Bejan, Constructal optimization of internal flow geometry in convection, J. Heat Transfer 120 (1998) 357–364.

[64] A Bejan, Simple methods for convection in porous media: scale analysis and the intersection of asymptotes, Int. J. Energy Res. 27 (2003) 859–874.

[65] A.H. Reis, A.F. Miguel, A. Bejan, Constructal theory of particle agglomeration and design of air-cleaning devices, J. Phys. D: Appl. Phys. 39 (2006) 2311–2318.

[66] J. Szargut, Anthropogenic and natural exergy losses (exergy balance of the Earths surface and atmosphere), Energy 28 (2003) 1047–1054.

[67] G.Q. Chen, Exergy consumption of the earth, Ecological Modelling 184 (2005) 363–380.

[68] W. Hermann, Quantifying global exergy resources, Energy 31 (2006) 1685–1702.

[69] C. Koroneos, T. Spachos, N. Moussiopoulos, Exergy analysis of renewable energy sources, Renewable Energy 28 (2003) 295–310.

[70] A. Hepbasli, A key review on exergetic analysis and assessment of renewable energy resources for a sustainable future, Renewable and Sustainable Energy Reviews 12 (2008) 593–661.

[71] K.C. Lee, Classification of geothermal resources by exergy, Geothermics 30 (2001) 431–442.

[72] D. Schmidt, M. Ala-Juusela, Low Exergy Systems for Heating and Cooling of Buildings, *in* Proceedings of The 21st Conference on Passive and Low Energy Architecture, The Netherlands, 2004.

[73] M.T. Balta, Y. Kalinci, A. Hepbasli, Evaluating a low exergy heating system from the power plant through the heat pump to the building envelope, Energy and Buildings 40 (2008) 1799–1804.

[74] H. Toro, A. Angelotti, D. Schmidt, Exergy analysis of renewable energy-based climatisation systems for buildings: A critical view, Energy and Buildings 41 (2009) 248–271.

[75] A.H. Reis, P. Canhoto, A.F. Miguel, R. Rosa, Non-flow exergy potential of the near-ground atmosphere with respect to soil in the vora region (Portugal), *in* Proceedings of the First International Exergy, Energy and Environment Symposium, Izmir, Turkey, 2003.

[76] M. Piechowski, Heat and mass transfer model of a ground heat exchanger: theoretical development, Int. J. Energy Res. 23 (1999) 571–588.

[77] M. Piechowski, Heat and mass transfer model of a ground heat exchanger: validation and sensitivity analysis, Int. J. Energy Res. 22 (1998) 965–979.

[78] Y. Bi, L. Chen, C. Wu, Ground heat exchanger temperature distribution analysis and experimental verification, Appl. Thermal Eng. 22 (2002) 183–189.

[79] N. Diao, Q. Li, Z. Fang, Heat transfer in ground heat exchangers with groundwater advection, Int. J. Thermal Sci. 43 (2004) 1203–1211.

[80] H. Esen, M. Inalli, M. Esen, Numerical and experimental analysis of a horizontal ground-coupled heat pump system, Building and Environment 42 (2007) 1126–1134.

[81] B. Sanner, C. Karytsas, D. Mendrinos, L. Rybach, Current status of ground source heat pumps and underground thermal energy storage in Europe, Geothermics 32 (2003) 579–588.

[82] J.C. Lam, W.W. Chan, Energy performance of air-to-water and water-to-water heat pumps in hotel applications, Energy conversion and Management 44 (2003) 1625–1631.

[83] P.S. Doherty, S. Al-Huthaili, S.B. Riffat, N. Abodahab, Ground source heat pump – description and preliminary results of the Eco House system, Appl. Thermal Eng. 24 (2004) 2627–2641.

[84] Y. Bi, T. Guo, L. Zhang, L. Chen, Solar and ground source heat-pump system, Applied Energy 78 (2004) 231–245.

[85] O. Ozgener, A. Hepbasli, Modeling and performance evaluation of ground source (geothermal) heat pump systems, Energy and Buildings 39 (2007) 66–75.

[86] A. Hepbasli, M.T. Balta, A study on modeling and performance assessment of a heat pump system for utilizing low temperature geothermal resources in buildings, Building and Environment 42 (2007) 3747–3756.

[87] O. Zogou, A. Stamatelos, Optimization of thermal performance of a building with ground source heat pump system, Energy Conversion and Management 48 (2007) 2853–2863.

[88] J.F. Urchueguía, M. Zacarés, J.M. Corberán, Á. Montero, J. Martos, H. Witte, Comparison between the energy performance of a ground coupled water to water heat pump system and an air to water heat pump system for heating

and cooling in typical conditions of the European Mediterranean coast, Energy Conversion and Management 49 (2008) 2917–2923.

[89] A. Hepbasli, Y. Kalinci, A review of heat pump water heating systems, Renewable and Sustainable Energy Reviews 13 (2009) 1211–1229.

[90] R. Karabacak, Ş.G. Acar, H. Kumsar, A. Gökgöz, Experimental investigation of the cooling performance of a ground source heat pump system in Denizli, Turkey, Int. J. Refrig. 34 (2011) 454–465.

[91] D.E. Kalz, J. Pfafferott, S. Herkel, A. Wagner, Energy and efficiency analysis of environmental heat sources and sinks: In-use performance, Renewable Energy 36 (2011) 916–929.

[92] O. Buyukalaca, F. Ekinci, T. Yilmaz , Experimental investigation of Seyhan River and dam lake as heat sourcesink for heat pump, Energy 28 (2003) 157–169.

[93] G. Gan, S.B. Riffat, C.S.A. Chong, A novel rainwaterground source heat pump – Measurement and simulation, Appl. Thermal Eng. 27 (2007) 430–441.

[94] Y. Bi, T. Guo, L. Zhang, L. Chen, Solar and ground source heat-pump system, Applied Energy 78 (2004) 231–245.

[95] W. Yang, M. Shi, H. Dong, Numerical simulation of the performance of a solar-earth source heat pump system, Appl. Thermal Eng. 26 (2006) 2367–2376.

[96] O. Ozgener, A. Hepbasli, Experimental performance analysis of a solar assisted ground-source heat pump greenhouse heating system, Energy and Buildings 37 (2005) 101–110.

[97] O. Ozgener, A. Hepbasli, Performance analysis of a solar-assisted ground-source heat pump system for greenhouse heating: an experimental study, Building and Environment 40 (2005) 1040–1050.

[98] O. Ozgener, A. Hepbasli, A parametrical study on the energetic and exergetic assessment of a solar-assisted vertical ground-source heat pump system used for heating a greenhouse, Building and Environment 42 (2007) 11–24.

[99] X. Wang, M. Zheng, W. Zhang, S. Zhang, T. Yang, Experimental study of a solar-assisted ground-coupled heat pump system with solar seasonal thermal storage in severe cold areas, Energy and Buildings 42 (2010) 2104–2110.

[100] P.J. Petit, J.P. Meyer, A techno-economic analytical comparison of the performance of air-source and horizontal-ground-source air-conditioners in South Africa, Int. J. Energy Res. 21 (1997) 1011–1021.

[101] O. Zogou, A. Stamatelos, Effect of climatic conditions on the design optimisation of heat pump systems for space heating and cooling, Energy Conversion and Management 39 (1998) 609–622.

[102] E. Bilgen, H. Takahashi, Exergy analysis and experimental study of heat pump systems, Exergy, Int. J. 2 (2002) 259–265.

[103] J. Szargut, Component efficiencies of a vapour-compression heat pump, Exergy, Int. J. 2 (2002) 99–104.

[104] A. Hepbasli, O. Akdemir, Energy and exergy analysis of a ground source (geothermal) heat pump system, Energy Conversion and Management 45 (2004) 737–753.

[105] H. Esen, M. Inalli, M. Esen, K. Pihtili, Energy and exergy analysis of a ground-coupled heat pump system with two horizontal ground heat exchangers, Building and Environment 42 (2007) 3606–3615.

[106] Y. Bi, X. Wang, Y. Liu, H. Zhang, L. Chen, Comprehensive exergy analysis of a ground-source heat pump system for both building heating and cooling modes, Applied Energy 86 (2009) 2560–2565.

[107] M.M. Alhazmy, The minimum work required for air conditioning process, Energy 31 (2006) 2739–2749.

[108] Y.A. Göğüş, Ü. Çamdali, M.Ş. Kavsaoğlu, Exergy balance of a general system with variation of environmental conditions and some applications, Energy 27 (2002) 625–646.

[109] C. Cheng, C. Chen, Performance optimization of an irreversible heat pump, J. Phys. D: Appl. Phys. 28 (1995) 2451–2454.

[110] J.S. Chiou, C.J. Liu, C.K. Chen, The performance of an irreversible Carnot refrigeration cycle, J. Phys. D: Appl. Phys. 28 (1995) 1314–1318.

[111] M. Ait-Ali, A class of internally irreversible refrigeration cycles, J. Phys. D: Appl. Phys. 29 (1996) 593–599.

[112] S.A. Klein, Design considerations for refrigeration cycles, Int. J. Refrig. 15 (1992) 181–185.

[113] M. El-Din, Optimization of totally irreversible refrigerators and heat pumps, Energy Conversion and Management 40 (1999) 423–436.

[114] L. Chen, F. Sun, C. Wu, Optimal allocation of heat-exchanger area for refrigeration and air-conditioning plants, Applied Energy 77 (2004) 339–354.

[115] J. Khan, S.M. Zubair, Thermodynamic optimization of finite time vapor compression refrigeration systems, Energy Conversion and Management 42 (2001) 1457–1475.

[116] J. Sarkar, S. Bhattacharyya, Overall conductance and heat transfer area minimization of refrigerators and heat pumps with finite heat reservoirs, Energy Conversion and Management 48 (2007) 803–808.

[117] J. Sarkar, S. Bhattacharyya, M.R. Gopal, Analytical minimization of overall conductance and heat transfer area in refrigeration and heat pump systems and its numerical confirmation, Energy Conversion and Management 48 (2007) 1245–1250.

[118] Z. Yan, L. Chen, Optimization of the rate of exergy output for an endoreversible Carnot refrigerator, J. Phys. D: Appl. Phys. 29 (1996) 3017–3021.

[119] L. Chen, Z. Xiaoqin, F. Sun, C. Wu, Ecological optimization for generalized irreversible Carnot refrigerators, J. Phys. D: Appl. Phys. 38 (2005) 113–118.

[120] L. Chen, Z. Xiaoqin, F. Sun, C. Wu, Exergy-based ecological optimization for a generalized irreversible Carnot heat-pump, Applied Energy 84 (2007) 78–88.

Chapter 2

Optimization of forced convection heat sinks with pumping power requirements[†]

Abstract

In this paper we address the optimization of a heat sink formed by parallel circular or non-circular ducts in a finite volume. The flow is considered to be laminar and steady and the fluid properties are assumed to be constant. Results for optimum dimensionless thermal length, optimum hydraulic diameter and maximum heat transfer rate density are presented for five different duct shapes subjected to a fixed pumping power constraint. Simple equations for the calculation of these optimum values are presented, and the influence of the local pressure drops at the inlet and outlet plenums, and of Prandtl number is discussed. The optimization results are then extended for the case of pumping power minimization at fixed heat transfer density.

Keywords: Heat sinks, Forced convection, Laminar flow, Pumping power, Optimization.

2.1 Introduction

Compact heat exchangers that are used in forced convection cooling systems must be optimally designed because space is valuable and demand for pumping power must be as low as possible. Generally, optimization is carried out with the purpose of reaching the maximum heat transfer rate density either with fixed pressure drop or fixed pumping power. Bejan and Sciubba [1] addressed this problem by using the method of the intersection of asymptotes for a parallel plates heat sink with application to cooling of electronic systems, and Mereu et al. [2] extend that work to the cases of fixed mass flow rate and fixed pumping power. This method is a straightforward tool for predicting the optimal internal geometric structure of volumes cooled

[†]Paulo Canhoto[(1)], A. Heitor Reis[(1)], Optimization of forced convection heat sinks with pumping power requirements, *International Journal of Heat and Mass Transfer* 54 (2011) 1441–1447.

[(1)] Physics Department and Geophysics Centre of Évora, University of Évora.

by forced convection and is part of the constructal method [3, 4].

More recent works report the application of the method of the intersection of asymptotes to other duct shapes, e.g. Muzychka [5] for microchannel heat sinks with fixed pressure drop and Wen *el al.* [6] for metallic cellular sandwich heat sinks with constant pumping power. In other recent works the constructal principle was used to optimize duct geometry at the entrance region of laminar flow [7] and to design multi-scale micro-tube heat sinks [8] with the purpose of increasing the heat transfer density.

Yilmaz [9] applied an exact method based on generalized empirical correlations to obtain the optimal geometry for circular, parallel plates, equilateral triangle and square duct shapes with fixed pressure drop, laminar flow conditions and uniform wall temperature. Li and Peterson [10] developed a parametric analysis for the optimization of rectangular microchannel heat sinks with fixed pumping power by using a detailed three-dimensional numerical simulation model. Also a computational fluid dynamics model was developed and compared with analytical solutions by Liu and Garimella [11] for the optimization of rectangular microchannel heat sinks assuming a prescribed pumping power as a design constraint.

Copeland [12] reported the influence of fin thickness and pitch of a parallel plates heat sink on pressure drop and pumping power with constant thermal resistance. Reduction of pumping power in fluid distribution networks with application to heat--generation plates cooling devices was studied by Gosselin [13], and simultaneous minimization of the global fluid flow resistance and global thermal resistance was reported by Wechsatol [14] for tree shaped heat convection network on a disc.

In this work we address the optimization of a heat sink formed by parallel circular or non-circular ducts in finite volume and subjected to fixed pumping power, for maximum heat transfer density. The duct geometries that have been considered were: circular, parallel plates, rectangular, square and equilateral triangle. An asymptotic analysis for ducts with small and large hydraulic diameter was also carried out. Next, the optimization results were extended and discussed for the case of pumping power minimization with fixed heat transfer density. This is relevant because in most practical cases the heat to be extracted from a system or device at a given temperature is known and the objective is to reduce the electric power input to the fan or pump.

2.2 General theory

The compact heat sink under consideration in the present work consists of a solid matrix of fixed dimensions H, W and L containing an array of circular or non--circular ducts as shown in Fig. 2.1-(a). The cross-sectional area is constant along

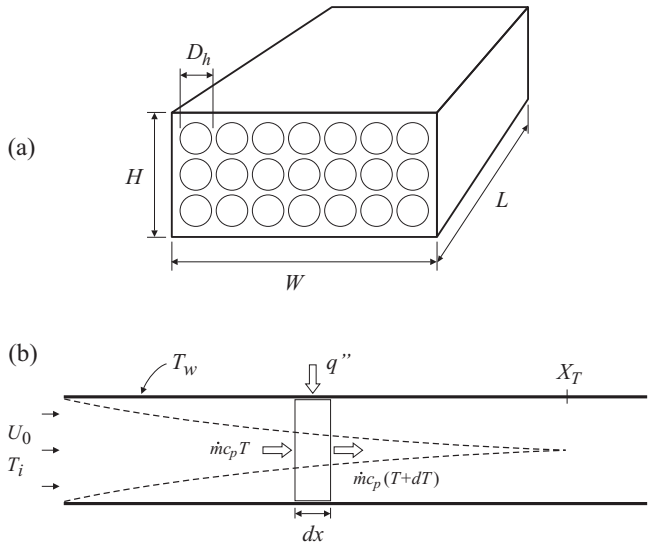

Fig. 2.1: Compact heat sink of parallel ducts. (a) Geometry. (b) Thermal boundary layer development and energy balance in an elemental volume of flow inside one duct.

the heat sink length and is equal for all ducts. The volume is cooled by internal laminar forced convection using a fluid with inlet temperature T_i and mean velocity U_0. It is assumed that the flow is steady and uniformly distributed, i.e. the mass flow rate is equal in all ducts, and that the walls are isothermal with temperature T_w.

This last assumption follows from neglecting the conduction resistance in the array, which is admissible if the solid matrix is made of a high thermal conductivity material, thus T_w is considered to be the scale for wall temperature, in line with recent works for similar multilayer channel configuration [5 – 9][1]. In particular, Wen *et al.* [6] presented a study where both the cases of uniform wall temperature and finite thermal conductivity substrate were considered[2]. However, we note that the error affecting the optimization results when this assumption is considered increases significantly only for values of heat sink porosity close to unity. The properties of

[1] Mereu et al. [2] also stressed that "*This assumption is not meant to imply in any way that the board substrate is a perfect thermal conductor.* [...] *in the present scale analysis the board temperature* T_w [...] *plays the same role as the L-averaged surface temperature when the board is modelled as uniform* [heat] *flux.*"

[2] As an example, for the case of a substrate with thermal conductivity of $100\,\mathrm{Wm^{-1}K^{-1}}$, using air as the coolant and for $H = 0.012\,\mathrm{m}$, $W = 5\,H$, $L = 5\,H$, $\varepsilon = 0.6$ and $\dot{P} = 0.5\,\mathrm{W}$, the optimization results shown in Fig. 8 of Wen's paper [6] indicate that the predicted optimum values of both the overall thermal resistance and the number of square channel layers are higher by approximately 10% with respect to the case when uniform wall temperature is assumed. If a highly conductive material is used (e.g. copper, $k \approx 400\,\mathrm{Wm^{-1}K^{-1}}$), the error due to the assumption of uniform wall temperature becomes even smaller.

the fluid are assumed to be constant.

The number of ducts with cross-sectional area A_n is

$$N \simeq \frac{\varepsilon HW}{A_n} \tag{2.1}$$

The volume fraction of ducts ε is defined and set fixed by the heat sink designer, and is a measure of the wall thickness. $\varepsilon = 1$ is assumed whenever thickness of parallel plates, square, rectangular or triangular ducts is neglected. In the case of circular tubes in a maximum packing square arrangement we have $\varepsilon \simeq 0.785$. Fig. 2.1-(b) schematically shows the thermal boundary layer development and an elemental volume in one duct. The energy balance in that elemental volume reads

$$\dot{m} c_p dT = q'' dA \tag{2.2}$$

where T and dA are, respectively, average bulk fluid temperature and elemental heat transfer area. The mass flow rate $\dot{m}$ is given by

$$\dot{m} = \rho U_0 A_n, \tag{2.3}$$

while the heat flux q'' at the wall reads

$$q'' = h_x \left(T_w - T\right) \tag{2.4}$$

with h_x standing for local heat transfer coefficient. By combining Eqs. (2.2) – (2.4) with $dT = -d\left(T_w - T\right)$ and $dA = pdx$, where p is perimeter of the duct, and then integrating along the total length, we obtain the mean temperature of the fluid at the heat sink exit T_o in the following dimensionless form:

$$\theta = \frac{T_w - T_o}{T_w - T_i} = \exp\left(-\frac{p h_{0-L} L}{\rho c_p U_0 A_n}\right) \tag{2.5}$$

with the average heat transfer coefficient h_{0-L} defined as

$$h_{0-L} = \frac{1}{L}\int_0^L h_x dx \tag{2.6}$$

Eq. (2.5) can be rewritten in terms of the dimensionless thermal length of the flow $x_* = (L/D_h)/(\mathrm{RePr})$, where $D_h = 4A_n/p$ is the hydraulic diameter of the duct, in the following simplified form:

$$\theta = \exp\left(-4 x_* \mathrm{Nu}_{0-L}\right). \tag{2.7}$$

The mean Nusselt number $\mathrm{Nu}_{0-L} = h_{0-L} D_h/k$ is a function of x_* and Pr and depends on the duct cross-sectional shape.

The mean Nusselt number is calculated by using the model proposed by Muzychka [15, 16] and now rewritten in terms of the hydraulic diameter:

$$\mathrm{Nu}_{0-L}\left(x_*\right) = \left[\mathrm{Nu}_{fd}^5 + \left(0.6135\left(\frac{f\mathrm{Re}}{x_*}\right)^{1/3}\right)^5 + \left(\frac{0.664}{\mathrm{Pr}^{1/6} x_*^{1/2}}\right)^5\right]^{1/5} \tag{2.8}$$

where Nu_{fd} and $f\mathrm{Re}$ are, respectively, Nusselt number and friction factor-Reynolds number group for fully developed flow, which are characteristic of each duct geometry. Table 2.1 summarizes these values for the five geometries considered in present work. Eq. (2.8) was compared with data [17 – 19] for the geometries in Table 2.1 and maximum differences fall in the range -8% to 15% for thermally developing flow ($\mathrm{Pr}\rightarrow\infty$) and -8% to 16% for simultaneously developing flow with $\mathrm{Pr}=0.7$.

Table 2.1: Hydraulic diameter, maximum duct fraction and fully developed flow Nusselt number and friction factor for different duct geometries.

Duct geometry	D_h	$\varepsilon_{\max}$	Nu_{fd}	$f\mathrm{Re}$
Circular tubes	D	0.785	3.66	16
Parallel plates	$2D$	1.0	7.54	24
Rectangular 1:4	$8D/5$	1.0	4.44	18.23
Square	D	1.0	2.98	14.23
Equilateral triangle	$D/\sqrt{3}$	1.0	2.47	13.33

The total heat transfer rate is obtained from the energy balance to the heat sink as

$$\dot{Q}_N = N\dot{m}c_p\left(T_o - T_i\right) \tag{2.9}$$

which, by combining with Eqs. (2.1), (2.3) and (2.7), yields

$$\dot{Q}_N = \varepsilon HW\frac{\rho k}{\mu}\mathrm{Pr}U_0\left(1-\theta\right)\left(T_w - T_i\right) \tag{2.10}$$

The mean velocity of the fluid can be related to the total pumping power by:

$$\dot{P}_N = \frac{1}{\rho}N\dot{m}\Delta p \tag{2.11}$$

where the pressure drop across the heat sink Δp is obtained with the apparent friction factor method through the following expression

$$\frac{\Delta p}{1/2\rho U_0^2} = 4x_+ f_{app}\mathrm{Re} + K_{SC} + K_{SE} \tag{2.12}$$

In Eq. (2.12), K_{SC} and K_{SE} are coefficients that account for specific pressure drops. The group $f_{app}\mathrm{Re}$ accounts for the friction along the walls and for the acceleration of the fluid core as the hydrodynamic boundary layer develops, and is determined through the formula

$$f_{app}\mathrm{Re} = \left[\left(\frac{3.44}{x_+^{1/2}}\right)^2 + \left(f\mathrm{Re}\right)^2\right]^{1/2}. \tag{2.13}$$

Note that the dimensionless hydrodynamic length $x_+ = (L/D_h)/\mathrm{Re}$ is related to the dimensionless thermal length through $x_+ = x_*\mathrm{Pr}$. Eq. (2.13) combines the Shapiro's limit for developing flow $f_{app}\mathrm{Re} = 3.44/x_+^{1/2}$ ([20] as quoted by Muzychka [15]), which is nearly independent of duct geometry, with the fully developed flow limit $f\mathrm{Re}$ through the asymptotic correlation method of Churchill and Usagi [21]. More recently, Muzychka [22] presented a detailed review and analysis of the friction factor in non-circular ducts and proposed new models for predicting the friction factor-Reynolds product for developing and fully developed flow.

The coefficients for local pressure drop at the inlet and outlet plenums are provided by models for sudden contraction (K_{SC}) and sudden expansion (K_{SE}) given respectively by [23]

$$K_{SC} = 0.42\,(1-\varepsilon) \tag{2.14}$$

and

$$K_{SE} = (1-\varepsilon)^2 \tag{2.15}$$

Finally, by combining Eqs. (2.1), (2.3) and (2.10) to (2.12) we obtain the overall heat transfer rate density in the following dimensionless form

$$Q_N^*/\varepsilon = \left[2x_* f_{app}\mathrm{Re} + \frac{K_{SC}+K_{SE}}{2\mathrm{Pr}}\right]^{-1/3} (1-\theta)\,\mathrm{Pr}^{2/3}\,(P_N^*/\varepsilon)^{1/3} \tag{2.16}$$

with

$$Q_N^* = \frac{L^2\dot{Q}_N/(HWL)}{k\,(T_w - T_i)} \tag{2.17}$$

and with the dimensionless pumping power per unit of volume defined as

$$P_N^* = \frac{\rho^2 L^4 \dot{P}_N/(HWL)}{\mu^3} \tag{2.18}$$

Note that the groups Q_N^*/ε and P_N^*/ε represent the dimensionless heat transfer rate and total pumping power per unit of volume that is effectively occupied by the fluid, respectively. As already stated above, the groups $f_{app}\mathrm{Re}$ and $1-\theta$ can be determined as functions of the dimensionless thermal length and of the Prandtl number, thus x_* emerges as the unique optimization variable in Eq. (2.16) when maximizing Q_N^* with fixed P_N^*. Then, the ratio of hydraulic diameter to duct length can also be expressed in terms of x_*, ε, Pr and P_N^* using Eqs. (2.1), (2.3), (2.11) and (2.12) with $U_0 = \nu\mathrm{Re}/D_h$. The result is

$$D_h/L = \left[2f_{app}\mathrm{Re} + \frac{K_{SC}+K_{SE}}{2x_*\mathrm{Pr}}\right]^{1/6} x_*^{-1/3}\mathrm{Pr}^{-1/3}\,(P_N^*/\varepsilon)^{-1/6} \tag{2.19}$$

In view of Eqs. (2.16) and (2.19) the heat transfer density scales with the group $\mathrm{Pr}^{2/3}\,(P_N^*/\varepsilon)^{1/3}$ while the ratio of hydraulic diameter to duct length scales with the group $\mathrm{Pr}^{-1/3}\,(P_N^*/\varepsilon)^{-1/6}$, as shown in Figs. 2.2 to 2.5 in which the existence of maximums is made evident.

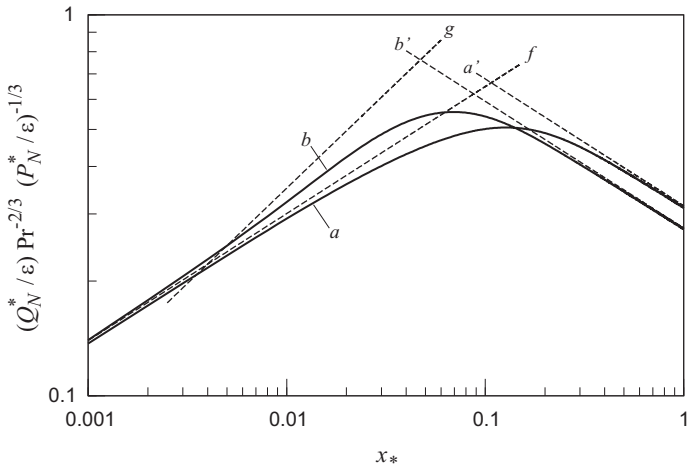

Fig. 2.2: Variation of dimensionless heat transfer density with x_* for (a) circular tubes and (b) parallel plates ducts with $K_{SC}=K_{SE}=0$ and $\mathrm{Pr}=0.7$.

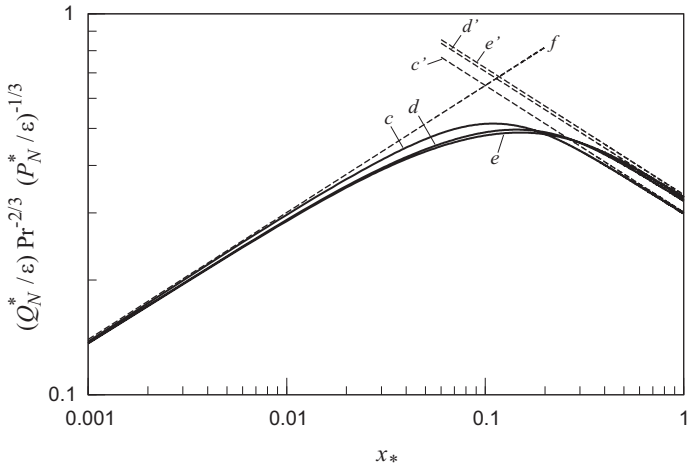

Fig. 2.3: Variation of dimensionless heat transfer density with x_* for (c) rectangular ducts 1:4, (d) square ducts and (e) equilateral triangular ducts with $K_{SC}=K_{SE}=0$ and $\mathrm{Pr}=0.7$.

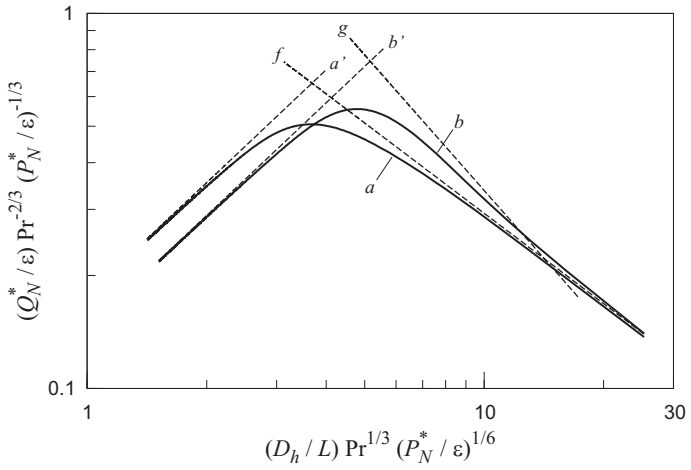

Fig. 2.4: Variation of dimensionless heat transfer density with the hydraulic diameter for (a) circular tubes and (b) parallel plates ducts with $K_{SC} = K_{SE} = 0$ and $\mathrm{Pr} = 0.7$.

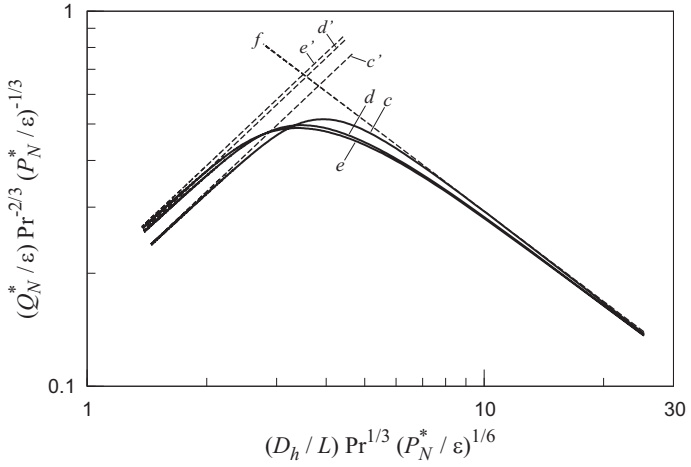

Fig. 2.5: Variation of dimensionless heat transfer density with the hydraulic diameter for (c) rectangular ducts 1:4, (d) square ducts and (e) equilateral triangular ducts with $K_{SC} = K_{SE} = 0$ and $\mathrm{Pr} = 0.7$.

2.3 Asymptotic analysis of heat sink optimization

In this section the limiting asymptotes for small and large ducts are presented and the order of magnitude of the optimum hydraulic diameter is predicted. The analysis is carried out using the formulation derived in the previous section and neglecting the local losses at the inlet and outlet plenums ($K_{SC}=K_{SE}=0$).

2.3.1 Heat transfer density for small ducts

In the case of ducts with vanishing small hydraulic diameter ($D_h \to 0$) the flow becomes fully developed ($x_* \to \infty$) and therefore $\theta \to 0$, i.e. the mean temperature of the fluid at the exit tends to the temperature of the walls. Additionally, the apparent friction factor of Eq. (2.13) tends to the fully developed flow value $f\mathrm{Re}$. Therefore, Eq. (2.16) reduces to

$$Q_N^*/\varepsilon = (2x_* f\mathrm{Re})^{-1/3}\,\mathrm{Pr}^{2/3}\,(P_N^*/\varepsilon)^{1/3} \tag{2.20}$$

We conclude that the heat transfer density varies with $x_*^{-1/3}$. Using Eq. (2.19) the asymptote of the expression above can be rewritten in terms of the hydraulic diameter as

$$Q_N^*/\varepsilon = (2f\mathrm{Re})^{-1/2}\,(D_h/L)\,\mathrm{Pr}\,(P_N^*/\varepsilon)^{1/2} \tag{2.21}$$

Thus, in the limit $D_h \to 0$ the heat transfer density decreases with D_h/L.

2.3.2 Heat transfer density for large ducts

In the case of ducts with large hydraulic diameter ($D_h \to \infty$) the flow is in both thermal and hydrodynamic development ($x_* \to 0$). Therefore we have

$$\theta \simeq 1 - 4x_*\mathrm{Nu}_{0-L} \tag{2.22}$$

In this limit both the mean Nusselt number and apparent friction factor are nearly independent of the cross-sectional shape of the duct and are well described, respectively, by the following equations [15]

$$\mathrm{Nu}_{0-L}\,(x_*) = \frac{0.664}{\mathrm{Pr}^{1/6}x_*^{1/2}} \tag{2.23}$$

and

$$f_{app}\mathrm{Re} = \frac{3.44}{x_+^{1/2}} \tag{2.24}$$

Note that Eq. (2.23) is the third component of the asymptotic correlation for mean Nusselt number presented in the right hand side of Eq. (2.8), and that Eq. (2.24) is the Shapiro's limit. Thus, Eq. (2.16) reduces to

$$Q_N^*/\varepsilon = 1.396x_*^{1/3}\mathrm{Pr}^{2/3}\,(P_N^*/\varepsilon)^{1/3} \tag{2.25}$$

In conclusion, the heat transfer density varies with $x_*^{1/3}$. This asymptote is independent of the cross-sectional shape and therefore holds for all duct geometries. Using Eq. (2.19) the expression above can be rewritten in terms of the hydraulic diameter as

$$Q_N^*/\varepsilon = 1.805\,(D_h/L)^{-4/5}\,\mathrm{Pr}^{1/3}\,(P_N^*/\varepsilon)^{1/5} \tag{2.26}$$

Thus, in the limit $D_h \to \infty$ the heat transfer density decreases as $(D_h/L)^{-4/5}$.

In the case of parallel plates and in the range $5\times10^{-3} < x_* < 5\times10^{-2}$ the heat transfer density is higher than the values given by the asymptote of Eq. (2.25) and approaches to the limiting curve that corresponds to the case $\mathrm{Pr} \to \infty$. This curve is derived as before but using in this case the second component of the asymptotic correlation in the right hand side of Eq. (2.8):

$$\mathrm{Nu}_{0-L}\,(x_*) = 0.6135\left(\frac{f\mathrm{Re}}{x_*}\right)^{1/3} \tag{2.27}$$

The result is:

$$Q_N^*/\varepsilon = 1.290\,(f\mathrm{Re})^{1/3}\,x_*^{1/2}\mathrm{Pr}^{5/6}\,(P_N^*/\varepsilon)^{1/3} \tag{2.28}$$

This shows that in the limit $x_* \to 0$, the heat transfer density decreases with $x_*^{1/2}$.

2.3.3 Scale analysis of optimum hydraulic diameter

The variation of the heat transfer density with respect to x_* is represented in Fig. 2.2 for circular tubes and parallel plates with $\mathrm{Pr} = 0.7$ and for the case when the local losses at inlet and outlet plenums may be neglected. Fig. 2.3 shows the same variation for the case of rectangular, square and equilateral triangular ducts. The limiting curves a' to e' are obtained from Eq. (2.20) and correspond to the small duct limit. The large duct limiting curve f is obtained from Eq. (2.25) while curve g is obtained from Eq. (2.28) for the case of parallel plates. In Figs. 2.4 and 2.5, the heat transfer density is represented as a function of D_h/L, exhibiting the existence of maximum values as well.

The maximum heat transfer density corresponds to the optimum D_h/L ratio, which is close to that obtained by intersecting the limits of Eqs. (2.21) and (2.26), as shown in Figs. 2.4 and 2.5. Thus, we can predict the order of magnitude of the optimum hydraulic diameter as

$$(D_h/L)_{\mathrm{opt}}\,(P_N^*/\varepsilon)^{1/6} = 1.388\,(2f\mathrm{Re})^{5/18}\,\mathrm{Pr}^{-10/27} \tag{2.29}$$

This result indicates that the optimum hydraulic diameter is nearly insensitive to both P_N^* and ε. With respect to optimum plate-to-plate spacing, in the case of parallel plates ($D_h = 2\,D$) the right hand side of Eq. (2.29) reduces to $2.03\,\mathrm{Pr}^{-10/27}$, which is very similar to the result obtained by Mereu et al. [2] for this duct geometry.

2.4 Optimization and discussion

From Eq. (2.16) whenever the plenum losses may be neglected we conclude that the optimum x_* that arises from the condition $\partial Q_N^*/\partial x_* = 0$ is independent of the duct fraction ε and, in that case, the maximum heat transfer density varies with $\varepsilon^{2/3}$ while, according to Eq. (2.19), the optimum ratio of hydraulic diameter to duct length varies with $\varepsilon^{1/6}$. The values of the optimum dimensional thermal length and maximum heat transfer density were found through numerical maximization of Eq. (2.16) using the Newton method. A maximum difference of 10^{-4} between two successive values of x_* was used as convergence criteria, with a maximum number of iteration of 100. The optimum hydraulic diameter was then calculated using Eq. (2.19).

2.4.1 Influence of the local losses

The influence of the local losses on the optimum dimensionless thermal length, maximum heat transfer density and optimum hydraulic diameter is shown in Figs. 2.6, 2.7 and 2.8, respectively. These variations are represented in percentage of the values for the case $K_{SC} = K_{SE} = 0$ and $\mathrm{Pr} = 0.7$. The optimum x_* decreases with increasing ε while the maximum heat transfer density and $(D_h/L)_{\mathrm{opt}}$ increase. This is explained by the increasing high values of local pressure drop at the plenums as ε decreases, leading to lower values of Q_N^*. The parallel plates geometry is more affected by local losses in terms of the maximum heat transfer density while the square and equilateral triangular ducts are the less affected. In terms of optimum hydraulic diameter the variations are small in all the cases (less than -1.5% for $\varepsilon = 0.5$).

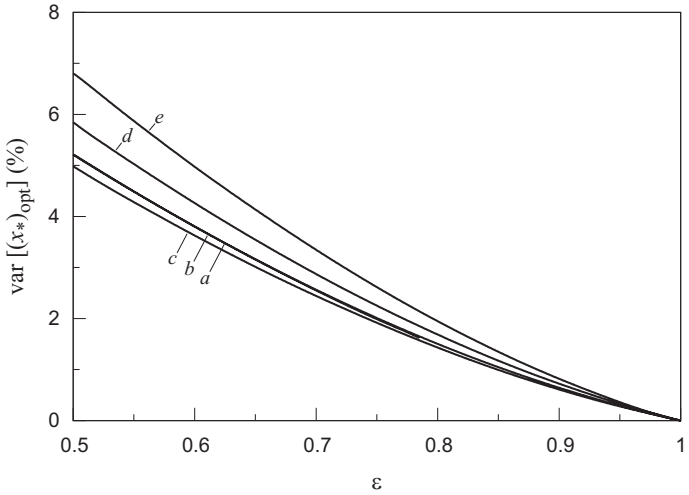

Fig. 2.6: Influence of plenum losses in the optimum dimensionless thermal length as percentage variation relative to the case $K_{SC} = K_{SE} = 0$ and $\mathrm{Pr} = 0.7$: (a) circular tubes; (b) parallel plates ducts; (c) rectangular ducts 1:4; (d) square ducts; (e) equilateral triangular ducts.

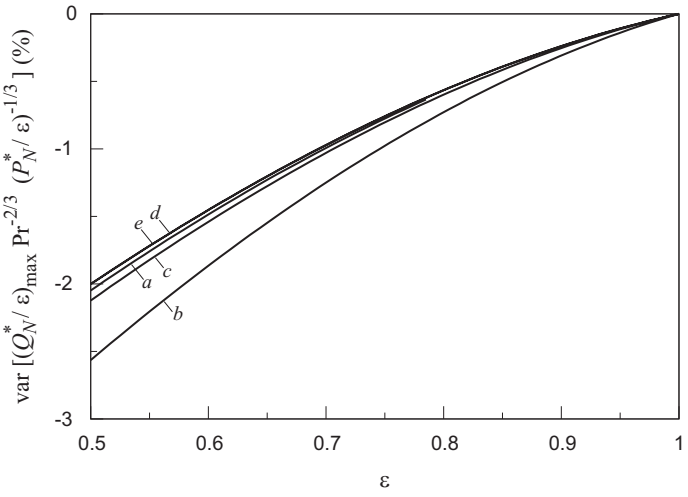

Fig. 2.7: Influence of plenum losses in the maximum heat transfer density as percentage variation relative to the case $K_{SC} = K_{SE} = 0$ and $\mathrm{Pr} = 0.7$: (a) circular tubes; (b) parallel plates ducts; (c) rectangular ducts 1:4; (d) square ducts; (e) equilateral triangular ducts.

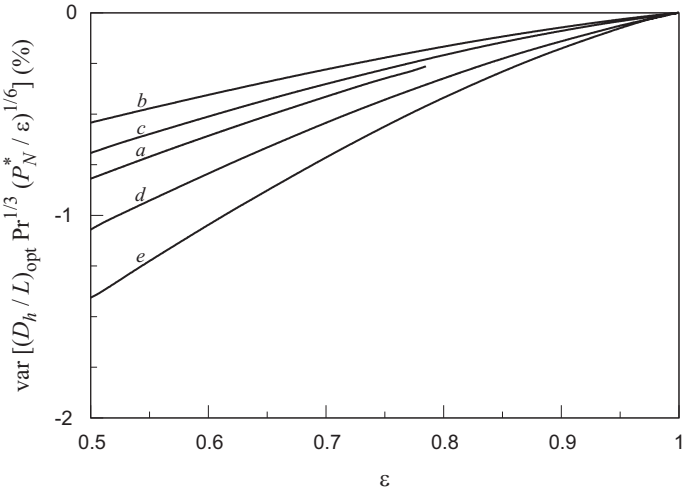

Fig. 2.8: Influence of plenum losses in the optimum hydraulic diameter as percentage variation relative to the case $K_{SC} = K_{SE} = 0$ and $\mathrm{Pr} = 0.7$: (a) circular tubes; (b) parallel plates ducts; (c) rectangular ducts 1:4; (d) square ducts; (e) equilateral triangular ducts.

2.4.2 Influence of the Prandtl number

For the case of circular tubes in which local losses may be neglected, both the variation of $(x_*)_{\text{opt}}$ and maximum heat transfer density with the Prandtl number is shown in Fig. 2.9. The optimum x_* decreases with Pr and tends to $(x_*)_{\text{opt}} \approx 0.1$ which corresponds to the optimum value for a thermally developing flow, while maximum heat transfer density increases with Pr. The values of $(x_*)_{\text{opt}}$, $(D_h/L)_{\text{opt}}$ and maximum Q_N^* are presented in Tables 2.2, 2.3 and 2.4, respectively, for various values of Pr.

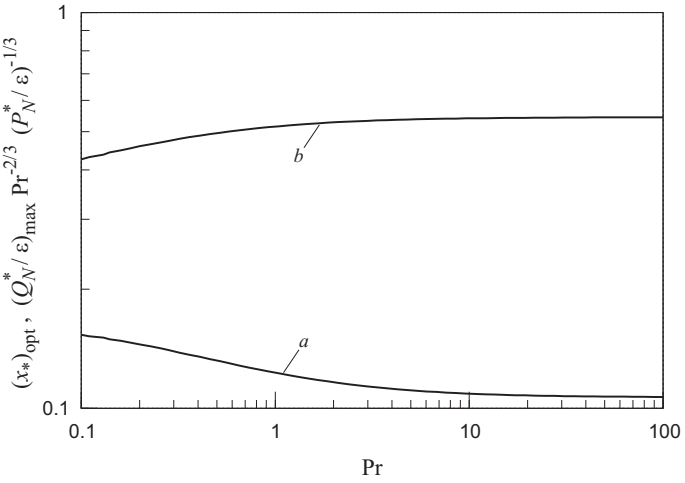

Fig. 2.9: Variation of (a) optimum dimensionless thermal length and (b) maximum heat transfer density with Pr for circular tubes and $K_{SC} = K_{SE} = 0$.

The optimum D_h/L ratio decreases with Pr as shown in Fig. 2.10 (solid lines), where the scaling factor $(P_N^*/\varepsilon)^{1/6}$ is used with the purpose of showing the effect of Prandtl number. These optimum values are found to be correlated for the geometries considered through the following expression:

$$(D_h/L)_{\text{opt}} \, (P_N^*/\varepsilon)^{1/6} = 2.265 \exp\left(\frac{f\text{Re}}{32}\right) \text{Pr}^{-0.33} \tag{2.30}$$

with a maximum error within -2.1% to 2.0% in the range $0.1 \leq \text{Pr} \leq 100$. On the other hand, the prediction made by Eq. (2.29) reproduces the numerical results with error within -8.6% to 13.5% for $0.1 \leq \text{Pr} \leq 10$ and for all the geometries considered except for parallel plates in which the lower limit of the error is -23%.

Once the optimum D_h/L ratio is known through Eq. (2.30), it is straightforward to determine the characteristic length scale of the duct (e.g. diameter of circular tubes, the length of the side of square ducts, etc) from the definition of hydraulic diameter (Table 2.1).

Table 2.2: Optimum x_* for different duct geometries and Pr numbers with $K_{SC}=K_{SE}=0$.

	Pr						
Duct geometry	0.1	0.7	1	5	10	50	100
Circular tubes	0.153	0.127	0.123	0.111	0.109	0.107	0.107
Parallel plates	0.083	0.069	0.067	0.063	0.062	0.061	0.061
Rectangular 1:4	0.132	0.110	0.106	0.097	0.096	0.095	0.094
Square	0.173	0.143	0.138	0.122	0.119	0.116	0.116
Equilateral triangle	0.180	0.150	0.143	0.123	0.119	0.116	0.116

Table 2.3: Optimum hydraulic diameter $(D_h/L)_{\text{opt}}\,\text{Pr}^{1/3}\,(P_N^*/\varepsilon)^{1/6}$ for different duct geometries and Pr numbers with $K_{SC}=K_{SE}=0$.

	Pr						
Duct geometry	0.1	0.7	1	5	10	50	100
Circular tubes	3.739	3.668	3.680	3.733	3.745	3.756	3.757
Parallel plates	4.854	4.781	4.790	4.826	4.834	4.840	4.841
Rectangular 1:4	3.989	3.926	3.937	3.981	3.991	3.999	4.000
Square	3.550	3.468	3.483	3.554	3.571	3.586	3.588
Equilateral triangle	3.481	3.389	3.409	3.502	3.526	3.548	3.551

Table 2.4: Maximum heat transfer density $(Q_N^*/\varepsilon)_{\max}\,\text{Pr}^{-2/3}\,(P_N^*/\varepsilon)^{-1/3}$ for different duct geometries and Pr numbers with $K_{SC}=K_{SE}=0$.

	Pr						
Duct geometry	0.1	0.7	1	5	10	50	100
Circular tubes	0.425	0.506	0.515	0.537	0.540	0.543	0.543
Parallel plates	0.472	0.556	0.564	0.585	0.588	0.590	0.591
Rectangular 1:4	0.436	0.515	0.523	0.544	0.547	0.549	0.550
Square	0.415	0.496	0.506	0.529	0.533	0.536	0.537
Equilateral triangle	0.408	0.488	0.497	0.522	0.526	0.529	0.529

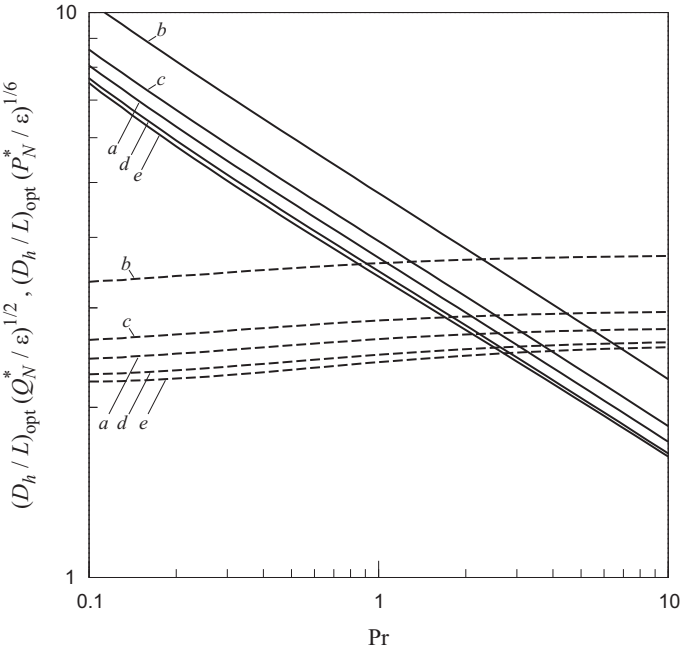

Fig. 2.10: Variation of optimum hydraulic diameter with Pr for heat transfer maximization (solid lines) and pumping power minimization (dashed lines) with $K_{SC} = K_{SE} = 0$: (a) circular tubes; (b) parallel plates ducts; (c) rectangular ducts 1:4; (d) square ducts; (e) equilateral triangular ducts.

For the maximum heat transfer density the formula

$$(Q_N^*/\varepsilon)_{\max} (P_N^*/\varepsilon)^{-1/3} = (0.42 + 0.0061 f\mathrm{Re})\,\mathrm{Pr}^a \tag{2.31}$$

is found to hold, with $a = 0.75$ for $0.1 \leq \mathrm{Pr} \leq 1$ and $a = 0.68$ for $1 \leq \mathrm{Pr} \leq 100$. In this case, the maximum error is -2.7% to 2.8% in the entire range of Pr. When $\mathrm{Pr} = 1$ the maximum absolute error is 1.6%.

2.4.3 Pumping power minimization

Given the proportionality between heat transfer and pumping power according to Eq. (2.16), the problem of minimizing P_N^* with fixed Q_N^* is equivalent to maximizing Q_N^* with fixed P_N^*, resulting in the same optimum x_* in both cases. The optimum hydraulic diameter for minimum pumping power is calculated from Eq. (2.19) by making $x_* = (x_*)_{\mathrm{opt}}$ and $P_N^* = (P_N^*)_{\min}$ that comes from Eq. (2.16). These values scale with $(Q_N^*/\varepsilon)^{1/2}$ and are shown in Fig. 2.10 (dashed lines) as function of Prandtl number.

For all the geometries considered the following expression it is found to hold:

$$(D_h/L)_{\mathrm{opt}} (Q_N^*/\varepsilon)^{1/2} = 2.265\,(0.42 + 0.0061 f\mathrm{Re})^{1/2} \exp\left(\frac{f\mathrm{Re}}{32}\right) \mathrm{Pr}^b \tag{2.32}$$

with $b = 0.045$ for $0.1 \leq \mathrm{Pr} \leq 1$ and $b = 0.01$ for $1 \leq \mathrm{Pr} \leq 100$. In this case, the maximum error is within -2.6% to 3.1% in the entire range of Pr. We can see that $(D_h/L)_{\mathrm{opt}} \left(Q_N^*/\varepsilon\right)^{1/2}$ is nearly constant for $\mathrm{Pr} \geq 0.7$ suggesting that, as an approximation, the heat sink can be firstly optimized geometrically for the required heat transfer density and then operated according to the kind of fluid for the purpose of achieving minimum pumping power, which is obtained from Eq. (2.16).

2.5 Conclusions

In this study we addressed the optimization of a heat sink formed by parallel ducts in a solid matrix of fixed volume. The optimum dimensionless thermal length and optimum hydraulic diameter were found for achieving maximum heat transfer density at fixed pumping power. We present simple equations for the calculation of those optimum values as function of Prandtl number. When local pressure losses at inlet and outlet plenums are considered we found that the optimum dimensionless thermal length varies inversely with the volume fraction of ducts while the maximum heat transfer density and the optimum hydraulic diameter vary directly with the same quantity. Results were extended and discussed for the case of pumping power minimization with fixed heat transfer density, and it was found that the optimum hydraulic diameter is nearly constant for $\mathrm{Pr} \geq 0.7$, thus suggesting that heat sinks can be firstly optimized geometrically for the required heat transfer density and then operated according to the fluid properties for achieving minimum pumping power.

References

[1] A. Bejan, E. Sciubba, The optimal spacing of parallel plates cooled by forced convection, Int. J. Heat Mass Transfer 35 (1992) 3259–3264.

[2] S. Mereu, E. Sciubba, A. Bejan, The optimal cooling of a stack of heat generating boards with fixed pressure drop, flowrate or pumping power, Int. J. Heat Mass Transfer 36 (1993) 3677–3686.

[3] A. Bejan, I. Dincer, S. Lorente, A.F. Miguel, A.H. Reis, Porous and Complex Flow Structures in Modern Technologies, Springer, New York, 2004.

[4] A.H. Reis, Constructal Theory: From Engineering to Physics, and How Flow Systems Develop Shape and Structure, Applied Mechanics Reviews 59 (2006) 269–282.

[5] Y. Muzychka, Constructal design of forced convection cooled microchannel heat sinks and heat exchangers, Int. J. Heat Mass Transfer 48 (2005) 3119–3127.

[6] T. Wen, F. Xu, T.J. Lu. Structural optimization of two-dimensional cellular metals cooled by forced convection, Int. J. Heat Mass Transfer 50 (2007) 2590–2604.

[7] T. Bello-Ochende, J.P. Meyer, A. Bejan, Constructal ducts with wrinkled entrances, Int. J. Heat Mass Transfer 52 (2009) 3628–3633.

[8] Y.S. Muzychka, Constructal multi-scale design of compact micro-tube heat sinks and heat exchangers, Int. J. Thermal Sciences 46 (2007) 245–252.

[9] A. Yilmaz, O. Buyukalaca, T. Yilmaz, Optimum shape and dimensions of ducts for convective heat transfer in laminar flow at constant wall temperature, Int. J. Heat Mass Transfer 43 (2000) 767–775.

[10] J. Li, G.P. Peterson, Geometric optimization of a micro heat sink with liquid flow, IEEE Transactions on Components and Packaging Technologies 29 (2006) 145–154.

[11] D. Liu, S.V. Garimella, Analysis and optimization of the thermal performance of microchannel heat sinks, Int. J. Numerical Heat Fluid Flow 15 (2005) 7–26.

[12] D. Copeland, Optimization of parallel plate heat sinks for forced convection, *in* Proceedings of the 16th IEEE SEMI-THERM Symposium, 2000, pp. 266–272.

[13] L. Gosselin, Fitting the flow regime in the internal structure of heat transfer systems, Int. Commun. Heat Mass Transfer 33 (2006) 30–38.

[14] W. Wechsatol, S. Lorente, A. Bejan, Dentritic heat convection on a disc, Int. J. Heat Mass Transfer 46 (2003) 4381–4391.

[15] Y. Muzychka, Analytical and Experimental Study of Fluid Friction and Heat Transfer in Low Reynolds Number Flow Heat Exchangers, Ph.D. Thesis, Department of Mechanical Engineering, University of Waterloo, Ontario, Canada, 1999.

[16] Y.S. Muzychka, M.M. Yovanovich, Laminar forced convection heat transfer in the combined entry region of non-circular ducts, J. Heat Transfer Trans. ASME 126 (2004) 54–61.

[17] R.K. Shah, A.L. London, Laminar Flow Forced Convection in Ducts, Academic Press, New York, 1978.

[18] P. Wibulswas, Laminar flow heat transfer in non-circular ducts, Ph.D. thesis, London University, London, 1966.

[19] A.R. Chandrupatla, V.M.K. Sastri, Laminar forced convection heat transfer of a non-Newtonian fluid in a square Duct, Int. J. Heat Mass Transfer 20 (1977) 1315–1324.

[20] A.H. Shapiro, R. Siegel, S.J. Kline, Friction factor in the laminar entry region of a smooth tube, *in* Proceedings of the Second US National Congress of Applied Mechanics, 1954, pp. 733–741.

[21] S.W. Churchill, R. Usagi, A general expression for the correlation of rates of transfer and other phenomena, Am. Inst. Chem. Eng. 18 (1972) 1121–1128.

[22] Y.S. Muzychka, M.M. Yovanovich, Pressure drop in laminar developing flow in noncircular ducts: a scaling and modelling approach, J. Fluids Eng. 131 (2009) 111105 (11 p.).

[23] F.M. White, Fluid Mechanics, fourth ed., McGraw-Hill, New York, 1999.

Nomenclature

A_n	cross-sectional area (m^2)
c_p	specific heat ($\mathrm{J\,kg^{-1}\,K^{-1}}$)
D_h	hydraulic diameter (m), $\equiv 4A_n/p$
f	friction factor
H	height (m)
h_x	local heat transfer coefficient ($\mathrm{W\,m^{-2}\,K^{-1}}$)
h_{0-L}	average heat transfer coefficient ($\mathrm{W\,m^{-2}\,K^{-1}}$)
L	length (m)
k	thermal conductivity ($\mathrm{W\,m^{-1}\,K^{-1}}$)
K	local pressure drop coefficient
$\dot{m}$	mass flow rate ($\mathrm{kg\,s^{-1}}$)
N	number of ducts
Nu_{0-L}	mean Nusselt number, $\equiv h_{0-L}D_h/k$
p	perimeter (m)
$\dot{P}_N$	total pumping power (W)
P_N^*	dimensionless pumping power, $\equiv \rho^2 L^4 \dot{P}_N/(\mu^3 HWL)$
Pr	Prandtl number, $\equiv \mu\, c_p/k$
q''	heat flux ($\mathrm{W\,m^{-2}}$)
$\dot{Q}_N$	total heat transfer rate (W)
Q_N^*	dimensionless heat transfer density, $\equiv L^2\dot{Q}_N/\left(kHWL\left(T_w - T_i\right)\right)$

Re	Reynolds number, $\equiv U_0 D_h/\nu$
T	temperature (K)
U_0	mean fluid velocity in ducts ($\mathrm{m\,s^{-1}}$)
x_+	dimensionless hydrodynamic length, $\equiv (L/D_h)/\mathrm{Re}$
x_*	dimensionless thermal length, $\equiv (L/D_h)/(\mathrm{RePr})$
W	width (m)

Greek symbols

Δp	pressure drop (Pa)
ε	volume fraction of ducts, $\equiv NA_nL/(HWL)$
μ	dynamic viscosity ($\mathrm{kg\,m^{-1}\,s^{-1}}$)
ν	kinematic viscosity ($\mathrm{m^2\,s^{-1}}$), $\equiv \mu/\rho$
ρ	density ($\mathrm{kg\,m^{-3}}$)

Subscripts

app	apparent
i	inlet
fd	fully developed flow
max	maximum
min	minimum
o	outlet
opt	optimum
SC	sudden contraction
SE	sudden expansion
w	wall

Chapter 3

Optimization of fluid flow and internal geometric structure of volumes cooled by forced convection in an array of parallel tubes[†]

Abstract

This paper reports the optimization of a heat sink composed of parallel tubes in a solid matrix of fixed dimensions for the following cases: (i) fixed pressure drop; (ii) fixed pumping power and (iii) fixed heat transfer rate density. The method of the intersection of asymptotes is employed using the dimensionless thermal length (x_*) as primary optimization variable, and approximate theoretical expressions for predicting the optimum ratio of diameter to tube length (D/L) are presented for each case. When the system is optimized with fixed heat transfer density it is found that the optimum values of both x_* and D/L are very close to those that correspond to the joint minimization of pressure drop and pumping power. These results are validated and complemented by means of numerical simulations.

Keywords: Heat sinks, Forced convection, Laminar flow, Optimization, Intersection of asymptotes method.

3.1 Introduction

The design of forced convection heat sinks is usually carried out in order to maximize the heat transfer density under the maximum surface temperature allowed for the system to be cooled. In this case, the optimal internal geometric structure depends on the imposed constraint, e.g. fixed pressure drop or fixed pumping power. The same procedure is also used either for determining the maximum packaging of heat generating devices in a fixed volume or, conversely, if the heat generated is fixed and

[†]Paulo Canhoto[(1)], A. Heitor Reis[(1)], Optimization of fluid flow and internal geometric structure of volumes cooled by forced convection in an array of parallel tubes, *International Journal of Heat and Mass Transfer* 54 (2011) 4288–4299.

[(1)] Physics Department and Geophysics Centre of Évora, University of Évora.

known, for minimizing the hot spot temperature.

Two different approaches are commonly considered in heat sink optimization: (1) numerical simulations of flow and temperature fields and; (2) scale analysis of flow and heat transfer variables. Although the numerical simulation is more accurate, it requires computing time and resources that are not negligible as compared with the second approach. In the second approach, the method of the intersection of asymptotes [1, 2] is a straightforward but powerful tool for predicting the optimal internal geometric structure of volumes cooled either by natural or forced convection, and is a tool of the constructal theory [3, 4, 5]. The constructal theory has extensive applicability in many domains, e.g. in optimization of engineered fluid flows and heat transfer networks [6, 7], and prediction of shape and structure in natural systems [8, 9] as well in living organisms [10].

The method of intersecting the asymptotes was first employed to predict the optimal spacing in a heat sink composed of parallel plates under natural convection [1], and thereafter applied to the optimization of a similar heat sink under forced convection and subjected to fixed pressure drop [2]. More recently, this last work was generalized to other duct geometries [11]. Optimization was also carried out for the case of a stack of heat generating boards with fixed mass flow rate and fixed pumping power [12] and for the cases of staggered plates [13] and cylinders in cross-flow [14, 15]. Recent works report the use of the constructal method in the optimization of aspect ratios of channels with fixed pressure drop [16, 17], and of metallic cellular sandwich heat sinks with constant pumping power [18]. The same method was used to design multi-scale compact micro-tube heat sinks [19] for maximum heat transfer density.

Yilmaz et al. [20] carried out an asymptotic analysis of forced convection heat transfer in ducts of different shapes for laminar flow with fixed pressure drop, and used an exact method based on correlations to obtain the optimal geometry. More recently, the optimization of a heat sink composed of parallel circular or non-circular ducts in a finite volume was reported for the case of fixed pumping power constraint, see Ref. [21][1]. This work also reports the optimum length scale of ducts for pumping power minimization with fixed heat transfer density at a given nominal or maximum temperature of operation.

The method of intersecting the asymptotes provides the geometric point that optimizes the trade-off of two distinct trends. For example, in the case of a heat sink composed of parallel channels, for small hydraulic diameters the flow becomes fully

[1]The paper "Optimization of forced convection heat sinks with pumping power requirements", *Int. J. Heat Mass Transfer* 54 (2011) 1441–1447 by P. Canhoto and A.H. Reis [21] is included in this thesis in the Chapter 2.

developed and the outlet temperature of the fluid approaches the wall temperature, while for large hydraulic diameters the flow is thermally developing and the temperature of the fluid in the core remains nearly unchanged. It is also possible to represent these limiting cases in terms of the dimensionless thermal length of the flow (x_*), thus allowing to directly verify if the fluid is 'efficiently used' for the cooling purpose: (i) if x_* is too small it means that the fluid in the core flow almost do not participate in the heat transfer process and; (ii) if x_* is too large the heat flux decreases and, in the limit, no more heat can be extracted by the fluid. The intersection of these two distinct trends makes it possible to predict the optimum length scale of the heat sink channels together with the optimum dimensionless thermal length under global constraints. For example, for a parallel plates heat sink subjected to fixed pressure drop the intersection of asymptotes underestimates by only 12% the optimum plate-to-plate spacing for maximum heat transfer density [2]. In this case the adjacent thermal boundary layers merge just at the exit of the channel.

However, we can recognize the concept beyond this method as a general rule that is likely independent of the imposed fluid flow constraints, because thermally developed and developing flow limits are still possible to reach if diverse conditions are considered. Specifically, we may assume that the method is able not only to predict the optimal internal geometric structure but also provide some guidelines about the better fluid flow conditions for a given heat transfer density.

The fluid flow constraint depends on the flow arrangement in which the heat sink is connected [12]. If several heat sinks or other components are connected in parallel thus receiving the flow from the same plenum then the fixed pressure drop is the appropriate constraint, while fixed mass flow rate constraint reveals appropriate when several components are placed in series. If a heat sink is the only component that is cooled by the flow imposed by a pump or fan, then the fixed pumping power assumption must be used. However, in this case we must also consider pumping power minimization with fixed heat transfer density, because in several practical installations the heat to be extracted from a system or device at a given design or maximum temperature is known, and the objective is reducing the electric power input to the fan or pump.

In this work, we explore the concept of the method of intersecting the asymptotes for the optimization of a heat sink composed of parallel tubes, by considering different constraints: fixed pressure drop, fixed pumping power, and fixed heat transfer density. The dimensionless thermal length is used as the primary optimization variable and the optimum ratio of diameter to tube length (D/L) is obtained for each case together with the maximum heat transfer density, minimum pressure drop or minimum pumping power. These results are validated and complemented by numerical simulations of fluid flow and temperature fields.

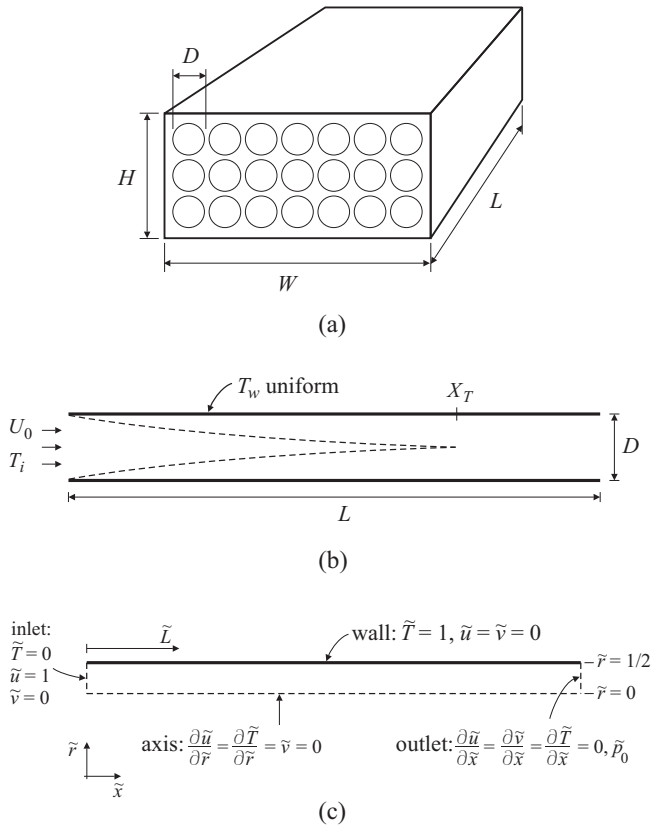

Fig. 3.1: Compact heat sink of parallel ducts in a finite volume: (a) geometry schematic; (b) physical domain of an elemental channel; (c) computational domain and boundary conditions.

3.2 Hydrodynamic and thermal analysis of heat sink optimization

The heat sink under consideration in the present work is composed of parallel tubes in a solid matrix of high thermal conductivity material with fixed dimensions H, W and L, as shown in Fig. 3.1(a). The number of tubes with diameter D in the array is given by

$$N \simeq \frac{4\varepsilon HW}{\pi D^2} \tag{3.1}$$

The volume fraction of the tubes ε is set fixed by the heat sink designer. For example, in the case of circular tubes in a maximum packing square arrangement $\varepsilon \simeq 0.785$ and $N \simeq HW/D^2$. A coolant flows in the tubes with mean velocity U_0 and inlet temperature T_i. It is assumed that the flow is steady, laminar, incompressible, and equally distributed among the tubes, together with negligible pressure losses at the inlet and outlet plenums.

The walls of the tubes are considered to be at uniform temperature T_w, thus neglecting the conduction resistance in the solid matrix, in line with recent works for similar multilayer channel configuration [11, 17 – 21]. This also means that we can

regard T_w as the scale of the surface temperature, which is distinct from the inlet and outlet temperatures of the fluid. Additionally, it is assumed that the thermodynamic and transport properties of the fluid are constant.

The mass flow rate in each tube is given by:

$$\dot{m} = \rho U_0 \pi D^2/4 \tag{3.2}$$

while the total rate of heat removed from the heat sink reads:

$$\dot{Q}_N = N\dot{m}c_p\left(T_o - T_i\right) \tag{3.3}$$

The mean temperature of the fluid at the outlet T_o is determined through the following expression [22]:

$$\theta = \frac{T_w - T_o}{T_w - T_i} = \exp\left(-4x_*\mathrm{Nu}_{0-L}\right) \tag{3.4}$$

where Nu_{0-L} is the mean Nusselt number and x_* is the dimensionless thermal length, which reads:

$$x_* = \frac{L/D}{\mathrm{RePr}} \tag{3.5}$$

By combining Eqs. (3.1) – (3.4) one finds the total heat transfer rate in the form:

$$\dot{Q}_N = \varepsilon HW\frac{\rho k}{\mu}\mathrm{Pr}U_0\left(1-\theta\right)\left(T_w - T_i\right) \tag{3.6}$$

The mean fluid velocity U_0 is related to the pressure drop across the heat sink through the apparent friction factor method by using the known formula:

$$\frac{\Delta p}{1/2\rho U_0^2} = 4x_+ f_{app}\mathrm{Re} \tag{3.7}$$

with the friction factor-Reynolds number group given by [23]

$$f_{app}\mathrm{Re} = \left[\left(\frac{3.44}{x_+^{1/2}}\right)^2 + \left(f\mathrm{Re}\right)^2\right]^{1/2} \tag{3.8}$$

Note that the dimensionless hydrodynamic length $x_+ = \left(L/D\right)/\mathrm{Re}$ may also read $x_+ = x_*\mathrm{Pr}$ and that $f\mathrm{Re}$ stands for friction factor of fully developed flow. More recently, Muzychka and Yovanovich [24, 25] presented a detailed analysis of heat transfer and friction factor in circular and non-circular ducts and proposed new models for developing and fully developed flow.

By combining Eqs. (3.6) and (3.7) we obtain

$$\dot{Q}_N = \underbrace{\left(\varepsilon HW\right)}_{\text{Geometry}}\underbrace{\left(\rho^{1/2}\mathrm{Pr}^{1/2}k/\mu\right)}_{\text{Fluid properties}}\underbrace{\left(2x_* f_{app}\mathrm{Re}\right)^{-1/2}}_{\text{Fluid flow}}\underbrace{\left(1-\theta\right)}_{\text{Heat transfer}}\Delta p^{1/2}(T_w - T_i) \tag{3.9}$$

In the right hand side of this equation four groups of factors are identified that relate to overall geometry, fluid properties and fluid flow and heat transfer conditions, respectively. Considering that both $f_{app}\mathrm{Re}$ and Nu_{0-L} can be determined as functions of dimensionless thermal length and Prandtl number, then x_* emerges as the unique free variable in Eq. (3.9) that can be adjusted for maximum heat transfer rate.

From previous works on heat sink optimization [2, 11, 20] it is known that when the imposed pressure drop is fixed an optimal internal geometry exists for which the total heat transfer rate is maximum. In fact, as for a given Pr both $f\mathrm{Re}$ and Nu_{0-L} decrease with x_*, and by a simple graphical analysis of Eq. (3.9) (not shown here for concision, see the next sections), if both Δp and $(T_w – T_i)$ are fixed we conclude that a maximum value of $\dot{Q}_N$ exists for a certain value of x_* (optimum). What is important to retain now is that the group $(1-\theta)x_*^{-1/2}$ makes it possible this maximum to exist, also for thermally developing flow ($f\mathrm{Re}=16$). If we rewrite Eq. (3.9) in the following simplified form:

$$\frac{\dot{Q}_N}{\Delta p^{1/2}(T_w - T_i)} = f(x_*) \tag{3.10}$$

where $f(x_*)>0$ stands for the four groups of factors identified before, it is straightforward to show that the optimum value of x_* that emerges from $\partial f(x_*)/\partial x_* = 0$ may be found either through maximization of $\dot{Q}_N$ at constant Δp and $T_w - T_i$, or equivalently through minimization of either Δp (at constant $\dot{Q}_N$ and $T_w - T_i$) or $T_w - T_i$ (at constant $\dot{Q}_N$ and Δp).

The relation between D/L, x_* and Δp may be derived from Eqs. (3.5) and (3.7) with $U_0 = \nu\mathrm{Re}/D$:

$$D/L = \left(\frac{2 f_{app}\mathrm{Re}}{x_*\mathrm{Pr}}\right)^{1/4} \Delta p^{*-1/4} \tag{3.11}$$

where $\Delta p^* = \rho L^2 \Delta p/\mu^2$ is dimensionless pressure drop. Once the optimum x_* is known, the optimum ratio of diameter to tube length can be determined through Eq. (3.11) by using either the fixed value or the minimum value of pressure drop.

In the case of heat transfer rate maximization the value of $(\dot{Q}_N)_{\max}$ is determined by making $x_* = (x_*)_{\mathrm{opt}}$ in Eq. (3.9), which can be rewritten in the following form:

$$Q_N^*/\varepsilon = (2x_* f_{app}\mathrm{Re})^{-1/2}\,(1-\theta)\,\mathrm{Pr}^{1/2}\Delta p^{*1/2} \tag{3.12}$$

with

$$Q_N^* = \frac{L^2\dot{Q}_N/(HWL)}{k(T_w - T_i)} \tag{3.13}$$

which is dimensionless heat transfer density.

From this analysis we may conclude that both the optimum dimensionless thermal length and the optimum D/L ratio are independent of porosity ε while the maximum heat transfer rate density varies with ε at fixed Δp, and the minimum

pressure drop varies with ε^{-2} at fixed $\dot{Q}_N$. Furthermore, one can verify that the maximum heat transfer rate scales with the group $(\mathrm{Pr}\Delta p^*)^{1/2}$ while the optimum diameter scales with $(\mathrm{Pr}\Delta p^*)^{-1/4}$.

If the mean velocity U_0 is related to the total pumping power in the form

$$\dot{P}_N = \frac{1}{\rho} N \dot{m} \Delta p \tag{3.14}$$

then, by using Eqs. (3.1), (3.2), (3.6), and (3.7), the heat transfer rate reads:

$$\dot{Q}_N = \underbrace{(\varepsilon HW)^{2/3}}_{\text{Geometry}} \underbrace{(\rho^{2/3}\mathrm{Pr}^{2/3}k/\mu)}_{\text{Fluid properties}} \underbrace{(2x_* f_{app}\mathrm{Re})^{-1/3}}_{\text{Fluid flow}} \underbrace{(1-\theta)}_{\text{Heat transfer}} \dot{P}_N^{1/3}(T_w - T_i) \tag{3.15}$$

Again, the dimensionless thermal length is the unique optimization variable. Similarly to the case before, by rewriting the last equation in the form:

$$\frac{\dot{Q}_N}{\dot{P}_N^{1/3}(T_w - T_i)} = g(x_*) \tag{3.16}$$

where $g(x_*) > 0$ stands for the four groups of factors identified in the right-hand side of Eq. (3.15), we can easily verify that the optimum value of x_* that emerges from $\partial g(x_*)/\partial x_* = 0$ may be found either when maximizing $\dot{Q}_N$ at constant $\dot{P}_N$ and $T_w - T_i$, or either when minimizing $\dot{P}_N$ (at constant $\dot{Q}_N$ and $T_w - T_i$) or $T_w - T_i$ (at constant $\dot{Q}_N$ and $\dot{P}_N$). Here, the existing extreme comes from the group $(1-\theta)x_*^{-1/3}$.

The relation between D/L, x_* and $\dot{P}_N$ is obtained from Eqs. (3.1), (3.2), (3.5), (3.7), and (3.14) with $U_0 = \nu\mathrm{Re}/D$:

$$D/L = \left(\frac{(2f_{app}\mathrm{Re})^{1/2}}{x_*\mathrm{Pr}} \right)^{1/3} (P_N^*/\varepsilon)^{-1/6} \tag{3.17}$$

where $P_N^* = \rho^2 L^4 \dot{P}_N/(\mu^3 HWL)$ is dimensionless pumping power. Again, once the optimum x_* is known the optimum ratio of diameter to tube length can be determined through Eq. (3.17) by using either the fixed value or the minimum value of pumping power.

In the case of heat transfer rate maximization the value of $(\dot{Q}_N)_{\max}$ is determined by making $x_* = (x_*)_{\mathrm{opt}}$ in Eq. (3.15), which can be rewritten in the following dimensionless form

$$Q_N^*/\varepsilon = (2x_* f_{app}\mathrm{Re})^{-1/3} (1-\theta)\, \mathrm{Pr}^{2/3} (P_N^*/\varepsilon)^{1/3} \tag{3.18}$$

Note that the groups Q_N^*/ε and P_N^*/ε represent the dimensionless heat transfer rate and total pumping power per unit of volume that is effectively occupied by the fluid, respectively.

In this case we may conclude that the optimum dimensionless thermal length is independent of ε while the optimum D/L ratio varies with $\varepsilon^{1/6}$, the maximum heat

transfer rate density varies with $\varepsilon^{2/3}$ at fixed $\dot{P}_N$, and the minimum pumping power varies with ε^{-2} at fixed $\dot{Q}_N$. One can also verify that the maximum Q_N^*/ε scales with the group $\mathrm{Pr}^{2/3}(P_N^*/\varepsilon)^{1/3}$ while the optimum diameter scales with $\mathrm{Pr}^{-1/3}(P_N^*/\varepsilon)^{-1/6}$.

3.3 Numerical heat sink modelling

The physical domain of one single tube of the heat sink together with the computational domain and the boundary conditions are shown in Fig. 3.1. The dimensionless governing equations for steady flow in cylindrical coordinates read:
Continuity

$$\frac{\partial \tilde{u}}{\partial \tilde{x}} + \frac{\tilde{v}}{\tilde{r}} + \frac{\partial \tilde{v}}{\partial \tilde{r}} = 0 \tag{3.19}$$

x–momentum

$$\tilde{u}\frac{\partial \tilde{u}}{\partial \tilde{x}} + \tilde{v}\frac{\partial \tilde{u}}{\partial \tilde{r}} = -\frac{\partial \tilde{p}}{\partial \tilde{x}} + \frac{1}{\mathrm{Re}}\left(\frac{\partial^2 \tilde{u}}{\partial \tilde{x}^2} + \frac{1}{\tilde{r}}\frac{\partial \tilde{u}}{\partial \tilde{r}} + \frac{\partial^2 \tilde{u}}{\partial \tilde{r}^2}\right) \tag{3.20}$$

r–momentum

$$\tilde{u}\frac{\partial \tilde{v}}{\partial \tilde{x}} + \tilde{v}\frac{\partial \tilde{v}}{\partial \tilde{r}} = -\frac{\partial \tilde{p}}{\partial \tilde{r}} + \frac{1}{\mathrm{Re}}\left(\frac{\partial^2 \tilde{v}}{\partial \tilde{x}^2} - \frac{\tilde{v}}{\tilde{r}^2} + \frac{1}{\tilde{r}}\frac{\partial \tilde{v}}{\partial \tilde{r}} + \frac{\partial^2 \tilde{v}}{\partial \tilde{r}^2}\right) \tag{3.21}$$

Energy

$$\tilde{u}\frac{\partial \tilde{T}}{\partial \tilde{x}} + \tilde{v}\frac{\partial \tilde{T}}{\partial \tilde{r}} = \frac{1}{\mathrm{RePr}}\left(\frac{\partial^2 \tilde{T}}{\partial \tilde{x}^2} + \frac{1}{\tilde{r}}\frac{\partial \tilde{T}}{\partial \tilde{r}} + \frac{\partial^2 \tilde{T}}{\partial \tilde{r}^2}\right) \tag{3.22}$$

The axial and radial velocity components are $\tilde{u}$ and $\tilde{v}$, respectively. These equations are obtained by defining the following variables transformations

$$(\tilde{u}, \tilde{v}) = (u, v)/U_0 \tag{3.23}$$

$$\left(\tilde{x}, \tilde{r}, \tilde{L}\right) = (x, r, L)/D \tag{3.24}$$

$$\tilde{p} = p/\left(\rho U_0^2\right) \tag{3.25}$$

$$\tilde{T} = \frac{T - T_i}{T_w - T_i} \tag{3.26}$$

No-slip condition at the wall and zero gradients at the outlet boundary are assumed. The heat transfer rate is calculated from the local heat flux at the wall $q'' = k(\partial T/\partial r)_{r=D/2}$.

The governing equations were solved with the help of the finite volume method by using a free source code for convection–diffusion problems [26]. The diffusion terms were discretised by means of a central differencing scheme, and convergence was considered to be achieved when the normalized residuals of the mass and momentum equations became smaller than 10^{-6}, and the residual of the energy equation smaller than 10^{-8}. A grid independence test was carried out for the following conditions:

$D = 0.004\,\mathrm{m}$, $L = 0.10\,\mathrm{m}$, $U_0 = 0.1\,\mathrm{m/s}$ and $\mathrm{Pr} = 5.0$. The numerical values generated in this simulation test were validated by comparison with the results presented in referenced literature [27], and it was found that mesh size of 100×50 assures a grid independent solution.

From the analysis presented in the previous section we concluded that the same value of optimum x_* is obtained either when maximizing heat transfer density or when minimizing either pressure drop or pumping power at fixed heat transfer density. Furthermore, the optimum x_* is independent of the volume fraction of tubes. Thus, the numerical simulations were carried out considering the following fixed values: $Q_N^* = 1 \times 10^3$, $\varepsilon = 0.6$ and $V = 1 \times 10^{-4}\,\mathrm{m}^3$.

In the case of simultaneously developing flow the numerical procedure can be briefly described as comprising the following steps: (1) obtain the fluid flow and temperature fields in a long tube ($D/L \leqslant 0.01$) for a given Reynolds number; (2) assume an initial number of tubes; (3) find the D/L ratio to obtain the required heat transfer density; (4) update the number of tubes and the D/L ratio according to the fixed volume constraint; (5) calculate the dimensionless thermal length, the pressure drop and the pumping power. The procedure above is repeated for various Reynolds numbers within the laminar fluid flow range and such that the dimensionless thermal length falls in the range $10^{-4} < x_* < 0.5$. The minimum pressure drop and the minimum pumping power are obtained with the help of an external numerical minimization procedure.

In the particular case of hydrodynamically fully developed flow the radial velocity component is zero and the axial component is $\tilde{u} = 2(1 - 4\tilde{r}^2)$. Then, by neglecting the effect of axial conduction ($\mathrm{RePr} \gg 1$), the energy conservation equation reduces to the classical Graetz problem formulation [28]. In this case the heat transfer rate is well modelled by using an appropriate estimate for the mean Nusselt number in Eqs. (3.12) and (3.18) along with $f\mathrm{Re} = 16$. We modelled the Nusselt number of thermally developing flow as:

$$\mathrm{Nu}_{dv} = 1.522 x_*^{-1/3} \tag{3.27}$$

This equation is deduced during the scale analysis presented in the next section and is very similar to the Lévêque solution ($\mathrm{Nu}_{dv} = 1.615 x_*^{-1/3}$) [29]. Then, the asymptotic correlation method outlined by Churchill and Usagi [30] was used to model the Nusselt number in the entire range of x_* in the form:

$$\mathrm{Nu}_{0-L} = \left(\mathrm{Nu}_{dv}^4 + \mathrm{Nu}_{fd}^4\right)^{1/4} \tag{3.28}$$

with $\mathrm{Nu}_{fd} = 3.66$. The values generated by Eq. (3.28) were compared with data from Shah and London [31] and maximum differences were found within -0.96% to 0.62% for $x_* \geqslant 1 \times 10^{-3}$. These differences fall in the range -3.04% to 0.62% for $x_* \geqslant 1 \times 10^{-4}$.

3.4 Scale analysis and intersection-of-asymptotes method

In the first part of this section, we present scale analysis and the method of intersection of asymptotes for predicting the optimal heat sink design that maximizes the heat transfer density with fixed pressure drop and fixed pumping power. In the second part, we present scale analysis of fluid flow optimization (minimization of pressure drop and pumping power) with fixed heat transfer density.

3.4.1 Scale analysis of heat transfer rate maximization

Bejan and Sciubba [2] and more recently Muzychka [11] used the method of the intersection of asymptotes for optimizing a parallel channels heat sink subjected to finite volume and fixed pressure drop constraints. In those works the optimal internal structure was predicted for maximum heat transfer rate, with the optimization variable D either representing the plate-to-plate spacing or the inner circular tube diameter or else other reference length scale of the duct shape. In that case, the mean velocity of the fluid (or equivalently the Reynolds number) and the dimensionless thermal length x_* implicitly vary according to the flow constraint. The method is based on the intersection of two distinct trends: (i) the fully developed flow asymptote ($D \to 0$ limit), in which the mean outlet temperature of the fluid approaches the temperature of the wall and the heat transfer rate varies as $\sim D^2$; and (ii) the developing flow asymptote ($D \to \infty$ limit), in which the mean temperature of the fluid in the flow core approaches the inlet temperature, and the total heat transfer rate varies as $\sim D^{-2/3}$.

In this section, the method of the intersection of asymptotes is employed using x_* as the optimization variable and for the cases when either pressure drop or pumping power are fixed. Firstly, the method is applied for the case of thermally developing flow and then the results are generalized for simultaneously developing flow, and formulae for predicting the optimum diameter of the tubes are presented.

Fixed pressure drop

In the fully developed flow limit the total heat transfer rate is given by the global energy balance in the array:

$$\dot{Q}_{fd} = N\dot{m}c_p\,(T_w - T_i) \tag{3.29}$$

The mass flow rate $\dot{m}$ or, alternatively, the mean velocity of the fluid in the tubes U_0 is related to pressure drop Δp through Eq. (3.7), where the friction factor-Reynolds number group in the case of circular tubes and fully hydrodynamically developed flow is $f\mathrm{Re}=16$. Then, by setting $x_*=x_+/\mathrm{Pr}$ as the optimization variable, the mean

velocity reads:

$$U_0 = \left(\frac{\Delta p}{2f\mathrm{Re}\rho\mathrm{Pr}x_*} \right)^{1/2} \tag{3.30}$$

By combining Eqs. (3.1), (3.2), (3.29), and (3.30), and with Prandtl number given by $\mathrm{Pr} = \mu c_p/k$, the total rate of heat transfer reads:

$$\dot{Q}_{fd} = \varepsilon HW \left(\frac{\rho\mathrm{Pr}\Delta p}{2f\mathrm{Re}\mu^2 x_*} \right)^{1/2} k\,(T_w - T_i) \tag{3.31}$$

This expression can be rewritten in dimensionless form as (see Eq. (3.13)):

$$Q^*_{fd} = \varepsilon \left(\frac{\mathrm{Pr}\Delta p^*}{2f\mathrm{Re}} \right)^{1/2} x_*^{-1/2} \tag{3.32}$$

Thus, in the limit $x_* \to \infty$ the heat transfer density varies as $x_*^{-1/2}$. The group $Be = \mathrm{Pr}\Delta p^*$ that appears in the last equation is also referred as the Bejan number [32].

In the thermally developing flow limit the total heat transfer rate that is removed from the entire array of tubes with transfer area $A_N = N\pi DL$ is given by

$$\dot{Q}_{dv} = A_N h_{0-L}\,(T_w - T_i) \tag{3.33}$$

The average heat transfer coefficient h_{0-L} may be approximated by the expression for laminar boundary layer flow over a flat plate [11, 28]:

$$\frac{Lh_{0-L}}{k} = 0.664\mathrm{Re}_L^{1/2}\mathrm{Pr}^{1/3} \tag{3.34}$$

for $\mathrm{Pr} \geqslant 0.5$. The Reynolds number based on the length Re_L is obtained from balancing the forces on the array:

$$\tau_w N\pi DL = N\frac{\pi D^2}{4}\Delta p \tag{3.35}$$

in which the mean wall shear stress τ_w is given by the velocity boundary layer solution [28]

$$\frac{\tau_w}{1/2\rho U_\infty^2} = 1.328\mathrm{Re}_L^{-1/2} \tag{3.36}$$

and U_∞ is the free stream (core flow) velocity. Combining Eqs. (3.35) and (3.36) with $U_\infty = \nu\mathrm{Re}_L/L$ yields:

$$\mathrm{Re}_L^{1/2} = 0.722\Delta p^{*1/3}\,(D/L)^{1/3} \tag{3.37}$$

The use of the square root of Re_L instead of the free stream velocity U_∞ is advantageous because $\mathrm{Re}_L^{1/2}$ accounts for the boundary layer slenderness ratio as noted by Bejan [28].

Finally, by combining Eqs. (3.11), (3.33), (3.34), and (3.37) we obtain the dimensionless heat transfer density in the form:

$$Q_{dv}^{*} = 1.918\varepsilon \frac{(\mathrm{Pr}\Delta p^{*})^{1/2}}{(2f\mathrm{Re})^{1/6}} x_{*}^{1/6} \tag{3.38}$$

Eq. (3.38) shows that in the limit $x \to 0$ the global heat transfer density varies as $\sim x_{*}^{1/6}$.

It is worth noting that by combining Eqs. (3.34) and (3.37) and eliminating the pressure drop through Eq. (3.11) we obtain the mean Nusselt number based on D in the form:

$$\frac{Dh_{0-L}}{k} = 0.604\,(f\mathrm{Re})^{1/3}\, x_{*}^{-1/3} \tag{3.39}$$

which in the case of circular tubes ($f\mathrm{Re}=16$) reduces to

$$\frac{Dh_{0-L}}{k} = 1.522 x_{*}^{-1/3} \tag{3.40}$$

This expression was already presented in the previous section (see Eq. (3.27)) (the difference to data [31] is smaller than 3.04% in the range $1\times10^{-4} \leqslant x_{*} \leqslant 1\times 10^{-2}$). Eq. (3.39) still holds for other duct geometries provided that the correspondent hydraulic diameter and friction factor-Reynolds number group are used, and good agreement can also be found for square and parallel plate channels. This confirms the correctness of the approximations assumed in the formulation of the developing flow asymptote and corresponds to $(\tau_w)_{plate} = (\tau_w)_{tube}$, i.e., the average heat transfer coefficient of a thermally developing flow in a circular tube is quite well described by the boundary layer solution of Eq. (3.34) when using values of $\mathrm{Re}_L^{1/2}$ such that the mean gradient of the fluid velocity near a flat plate surface $\overline{(\partial u/\partial y)}_{y=0}$ (that is the fluid that effectively participates in the heat transfer) is equal to the gradient of the fluid velocity at the wall of the tube.

The asymptotes described by Eqs. (3.32) and (3.38) as well as the actual dimensionless heat transfer density from Eq. (3.12) are depicted in Fig. 3.2. The optimum x_{*} that emerges from the intersection of these asymptotes is given by

$$(x_{*})_{\mathrm{opt}} = \frac{1}{1.918^{3/2}\,(2f\mathrm{Re})^{1/2}} \tag{3.41}$$

while the optimum ratio of diameter to tube length can be predicted through Eq. (3.11) by making $x_{*} = (x_{*})_{\mathrm{opt}}$:

$$(D_h/L)_{\mathrm{opt}} \approx 1.277\,(2f\mathrm{Re}_{D_h})^{3/8}\,(\mathrm{Pr}\Delta p^{*})^{-1/4} \tag{3.42}$$

This equation is intentionally presented in its generalized form based on hydraulic diameter with the purpose of highlighting two aspects: (i) the present result still holds for other duct geometries, in particular, we note that the application of

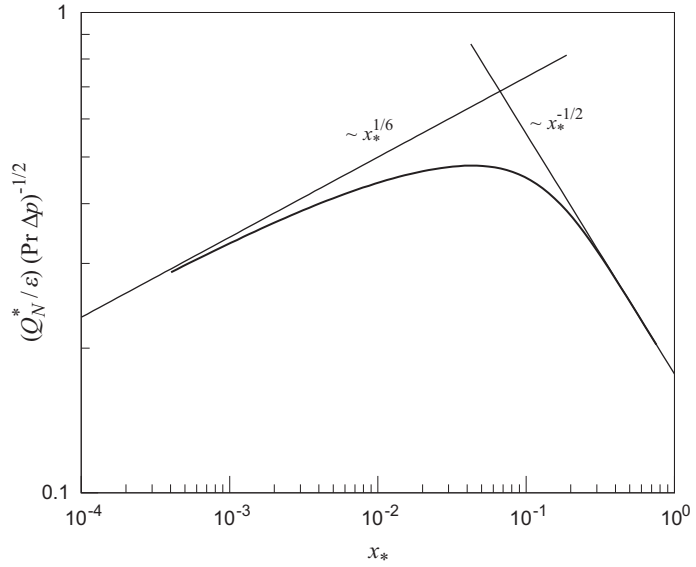

Fig. 3.2: Heat transfer asymptotes as function of dimensionless thermal length at fixed pressure drop.

Eq. (3.42) to parallel plates heat sink ($D_h = 2D$, $f\mathrm{Re}_{D_h} = 24$) leads to $D_{\mathrm{opt}}/L \cong 2.73Be^{-1/4}$ with $Be = \mathrm{Pr}\Delta p^*$, which matches exactly the optimum plate-to-plate spacing (D_{opt}) found by Bejan [2] for that geometry; and (ii) Eq. (3.42) is a straightforward form alternative to the result obtained by Muzychka [11] that used the geometric length scale D_h as optimization variable in the case of simultaneously developing flow. In the case of the present work, for circular tubes we have $(x_*)_{\mathrm{opt}} \approx 0.067$ and

$$D_{\mathrm{opt}}/L \approx 4.684\,(\mathrm{Pr}\Delta p^*)^{-1/4} \tag{3.43}$$

As conclusion, we can extend the use of Eqs. (3.42) and (3.43) to simultaneously developing flow and, by comparison with Eq. (3.11), to find out $(x_*)_{\mathrm{opt}}$ from

$$\left(\frac{2f_{app}\mathrm{Re}}{(x_*)_{\mathrm{opt}}}\right)^{1/4} = 4.684 \tag{3.44}$$

The solution of this equation depends on Prandtl number due to the relation between dimensionless hydrodynamic and thermal lengths $x_+ = x_*\mathrm{Pr}$. A polynomial equation on $(x_*)_{\mathrm{opt}}$ is obtained by substituting Eq. (3.8) in Eq. (3.44), and the optimum x_* decreases and approaches 0.067 for $\mathrm{Pr} \gg 1$. The feasible solution of this polynomial equation is presented and discussed in Section 3.5 for various values of Pr.

From Eq. (3.32) (or Eq. (3.38)) one finds that the maximum heat transfer density corresponding to $x_* = (x_*)_{\mathrm{opt}}$ is given by:

$$(Q_N^*/\varepsilon)_{\max} < 1.630\,(2f\mathrm{Re})^{-1/4}\,(\mathrm{Pr}\Delta p^*)^{1/2} \tag{3.45}$$

The maximum heat transfer density is directly proportional to ε and to the square root of Prandtl number. In the case of a parallel tubes heat sink in a maximum square packing arrangement ($\varepsilon \approx 0.785$) one has $Q^*_{N,\max} < 0.538\,(\mathrm{Pr}\Delta p^*)^{1/2}$.

Fixed pumping power

The heat transfer asymptotes at fixed pumping power can be derived in a way similar to that of fixed pressure drop. Again, we start by considering a thermally developing flow. By using Eqs. (3.7) and (3.14) together with Eqs. (3.1) and (3.2) the mean velocity reads:

$$U_0 = \left(\frac{\dot{P}_N}{\varepsilon H W 2 f \mathrm{Re} \rho \mathrm{Pr} x_*} \right)^{1/3} \tag{3.46}$$

while pressure drop relates to pumping power as:

$$\Delta p^* = (2 f \mathrm{Re} x_* \mathrm{Pr})^{1/3} \left(\frac{P^*_N}{\varepsilon} \right)^{2/3} \tag{3.47}$$

Then, by using Eqs. (3.32) and (3.47) the fully developed flow asymptote reads:

$$Q^*_{fd} = \frac{\varepsilon^{2/3}}{(2 f \mathrm{Re})^{1/3}} \mathrm{Pr}^{2/3} P^{*1/3}_N x_*^{-1/3} \tag{3.48}$$

Thus, in the limit $x_* \to \infty$ the heat transfer density varies with $x_*^{-1/3}$. In the same way the developing flow asymptote of Eq. (38) turns into:

$$Q^*_{dv} = 1.918 \varepsilon^{2/3} \mathrm{Pr}^{2/3} P^{*1/3}_N x_*^{1/3} \tag{3.49}$$

In the limit $x_* \to 0$ the heat transfer density varies with $x_*^{1/3}$. It must be also noted that this asymptote is independent of the duct shape.

Both the asymptotes and the actual dimensionless heat transfer density calculated from Eq. (3.18) are shown in Fig. 3.3. Due to proportionality between pressure drop and pumping power shown by Eq. (3.47), it is expected that the intersection of the asymptotes with fixed P^*_N will predict the same optimum x_* as with the asymptotes at fixed Δp^*. In fact, from the combination of Eqs. (3.48) and (3.49) we obtain again Eq. (3.41). This shows that in the case of thermally developing flow, the optimum x_* predicted by intersecting the asymptotes is independent of the constraint imposed to fluid flow.

The optimum ratio of diameter to tube length is predicted by making $x_* = (x_*)_{\mathrm{opt}}$ in Eq. (3.17):

$$(D_h/L)_{\mathrm{opt}} \approx 1.385\,(2 f \mathrm{Re}_{D_h})^{1/3}\,\mathrm{Pr}^{-1/3}\,(P^*_N/\varepsilon)^{-1/6} \tag{3.50}$$

Again we present a generalization based on the hydraulic diameter to show that this result still holds for other duct geometries. In particular, we note that the

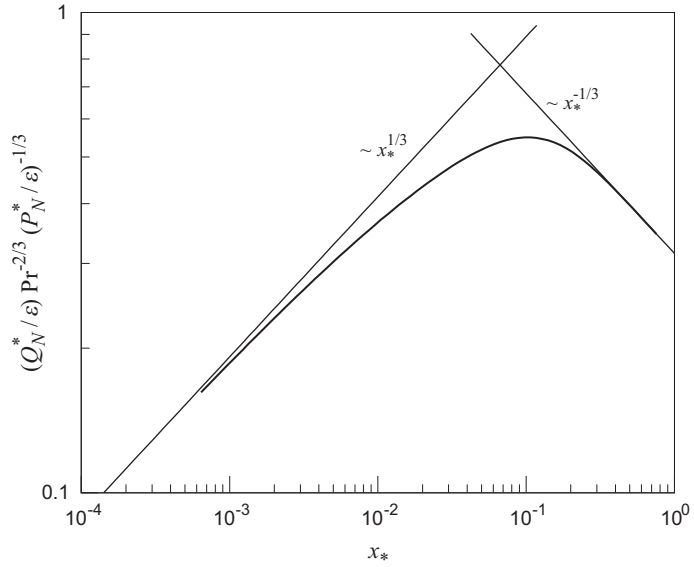

Fig. 3.3: Heat transfer asymptotes as function of dimensionless thermal length at fixed pumping power.

application of Eq. (3.50) to a parallel plates heat sink ($D_h = 2D$, $f\mathrm{Re}_{D_h} = 24$, $\varepsilon = 1$) yields $D_{\mathrm{opt}}/L \cong 2.52\,\mathrm{Pr}^{-1/3} P_N^{*-1/6}$, which is similar and matches the optimum plate-to-plate spacing (D_{opt}) found by Mereu et al. [12] very closely, in which the dimensionless pumping power raised to the power $-1/6$ is multiplied by the group $2.26\,\mathrm{Pr}^{-10/27}$. The result by Mereu was obtained by using the plate-to-plate spacing as the optimization (free) variable together with simultaneously developing flow, and assuming that the mean velocity of the fluid U_0 is equal to the free stream velocity U_∞ when deriving the developing flow asymptote.

The values of $(D_h/L)_{\mathrm{opt}}$ obtained from the present work are tabulated and summarized in Table 3.1 for some duct geometries. In the case of circular tubes we have $(x_*)_{\mathrm{opt}} \approx 0.067$ and

$$D_{\mathrm{opt}}/L \approx 4.397 \mathrm{Pr}^{-1/3}\,(P_N^*/\varepsilon)^{-1/6} \tag{3.51}$$

We can extend the use of Eqs. (3.50) and (3.51) to simultaneously developing flow and, by comparison with Eq. (3.17), determine $(x_*)_{\mathrm{opt}}$ for that case from:

$$\left(\frac{(2f_{app}\mathrm{Re})^{1/2}}{(x_*)_{\mathrm{opt}}}\right)^{1/3} = 4.397 \tag{3.52}$$

The optimum x_* decreases and approaches 0.067 for $\mathrm{Pr} \gg 1$, and the results for various values of Prandtl number are presented in Section 3.5.

The maximum heat transfer density is predicted through Eq. (3.48) (or Eq. (3.49)) and is given by:

$$(Q_N^*/\varepsilon)_{\max} < 1.385\,(2f\mathrm{Re}_{D_h})^{-1/6}\,\mathrm{Pr}^{2/3}\,(P_N^*/\varepsilon)^{1/3} \tag{3.53}$$

Table 3.1: Values of optimum hydraulic diameter $(D_h/L)_{\rm opt}{\rm Pr}^{1/3}(P_N^*/\varepsilon)^{1/6}$ and maximum heat transfer density $(Q_N^*/\varepsilon)_{\rm max}{\rm Pr}^{-2/3}(P_N^*/\varepsilon)^{-1/3}$ as predicted by the method of the intersection of asymptotes for different duct geometries at fixed pumping power.

Duct geometry	D_h	$f{\rm Re}_{D_h}$	Optimum D_h	Maximum Q_N^*
Parallel plates	$2D$	24	5.033	0.727
Circular tubes	D	16	4.397	0.777
Square	D	14.24	4.230	0.793
Equilateral triangle	$D/\sqrt{3}$	13.33	4.137	0.801

The maximum heat transfer density is proportional to $\varepsilon^{2/3}$ and varies with ${\rm Pr}^{2/3}$. The estimated values of maximum Q_N^* are presented in Table 3.1 for some duct geometries. In the case of a parallel tubes heat sink with $\varepsilon \approx 0.785$ we have $Q_{N,\max}^* < 0.661\,{\rm Pr}^{2/3}P_N^{*1/3}$.

3.4.2 Scale analysis of fluid flow optimization with fixed heat transfer density

In this section we present a scale analysis of fluid flow optimization with fixed heat transfer density through the method of the intersection of asymptotes, allowing predicting the optimum D/L ratio for minimum pressure drop and minimum pumping power. This method is also used for fixed heat transfer density without imposing any fluid flow condition.

Scale analysis of fluid flow optimization

The model and analysis developed in Sections 3.2 and 3.3 are now used for studying the optimal fluid flow conditions at a given (fixed) heat transfer density. Fig. 3.4 shows total mass flow rate $\dot{m}_N$ and fluid flow resistance R_N as function of x_*. Both variables are presented in its dimensionless form through $m_N^* = L^2 m_N'''/\mu$ with $m_N''' = N\dot{m}/(HWL)$ and $R_N^* = R_N(HWL)/\nu$ with $R_N = \Delta p/(N\dot{m})$, respectively. Increasing x_* imply decreasing mass flow rate together with increasing fluid flow resistance.

Fig. 3.5 presents the parametric plot of dimensionless pressure drop and dimensionless pumping power with x_* shown along the curve. The two minima evidenced in this curve are $\Delta p_{\rm min}^*{\rm Pr}(Q_N^*/\varepsilon)^{-2} = 4.343$ and $(P_N^*/\varepsilon)_{\rm min}{\rm Pr}^2(Q_N^*/\varepsilon)^{-3} = 6.033$ which correspond to $x_* \sim 0.043$ and $x_* \sim 0.102$, respectively. In view of the analysis of Section 3.2, and for thermally developing flow, these values of x_* do not depend on Pr, and thus are constant.

Also noticed in the Section 2 was the fact that maximization of Q_N^* with x_* as the free variable is equivalent to minimization of either Δp^* or P_N^*. Thus, the asymptotes derived in the previous section can be rearranged so as to predict the

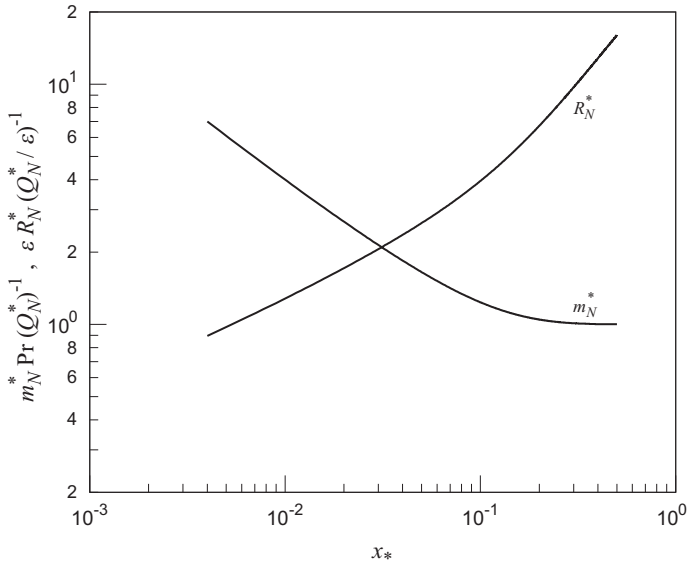

Fig. 3.4: Dimensionless mass flow rate (m_N^*) and fluid flow resistance (R_N^*) at fixed heat transfer density.

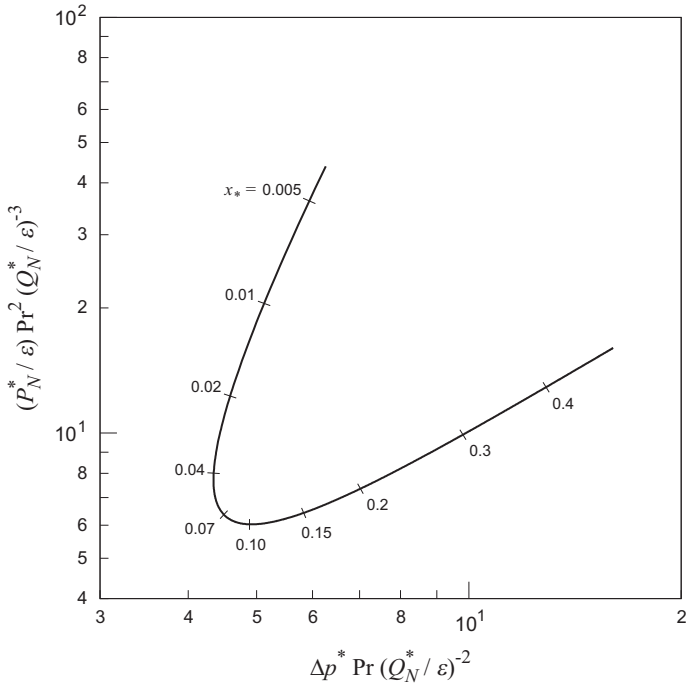

Fig. 3.5: Parametric plot of pressure drop and pumping power at fixed heat transfer density.

optimal heat sink designs corresponding either to minimum Δp^*, or to minimum P_N^*. In both cases the optimum dimensionless thermal length is the same, and is given by Eq. (3.41). On the other hand, from Eq. (3.45) we have

$$\Delta p^*_{\min} > 0.376\,(2f\mathrm{Re}_{D_h})^{1/2}\,\mathrm{Pr}^{-1}\,(Q_N^*/\varepsilon)^2 \tag{3.54}$$

where the sign $>$ means that the actual minimum pressure drop is higher than the predicted value.

Similarly, from Eq. (3.53) we have

$$(P_N^*/\varepsilon)_{\min} > 0.376\,(2f\mathrm{Re}_{D_h})^{1/2}\,\mathrm{Pr}^{-2}\,(Q_N^*/\varepsilon)^3 \tag{3.55}$$

Again, the sign $>$ reminds that the actual pumping power is higher than the predicted value. We note that the factor $0.376(2f\mathrm{Re}_{D_h})^{1/2}$ is present in both the Eqs. (3.54) and (3.55). More remarkable is the result that the estimate of the optimum diameter is exactly the same either for $(\Delta p^*)_{\min}$ (Eqs. (3.11), (3.41), and (3.54)) or $(P_N^*)_{\min}$ (Eqs. (3.17), (3.41), and (3.55)) and is given by:

$$(D_h/L)_{\mathrm{opt}} \approx 1.630\,(2f\mathrm{Re}_{D_h})^{1/4}\,(Q_N^*/\varepsilon)^{-1/2} \tag{3.56}$$

It is also interesting to note that the estimated $(D/L)_{\mathrm{opt}}$ ratio does not depend on Prandtl number, thus suggesting that firstly one may design geometrically the heat sink for the required heat transfer density, and then operate it in the optimal flow conditions according to the fluid in use.

In the next section we proceed with a further examination of the implications of these results.

Intersection of asymptotes and fluid flow optimization

The results presented above justify a more close analysis of the relation between optimal design predicted by the method of the intersection of asymptotes and by fluid flow optimization. By inspection of Fig. 3.5 we note that the predicted optimum value $(x_*)_{\mathrm{opt}} \approx 0.067$ is located in between the values of x_* corresponding to the minima of Δp^* and P_N^*. Furthermore, it seems to be very close to the joint minimization of both these quantities.

We explore this aspect by rewriting the asymptotes for a fixed heat transfer density without any fluid flow constraint and using two design variables: the D/L ratio that is related uniquely to the internal geometry; and the Reynolds number that is related to the fluid flow characteristics. In the following, for the sake of exemplification, thermally developing flow is considered with the values $Q_N^* = 5{\times}10^3$, $\varepsilon = 0.6$ and $\mathrm{Pr} = 5.0$.

The fully developed flow asymptote (small D and small Re) is derived as before by considering the outlet temperature approaching the wall temperature. Thus, by

combining Eqs. (3.1), (3.2), and (3.29), with $U_0 = \nu \mathrm{Re}/D$ and Prandtl number $\mathrm{Pr} = \mu c_p/k$, we obtain the dimensionless heat transfer density in the form:

$$Q_{fd}^* = \varepsilon \mathrm{RePr}\,(L/D) \tag{3.57}$$

We conclude that in this limit the D/L ratio varies with Re at fixed Q_N^*.

The developing flow asymptote (large D and large Re) is derived using the boundary layer solution and assuming that the temperature of the fluid in the core flow approaches the inlet temperature. By combining Eqs. (3.33) and (3.39) with $x_* = (L/D)/(\mathrm{RePr})$, the dimensionless heat transfer density reads:

$$Q_{dv}^* = 4 \cdot 0.604\,(f\mathrm{Re})^{1/3}\,\varepsilon\,(\mathrm{RePr})^{1/3}\,(L/D)^{5/3} \tag{3.58}$$

Then, in this limit, for a fixed value of Q_N^* the D/L ratio varies with $\mathrm{Re}^{1/5}$.

The asymptotes of Eqs. (3.57) and (3.58) intersect each other at the dimensionless thermal length defined by Eq. (3.41) and at the D/L ratio given by Eq. (3.56), as expected, and as shown in Fig. 3.6 for the case of circular tubes analysed in the present work. In this case, however, it is particularly useful to find out the optimum D/L ratio along the Q_N^* curve (i.e., the point of intersection of the dashed line with the solid curve in Fig. 3.6). Thus, by using Eq. (3.6) with $U_0 = \nu \mathrm{Re}/D_h$ we obtain:

$$(D_h/L)_{\mathrm{opt}} = \left(\frac{1-\theta_{\mathrm{opt}}}{(x_*)_{\mathrm{opt}}}\right)^{1/2} (Q_N^*/\varepsilon)^{-1/2} \tag{3.59}$$

For thermally developing flow we have $(x_*)_{\mathrm{opt}} \approx 0.067$, $\mathrm{Nu}_{0-L} = 4.41$ and $\theta_{\mathrm{opt}} = 0.307$, and therefore the estimate of the optimum diameter given by Eq. (3.59) reduces to:

$$(D_h/L)_{\mathrm{opt}} = 3.221\,(Q_N^*/\varepsilon)^{-1/2} \tag{3.60}$$

Again we verify that this estimate does not depend on Pr.

Assuming that the numerical factor in the equation above is constant, in the same way as in the previous cases, to find out the optimum x_* as function of Pr for a simultaneously developing flow we can use the following expression:

$$\left(\frac{1-\theta_{\mathrm{opt}}}{(x_*)_{\mathrm{opt}}}\right)^{1/2} = 3.221 \tag{3.61}$$

The mean Nusselt number can be determined from correlations available in literature (e.g. [33]):

$$\mathrm{Nu}_{0-L} = \mathrm{Nu}_{fd}\left[1 + 0.067\,(x_*\mathrm{Pr})^{-0.62}\right]^{0.27} \tag{3.62a}$$

$$\mathrm{Nu}_{fd} = \begin{cases} -0.5632 + 1.57x_*^{-0.3351}, & 10^{-6} \leqslant x_* \leqslant 10^{-3} \\ 0.9828 + 1.129x_*^{-0.3686}, & 10^{-3} \leqslant x_* \leqslant 10^{-2} \\ 3.6568 + 0.1272x_*^{-0.7373}\exp\left(-3.1563x_*\right), & x_* > 10^{-2} \end{cases} \tag{3.62b}$$

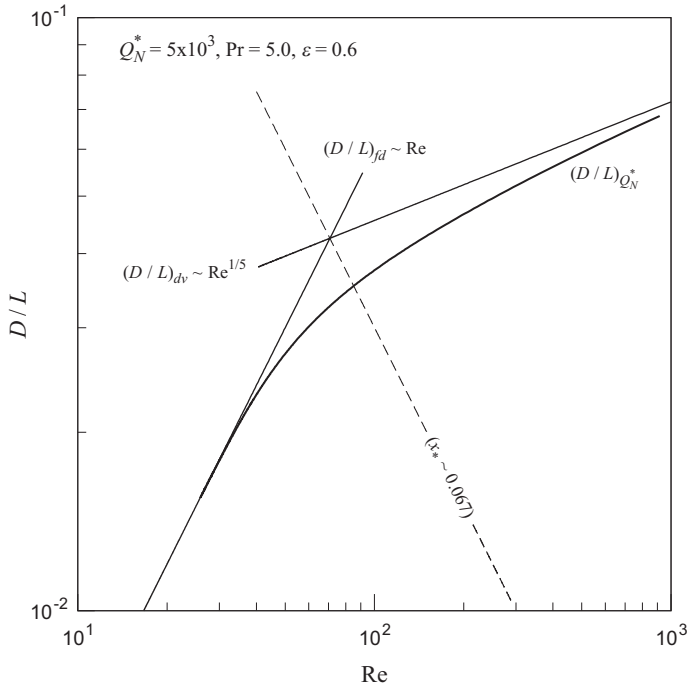

Fig. 3.6: Intersection of asymptotes at fixed heat transfer density and thermally developing flow.

Because the mean Nusselt number varies inversely with Pr in the developing region, the optimum x_* decreases and tends to 0.067. The solution of Eq. (3.61) is presented and discussed in the next section. The values of pressure drop and pumping power that corresponds to these values of $(x_*)_{\text{opt}}$ and $(D/L)_{\text{opt}}$ along the curve Q_N^* (fixed) are now easily calculated using Eqs. (3.11) and (3.17), respectively.

We proceed by considering the graphical representation of D/L .vs. Re as some kind of map where not only the heat transfer density can be represented, the same happening with the other variables involved, thus allowing to find out the order of magnitude of the optimum diameter and Reynolds number that match the minima of Δp^* and P_N^*. Then from Eq. (3.11) with $x_* = (L/D)/(\text{RePr})$ one has

$$(D/L)_{\Delta p} = \left(\frac{2f\text{Re}}{\Delta p^*}\right)^{1/3} \text{Re}^{1/3} \tag{3.63}$$

Similarly, from Eq. (3.17):

$$(D/L)_{P_N} = \left(\frac{2f\text{Re}}{P_N^*/\varepsilon}\right)^{1/4} \text{Re}^{1/2} \tag{3.64}$$

By considering $\Delta p^* = \Delta p^*_{\min}$ and $P_N^* = P^*_{N,\min}$ respectively in Eqs. (3.63) and (3.64), with $f\text{Re} = 16$, the tangents to the Q_N^* curve can be drawn as shown in Fig. 3.7. Note that the points of tangency correspond to $x_* = 0.043$ and $x_* = 0.102$, respectively.

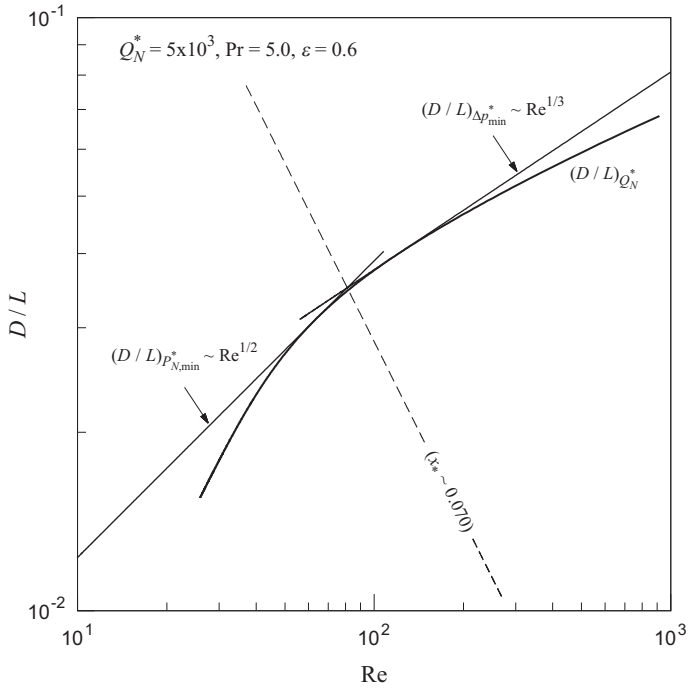

Fig. 3.7: Intersection of minimum Δp^* and minimum P_N^* limits at fixed heat transfer density and thermally developing flow.

The optimum values of D/L ratio and Reynolds number corresponding to the minima of Δp^* and P_N^* meet at the intersection of these lines, and the following function of $(x_*)_{\text{opt}}$ is obtained

$$2\,(x_*)_{\text{opt}}\, f\text{RePr} = \frac{(\Delta p^*)^3_{\text{min}}}{(P_N^*/\varepsilon)^2_{\text{min}}} \tag{3.65}$$

With the numerical values presented at the beginning of this section we have $x_* = 0.070$. This value is very close to that of the intersection of asymptotes. The solution of Eq. (3.65) for simultaneously developing flow is presented and discussed in the next section.

3.5 Heat sink optimization results

In this section we present and discuss the main results of the present work according to the optimization objectives and the imposed constraints. The results are summarized in various tables in such a way that useful information is easily extracted, together with the equations for predicting the optimal heat sink design deduced in the previous section. The numerical results were obtained using the model described in Section 3.3.

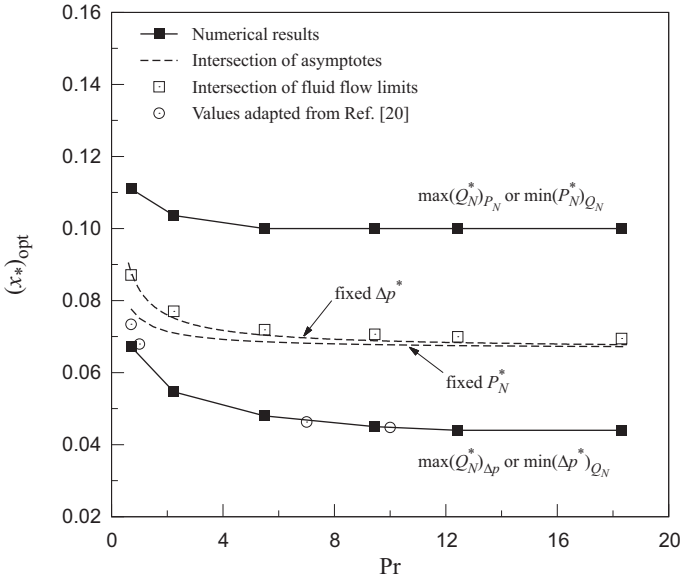

Fig. 3.8: Variation of $(x_*)_{opt}$ with the Prandtl number for minimum pressure drop, minimum pumping power, intersection of asymptotes and intersection of fluid flow limits.

3.5.1 Results of optimum dimensionless thermal length

When maximizing the heat transfer density and considering a thermally developing flow, the scale analysis carried out in the previous section shows that the optimum dimensionless thermal length $(x_*)_{\mathrm{opt}}$ predicted by the method of the intersection of asymptotes is independent of the imposed fluid flow constraint (e.g. fixed pressure drop or fixed pumping power). The value $(x_*)_{\mathrm{opt}} \approx 0.067$ was found to hold for circular tubes. In fact, it is possible to find out the fully developed and developing flow limits on which this method is based if diverse fluid flow conditions are imposed.

In the case of simultaneously developing flow the values of $(x_*)_{\mathrm{opt}}$ depend on the fluid flow constraint and Prandtl number due to the existence of a hydrodynamic boundary layer and to the relation between the hydrodynamic and thermal entrance lengths. These values of $(x_*)_{\mathrm{opt}}$ are shown in Fig. 3.8 (dashed lines) as function of Prandtl number for a fixed value of Δp^* (from the solution of Eq. (3.44)) and for a fixed value of P_N^* (from Eq. (3.52)). For small Pr, the optimum dimensionless thermal length in the case of fixed Δp^* is slightly higher than in the case of fixed P_N^*, and in both cases $(x_*)_{\mathrm{opt}}$ decreases with Pr, and tends to the value obtained for thermally developing flow. This is explained by the fact that the hydrodynamic entrance length is very small as compared with the thermal entrance length for higher Pr. The curve representing a fixed Q_N^* (from Eq. (3.61)) is not shown for concision, but some values are presented in Table 3.5. For increasing values of Pr we found a variation similar to that of the previous cases with values decreasing from $(x_*)_{\mathrm{opt}} \approx 0.0722$ for $\mathrm{Pr} = 0.7$ and tending to $(x_*)_{\mathrm{opt}} \approx 0.067$.

Also represented in the graph are the values of $(x_*)_{\text{opt}}$ obtained numerically through the model described in Section 3.3. The two series of values show the same dependency on Prandtl number as the estimated values, and tend to the values of x_* obtained for the case of thermally developing flow ($x_* \approx 0.043$ and $x_* \approx 0.102$, respectively). The values adapted from the work of Yilmaz et al. [20] for fixed Δp^* are presented for comparison. The results of Yilmaz's study were obtained using correlations for Nusselt number and are not expressed in terms of x_* thus requiring to be rewritten in terms of the solution of an equation similar to Eq. (3.44).

In average, the estimated values of $(x_*)_{\text{opt}}$ surpass by 32% the numerical values in the case of fixed Δp^*, while in the case of fixed P_N^* the numerical values are underestimated by 48% in average. The differences between the predicted and the numerical results slightly increase with Prandtl number. The intersection of the fluid flow limits are calculated from Eqs. (3.8) and (3.65) and by using the values of minimum pressure drop and minimum pumping power obtained numerically. We can see that these values are very close to the values that emerge from the intersection of asymptotes and tend to $x_* \approx 0.070$.

3.5.2 Results of optimum diameter for the maximization of Q_N^*

The numerical results of $(D/L)_{\text{opt}}$ for maximum Q_N^* are summarized in Table 3.2. These values are in average 11% higher than the estimate of Eq. (3.43) for the case of fixed Δp^*, and for the values of Pr shown, while in the case of fixed P_N^* are in average 12% lower than the estimate of Eq. (3.51). The results of maximum heat transfer density are summarized in Table 3.3, and show a mean difference of 13% as compared to the order-of-magnitude of Eq. (3.45) in the case of fixed Δp^* and of 17% compared with the estimate of Eq. (3.53) in the case of fixed P_N^*. These differences increase with Prandtl number in the case of $(D/L)_{\text{opt}}$ while they decrease in the case of $(Q_N^*/\varepsilon)_{\max}$.

3.5.3 Results of optimum diameter for the fluid flow optimization

In Table 3.4 the values of the optimum diameter are presented for minimum pressure drop and minimum pumping power at fixed heat transfer density. These values are in average only 8% lower than the estimate of Eq. (3.56) in the first case, and 26% in the second. If compared with the more reasonable estimate of Eq. (3.60) we found mean differences of order 11% in both cases.

A more noticeable result is presented in Table 3.5 that shows that the minimum pressure drop and the minimum pumping power are in average, respectively 4% and 9% lower than the values obtained using the optimum diameter estimate of Eq. (3.60) together with Eq. (3.11) and Eq. (3.17).

Table 3.2: Optimum diameter of the tubes for maximum heat transfer density at fixed pressure drop $(D/L)_{\text{opt}}(\text{Pr}\Delta p^*)^{1/4}$ and fixed pumping power $(D/L)_{\text{opt}}\text{Pr}^{1/3}(P_N^*/\varepsilon)^{1/6}$ for different values of Pr number.

Pr	Fixed Δp^*	Fixed P_N^*
0.70	5.088	3.854
2.23	5.121	3.852
5.49	5.185	3.865
9.45	5.231	3.854
12.43	5.246	3.850
18.30	5.229	3.847
∞	5.223	3.814

Table 3.3: Maximum heat transfer density at fixed pressure drop $(Q_N^*/\varepsilon)_{\max}(\text{Pr}\Delta p^*)^{-1/2}$ and fixed pumping power $(Q_N^*/\varepsilon)_{\max}\text{Pr}^{-2/3}(P_N^*/\varepsilon)^{-1/3}$ for different values of Pr number.

Pr	Fixed Δp^*	Fixed P_N^*
0.70	0.420	0.523
2.23	0.460	0.546
5.49	0.478	0.554
9.45	0.483	0.557
12.43	0.486	0.558
18.30	0.488	0.559
∞	0.480	0.549

Table 3.4: Optimum diameter of the tubes $(D/L)_{\text{opt}}(Q_N^*/\varepsilon)^{1/2}$ for minimum pressure drop and minimum pumping power at fixed heat transfer density.

	Numerical	
Pr	Minimum Δp^*	Minimum P_N^*
0.70	3.299	2.787
2.23	3.475	2.845
5.49	3.584	2.877
9.45	3.637	2.876
12.43	3.656	2.876
18.30	3.652	2.876
∞	3.619	2.826

Table 3.5: Numerical and predicted values of minimum $\Delta p^* \mathrm{Pr}(Q_N^*/\varepsilon)^{-2}$ and minimum $(P_N^*/\varepsilon)\mathrm{Pr}^2(Q_N^*/\varepsilon)^{-3}$ at fixed heat transfer density.

	Numerical		Intersection of asymptotes		
Pr	$(\Delta p^*)_{min}$	$(P_N^*)_{min}$	x_*	Δp^*	P_N^*
0.70	5.657	7.000	0.0722	5.698	7.606
2.23	4.718	6.152	0.0698	4.854	6.708
5.49	4.381	5.882	0.0685	4.602	6.479
9.45	4.281	5.795	0.0681	4.522	6.403
12.43	4.241	5.763	0.0678	4.505	6.406
18.30	4.203	5.730	0.0676	4.478	6.383
∞	4.343	6.033	0.0666	4.464	6.460

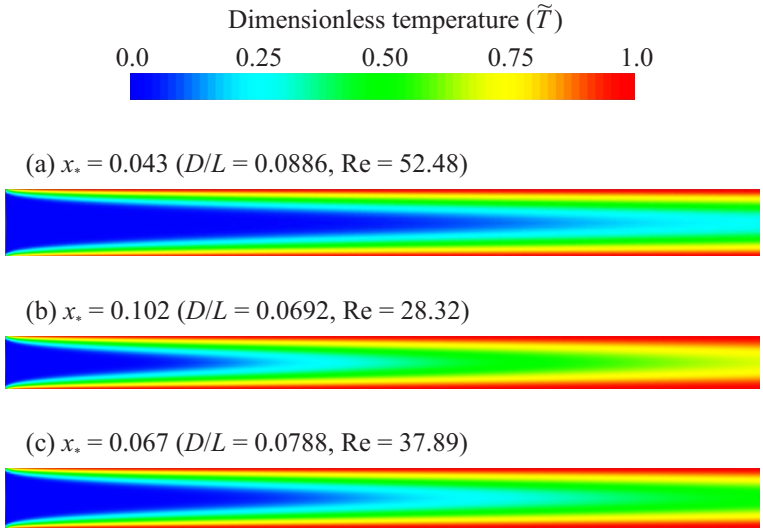

Fig. 3.9: Temperature field in an elemental tube for three distinct optimal designs: (a) minimum pressure drop; (b) minimum pumping power and (c) intersection of asymptotes ($Q_N^* = 1\times10^3$, $\mathrm{Pr} = 5.0$, $\varepsilon = 0.6$).

Fig. 3.9 shows an example of the temperature field of a thermally developing flow within a single tube for three different heat sink designs with $Q_N^* = 1\times10^3$, $\varepsilon = 0.6$ and $\mathrm{Pr} = 5.0$. The first temperature field corresponds to minimum pressure drop where the thermal boundary layer merge just at the tube outlet, while the second corresponds to minimum pumping power where the boundary layer merge approximately at the middle length of tube, and the third corresponds to the optimal design as defined from the intersection of asymptotes, the case in which the boundary layer merge closely before the tube outlet.

3.6 Conclusions

In the present work, we developed a set of theoretical results based on the method of intersection of asymptotes for predicting the optimal design of a heat sink composed of parallel tubes in a fixed volume and for various optimization objectives and imposed constraints. The estimated values were validated and complemented by numerical simulations. The optimization procedures lead to the following conclusions:

(a) *Maximization of heat transfer density with fixed pressure drop and fixed pumping power.*
The estimate of the optimum dimensionless thermal length obtained through the method of the intersection of asymptotes is nearly independent of the constraints imposed to fluid flow and tends to a fixed value with increasing Pr. For lower values of Pr the predicted values of $(x_*)_{\text{opt}}$ are slightly higher in the case of fixed pressure drop as compared to the values found for fixed pumping power. Estimates of optimum diameter of the tubes, and of the order of magnitude of maximum heat transfer density were obtained in both the case of fixed pressure drop and fixed pumping power. Results of the numerical procedure used for validation are also presented.

(b) *Minimization of pressure drop and pumping power with fixed heat transfer density.*
The estimates of the optimum diameter provided the same value when considering either pressure drop minimization or pumping power minimization. The order of magnitude of minimum pressure drop and minimum pumping power are presented together with numerical results for comparison and validation. Additionally, it was found that the estimate of the optimum diameter does not depend on Prandtl number.

(b) *Joint minimization of Δp^* and P_N^* with fixed heat transfer density.*
Scale analysis together with the method of the intersection of asymptotes was used in the case when heat transfer density is fixed. In this case two optimization variables are used: one of geometric nature that is represented by diameter to length ratio; and the other relative to fluid flow conditions, which is represented by the Reynolds number. The predicted $(x_*)_{\text{opt}}$ is very close to the values corresponding to the case of joint minimization of pressure drop and pumping power. A more reasonable estimate of the optimum diameter is also presented together with the corresponding values of pressure drop and pumping power, which are found to overestimate the respective minima by only 4% and 9% in average.

References

[1] A. Bejan, Convection Heat Transfer, Wiley, New York, 1984, Problem 11, p. 157; Solutions Manual pp. 93–95.

[2] A. Bejan, E. Sciubba, The optimal spacing of parallel plates cooled by forced convection, Int. J. Heat Mass Transfer 35 (1992) 3259–3264.

[3] A. Bejan, Shape and Structure, from Engineering to Nature, Cambridge University Press, Cambridge, UK, 2000.

[4] J. Lewins, Bejan's constructal theory of equal potential distribution, Int. J. Heat Mass Transfer 46 (2003) 1541–1543.

[5] A.H. Reis, Constructal Theory: From Engineering to Physics, and How Flow Systems Develop Shape and Structure, Appl. Mech. Rev. 59 (2006) 269–282.

[6] A.H. Reis, A.F. Miguel, A. Bejan, Constructal theory of particle agglomeration and design of air-cleaning devices, J. Phys. D: Appl. Phys. 39 (2006) 2311–2318.

[7] A. Bejan, I. Dincer, S. Lorente, A.F. Miguel, A.H. Reis, Porous and Complex Flow Structures in Modern Technologies, Springer, New York, 2004.

[8] A. Bejan, A.H. Reis, Thermodynamic optimization of global circulation and climate, Int. J. Energy Res. 29 (2005) 303–316.

[9] A.H. Reis, C. Gama, Sand size versus beachface slope An explanation based on the Constructal Law, Geomorphology 114 (2010) 276–283.

[10] A.H. Reis, A.F. Miguel, M. Aydin, Constructal theory of flow architecture of the lungs, Medical Physics 31 (2004) 1135–1140.

[11] Y. Muzychka, Constructal design of forced convection cooled microchannel heat sinks and heat exchangers, Int. J. Heat Mass Transfer 48 (2005) 3119–3127.

[12] S. Mereu, E. Sciubba, A. Bejan, The optimal cooling of a stack of heat generating boards with fixed pressure drop, flowrate or pumping power, Int. J. Heat Mass Transfer 36 (1993) 3677–3686.

[13] A.J. Fowler, G.A. Ledezma, A. Bejan, Optimal geometric arrangement of staggered plates in forced convection, Int. J. Heat Mass Transfer 40 (1997) 1795–1805.

[14] A. Bejan, Optimal spacings for cylinders in crossflow forced convection, J. Heat Transfer 117 (1995) 767–770.

[15] G. Stanescu, A.J. Fowler, A. Bejan, The optimal spacing of cylinders in free-stream crossflow forced convection, Int. J. Heat Mass Transfer 39 (1996) 311–317.

[16] T. Bello-Ochende, L. Liebenberg, J.P. Meyer, Constructal cooling channels for microchannel heat sinks, Int. J. Heat Mass Transfer 50 (2007) 4141–4150.

[17] T. Bello-Ochende, J.P. Meyer, A. Bejan, Constructal ducts with wrinkled entrances, Int. J. Heat Mass Transfer 52 (2009) 3628–3633.

[18] T. Wen, F. Xu, T.J. Lu, Structural optimization of two-dimensional cellular metals cooled by forced convection, Int. J. Heat Mass Transfer 50 (2007) 2590–2604.

[19] Y.S. Muzychka, Constructal multi-scale design of compact micro-tube heat sinks and heat exchangers, Int. J. Thermal Sciences 46 (2007) 245–252.

[20] A. Yilmaz, O. Buyukalaca, T. Yilmaz, Optimum shape and dimensions of ducts for convective heat transfer in laminar flow at constant wall temperature, Int. J. Heat Mass Transfer 43 (2000) 767–775.

[21] P. Canhoto, A.H. Reis, Optimization of forced convection heat sinks with pumping power requirements, Int. J. Heat Mass Transfer 54 (2011) 1441–1447.

[22] W.M. Kays, M.E. Crowford, Convective Heat and Mass Transfer, McGraw-Hill, New York, 1993, pp. 108–158.

[23] Y. Muzychka, Analytical and Experimental Study of Fluid Friction and Heat Transfer in Low Reynolds Number Flow Heat Exchangers, Ph.D. Thesis, Department of Mechanical Engineering, University of Waterloo, Ontario, Canada, 1999.

[24] Y.S. Muzychka, M.M. Yovanovich, Pressure drop in laminar developing flow in noncircular ducts: a scaling and modelling approach, J. Fluids Eng. 131 (2009) 111105 (11 p.).

[25] Y.S. Muzychka, M.M. Yovanovich, Laminar forced convection heat transfer in the combined entry region of non-circular ducts, J. Heat Transfer Trans. ASME 126 (2004) 54–61.

[26] www.openfoam.com

[27] M.A. Ebadian, Z.F. Dong, Forced Convection, Internal Flow in Ducts, *in* Handbook of Heat Transfer, Eds.: W.M. Rohsenow, J.P. Harnett, Y.I. Cho, McGraw-Hill, New York, Third Edition, 1998.

[28] A. Bejan, Convection Heat Transfer, Wiley, New York, 1995.

[29] R.B. Bird, W.E. Stewart, E.N. Lightfoot, Transport Phenomena, Wiley, New York, 1960.

[30] S.W. Churchill, R. Usagi, A general expression for the correlation of rates of transfer and other phenomena, American Institute of Chemical Engineers 18 (1972) 1121–1128.

[31] R.K. Shah, A.L. London, Advances in Heat Transfer, Supplement 1, Laminar Forced Flow Convection in Ducts, Academic Press, New York, 1978.

[32] S. Petrescu, Comments on the optimal spacing of parallel plates cooled by forced convection, Int. J. Heat Mass Transfer 37 (1994) 1283.

[33] B. Shome, Mixed convection laminar flow and heat transfer of liquids in isothermal horizontal circular tubes, Int. J. Heat Mass Transfer 38 (1995) 1945–1956.

Nomenclature

A	area (m^2)
c_p	specific heat ($\mathrm{J\,kg^{-1}\,K^{-1}}$)
D	diameter (m)
D_h	hydraulic diameter (m)
f	friction factor
H	height (m)
h_{0-L}	average heat transfer coefficient ($\mathrm{W\,m^{-2}\,K^{-1}}$)
L	length (m)
k	thermal conductivity ($\mathrm{W\,m^{-1}\,K^{-1}}$)
$\dot{m}$	mass flow rate ($\mathrm{kg\,s^{-1}}$)
N	number of tubes
Nu_{0-L}	mean Nusselt number, $\equiv h_{0-L}D/k$
p	pressure (Pa)
$\dot{P}_N$	total pumping power (W)
P_N^*	dimensionless pumping power, $\equiv \rho^2 L^4 \dot{P}_N/(\mu^3 HWL)$
Pr	Prandtl number, $\equiv c_p\,\mu/k$
q''	heat flux ($\mathrm{W\,m^{-2}}$)
$\dot{Q}_N$	total heat transfer rate (W)

Q_N^*	dimensionless heat transfer rate density, $\equiv L^2\dot{Q}_N/(kHWL(T_w - T_i))$
r	radial coordinate (m)
R	fluid flow resistance ($\mathrm{m}^{-1}\,\mathrm{s}^{-1}$)
Re	Reynolds number based on diameter, $\equiv U_0 D/\nu$
Re_L	Reynolds number based on length, $\equiv U_\infty L/\nu$
T	temperature (K)
U_0	mean velocity in tubes ($\mathrm{m\,s}^{-1}$)
U_∞	free stream velocity ($\mathrm{m\,s}^{-1}$)
(u,v)	velocity components ($\mathrm{m\,s}^{-1}$)
x	axial coordinate (m)
x_+	dimensionless hydrodynamic length, $\equiv (L/D)/\mathrm{Re}$
x_*	dimensionless thermal length, $\equiv (L/D)/(\mathrm{RePr})$
W	width (m)

Greek symbols

α	thermal diffusivity ($\mathrm{m}^2\,\mathrm{s}^{-1}$), $\equiv k/(\rho c_p)$
Δp	pressure drop (Pa)
Δp^*	dimensionless pressure drop, $\equiv \rho L^2 \Delta p/\mu^2$
ε	volume fraction of tubes
μ	dynamic viscosity ($\mathrm{kg\,m}^{-1}\,\mathrm{s}^{-1}$)
ν	kinematic viscosity ($\mathrm{m}^2\,\mathrm{s}^{-1}$), $\equiv \mu/\rho$
ρ	density ($\mathrm{kg\,m}^{-3}$)
θ	dimensionless temperature, $\equiv (T_w - T_o)/(T_w - T_i)$
τ_w	mean wall shear stress (Pa)

Subscripts

app	apparent
D_h	refers to hydraulic diameter
dv	developing
i	inlet
fd	fully developed
max	maximum
min	minimum
N	total for N tubes

o	outlet
opt	optimum
P_N	refers to fixed pumping power
Q_N	refers to fixed heat transfer density
w	wall
Δp^*	refers to fixed pressure drop

Superscripts

$(\tilde{})$	dimensionless variables, Eqs. (3.23) to (3.26)

Chapter 4

Utilisation of air-groundwater exergy potential for improvement of the performance of heat pump systems[†]

Abstract

This paper reports a study on the use of the non-flow air-groundwater exergy potential for improving heat pump performance. It is shown that for air/groundwater temperature differences of order 15^{o}C, energy savings up to 50% may be expected for heat pumps operating either in the heating mode or in the cooling mode. It is also shown that the reduction in the energy required to drive the heat pump is proportional to the square root of the exergy potential. In the Évora region the exergy potential peaks during wintertime and during summertime. It is concluded that the use of the non-flow air-groundwater exergy potential is attractive either for heating purposes in wintertime, when energy savings can reach 20%, or for cooling purposes during summertime when they can reach 10%.

Keywords: Environment, Exergy potential, Heat pumps, Performance improvement.

4.1 Introduction

Exergy, that is the maximum work that can be extracted from a system as it comes to equilibrium with a reference environment, has been recognised as a fundamental tool for planning the adequate use of the energy resources. The air-to-ground temperature difference generates an exergy potential that may be used for improving either the performance of thermal machines or heating/cooling systems.

The importance of the use of environmental heat sources and sinks (air, ground, groundwater and wastewater) on the improvement of the performance of heat pumps

[†]Paulo Canhoto[(1)], A. Heitor Reis[(1)], A.F. Miguel[(1)], R. Rosa[(1)], Utilisation of air-groundwater exergy potential for improvement of the performance of heat pump systems, *International Journal of Exergy* 3 (2006) 1–15.

[(1)] Physics Department and Geophysics Centre of Évora, University of Évora.

is widely recognised [1, 2]. It is well known that significant energy savings may be achieved by using available heat sources and sinks properly.

The most common type is the air-source heat pump (AHP) that uses outside air as the heat source during the heating season and as the heat sink during the cooling season [3]. However, AHPs performance decreases sharply when the outside air temperature increases during cooling or decreases during heating.

Water and ground-source heat pumps, referred to as geothermal heat pumps (GHP), have several advantages over AHP [4 – 8]. They benefit from the circumstance that water or rock or soil display rather more moderate temperature change than the surface air. Besides, GHPs seem to have better performance and lower maintenance costs. Recent studies (e.g. [4 – 6]) show that improvements on performance of heat pumps using water and ground heat sources are being achieved in a variety of circumstances. In order to evaluate the potential of energy savings from the utilisation of heat pumps, the knowledge of the exergy potential of heat sources or sinks is required. Exergy analysis has proved to be useful in energy policymaking [9], as well as for dealing with environmental issues [10].

As the exergy potentials of available heat sources or sinks change in time due to climatic conditions and also because of the finiteness of the exergy 'reservoirs', the exergy potential provides a tool for taking into account the magnitude of the exergy 'reservoir' and for making more realistic evaluations of the potential of energy savings ensuing from its utilisation.

In this study we address heat pump performance in relation with the non-flow air-groundwater exergy potential that changes over a year. The surface–underground environmental exergy potential of the Évora region which is situated in the south of Portugal, is evaluated and presented here. The Évora region is sparsely populated but has many farm buildings and other installations dispersed over the region that require the use of either fuel or electricity. Due to its dispersion, providing these installations with electricity or fuel has considerable distribution and transportation costs, which are higher than in other regions of Portugal. This is why the estimation of the environmental exergy potential is of great importance for evaluating the opportunities for the implementation of heat pumps for an ever-increasing number of applications that includes the acclimatisation of buildings, water heating, crop drying, agricultural greenhouses, etc. [11, 12].

4.2 Heat pump performance

The heat pump system used in this study is schematically represented in Fig. 4.1. Steady state operation is assumed and in addition that the refrigerant vapour at the compressor inlet and the liquid at the condenser outlet are saturated at the

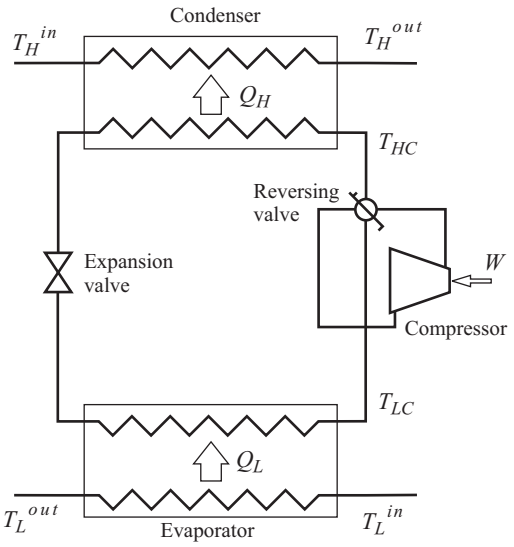

Fig. 4.1: Dual mode heat pump flow diagram.

temperatures T_{LC} and T_{HC}, respectively. After leaving the condenser the refrigerant flows into the evaporator through the expansion valve.

The heat transfer rate in the condenser can be written as

$$\dot{Q}_H = \varepsilon_H \dot{C}_H \left(T_{HC} - T_H^{in}\right) \tag{4.1}$$

and the heat transfer rate in the evaporator as

$$\dot{Q}_L = \varepsilon_L \dot{C}_L \left(T_L^{in} - T_{LC}\right) \tag{4.2}$$

where the heat capacitances rates of the external fluids in the condenser and in the evaporator are given, respectively, by

$$\dot{C}_H = \dot{m}_h c_{p,h} \tag{4.3}$$

$$\dot{C}_L = \dot{m}_l c_{p,l} \tag{4.4}$$

Considering that both the heat transfer processes occur at constant refrigerating fluid temperature, the effectiveness of the condenser, ε_H, and of the evaporator, ε_L, read, respectively [13]:

$$\varepsilon_H = 1 - \exp\left(-\frac{A_H U_H}{\dot{C}_H}\right) \tag{4.5}$$

$$\varepsilon_L = 1 - \exp\left(-\frac{A_L U_L}{\dot{C}_L}\right) \tag{4.6}$$

where A is area and U is the overall heat transfer coefficient. It is assumed that the cycle is endo-reversible, therefore the entropy balance of the internal fluid reads

$$\frac{\dot{Q}_H}{T_{HC}} = \frac{\dot{Q}_L}{T_{LC}} \tag{4.7}$$

By using Eqs. (4.1), (4.2) and (4.7), the refrigeration COP can be written as a function of the heat transfer rate at the evaporator [14]:

$$COP_c = \frac{T_L^{in} - \dot{Q}_L/K}{T_H^{in} - T_L^{in} + \dot{Q}_L/K} \tag{4.8}$$

where

$$\frac{1}{K} = \frac{1}{\varepsilon_H \dot{C}_H} + \frac{1}{\varepsilon_L \dot{C}_L} \tag{4.9}$$

and K is the overall heat conductance. By defining an equivalent temperature of the external fluid at evaporator inlet as

$$T_L^{in^*} = T_L^{in} - \frac{\dot{Q}_L}{K} \tag{4.10}$$

the refrigeration COP assumes the following form:

$$COP_c = \frac{T_L^{in^*}}{T_H^{in} - T_L^{in^*}} \tag{4.11}$$

Using the same procedure as above, the heating COP is obtained as a function of the heat transfer rate at the condenser as:

$$COP_h = \frac{T_H^{in^*}}{T_H^{in^*} - T_L^{in}} \tag{4.12}$$

with the equivalent temperature of the external fluid at the condenser inlet given by:

$$T_H^{in^*} = T_H^{in} + \frac{\dot{Q}_H}{K} \tag{4.13}$$

4.3 Utilisation of air/groundwater exergy potential

We compared the performance of the above-described heat pump operating as air-to--air system with the performance of a similar heat pump operating as air-to-ground system. We assumed that the heat exchanger, operating as the evaporator in wintertime and as the condenser in summertime, could be embedded in the ground, or submerged into a well, or having groundwater forced as external fluid. This purpose can be achieved with only one of the two heat pumps' heat exchangers because the heat pump can operate reversibly.

Due to the fact that the ground (or the water) has finite heat conductivity its temperature will change during operation. Therefore, by using the presented heat pump model we investigated the range of interest for the operating conditions in the Évora region. Another relevant aspect is that the energy savings ultimately result from the utilisation of the surface-air/groundwater exergy potential.

If the air temperature, T_a, is higher than the groundwater temperature, T_w, its specific exergy relatively to the water/ground conditions is given by[1]

$$Ex_{air/ground} = \frac{c_{p,a}\left(T_a - T_w\right)^2}{2T_w} \tag{4.14}$$

where $c_{p,a}$ is the air specific heat. On the other hand, if groundwater temperature is higher than the air temperature its specific exergy with respect to air is

$$Ex_{ground/air} = \frac{c_{p,w}\left(T_a - T_w\right)^2}{2T_a} \tag{4.15}$$

where $c_{p,w}$ is the groundwater specific heat[2]. Using Eq. (4.11) for the refrigeration mode of operation, the ratio of the coefficients of performance of the air-to-ground and of the air-to-air systems is given by

$$\phi_c = \frac{COP_c^w}{COP_c^a} = \frac{T_{c,w}^*\left(T_a - T_{c,a}^*\right)}{T_{c,a}^*\left(T_w - T_{c,w}^*\right)} \tag{4.16}$$

where $T_{c,a}^*$ and $T_{c,w}^*$ are the equivalent temperatures at the evaporator inlet for the air-to-air and air-to-ground systems, respectively, corresponding to the air comfort temperature, T_c. Those temperatures also depend on the heat transfer rate at the evaporator and on the overall thermal conductance, K_a and K_w, according to Eq. (4.10). Using Eq. (4.12) a similar expression can be obtained for the heating COP ratio

$$\phi_h = \frac{COP_h^w}{COP_h^a} = \frac{T_{h,w}^*\left(T_{h,a}^* - T_a\right)}{T_{h,a}^*\left(T_{h,w}^* - T_w\right)} \tag{4.17}$$

where $T_{h,a}^*$ and $T_{h,w}^*$ are the equivalent temperatures at condenser inlet for the air-to-air and air-to-ground systems, respectively, corresponding to the air comfort temperature, T_h.

---

[1] The specific physical exergy of air is

$$Ex = (h - h_0) - T_0\,(s - s_0)$$

where h and s refer to specific enthalpy and specific entropy, respectively, and T_0 is reference temperature. Assuming the air as an ideal gas and neglecting the pressure difference ($p{=}p_0$, p_0 – reference pressure), we have $h - h_0 = c_p\,(T - T_0)$ and $s - s_0 = c_p \ln\,(T/T_0)$, where c_p stands for specific heat. Thus, the specific exergy reads

$$Ex = c_p\,(T - T_0) - c_p T_0 \ln\,(T/T_0)$$

For $T/T_0 \sim 1$ this equation can be rewritten in the following simplified form:

$$Ex \approx c_p\,(T - T_0)^2\,/\,(2\,T_0)$$

Furthermore, in the present case it is also assumed that the moisture content of the air does not change due to water vapour condensation if it comes to equilibrium with the soil.

[2] It must be also noted that both Eqs. (4.14) and (4.15) still to hold either if $T_a < T_w$ or $T_a > T_w$, respectively.

Some simplifications can be made, assuming the same comfort temperature for the cooling and heating operation and assuming that the equivalent temperatures of the two systems are equal in each mode of operation. Then Eqs. (4.16) and (4.17) can be written in the following form

$$\phi = \left(1 - \frac{|T_a - T_w|}{|T_a - T_i^*|}\right)^{-1} \tag{4.18}$$

where T_i^* is the equivalent temperature of the air comfort temperature, T_i, in the conditioned space which, for the cooling mode of operation, is given by

$$T_i^* = T_i - \frac{\dot{Q}_L}{K} \tag{4.19}$$

and for the heating mode of operation is given by

$$T_i^* = T_i + \frac{\dot{Q}_H}{K} \tag{4.20}$$

In this case the comfort temperature is assumed to be the same for the heating and cooling operation mode. A further simplification was been implicitly made assuming that the overall thermal conductance is equal in the two modes of operation.

Now, by using Eqs. (4.14) and (4.18) we obtain

$$\phi = \left(1 - \frac{Ex^{1/2}}{|T_a - T_i^*|}\left(\frac{2T_w}{C_{p,a}}\right)^{1/2}\right)^{-1} \tag{4.21}$$

Furthermore, if it is assumed that the heat transfer rate is equal for the two systems, the magnitude of the reduction of the energy consumption by the compressor is related to the ratio ϕ in the following way

$$\frac{\Delta W}{W_a} = 1 - \frac{1}{\phi} \tag{4.22}$$

$$\frac{\Delta W}{W_a} = \frac{Ex^{1/2}}{|T_a - T_i^*|}\left(\frac{2T_w}{C_{p,a}}\right)^{1/2} \tag{4.23}$$

Eq. (4.23) shows that the energy savings are proportional to the square root of the surface-air/groundwater exergy potential and depend upon the ambient temperature (T_a) and the groundwater temperature (T_w).

A graphical interpretation is shown in Figs. 4.2 to 4.5, which display the improvement in performance and the energy consumption reduction due to the use of the exergy potential against ambient temperature, either in the heating or in the cooling modes. The comfort temperature is equal to 293 K, the equivalent temperature for the cooling mode is set to 273 K, and for heating mode is set to 313 K. Because of its finite size, the temperature of the groundwater reservoir will tend to increase when the heat pump is working for cooling while the opposite will occur when it is working for heating. From Figs. 4.2 to 4.5 we can conclude that for air/groundwater temperature differences of order 15^{o}C, reductions up to 25% in energy consumption may be expected for the heating mode and up to 50% for the cooling mode.

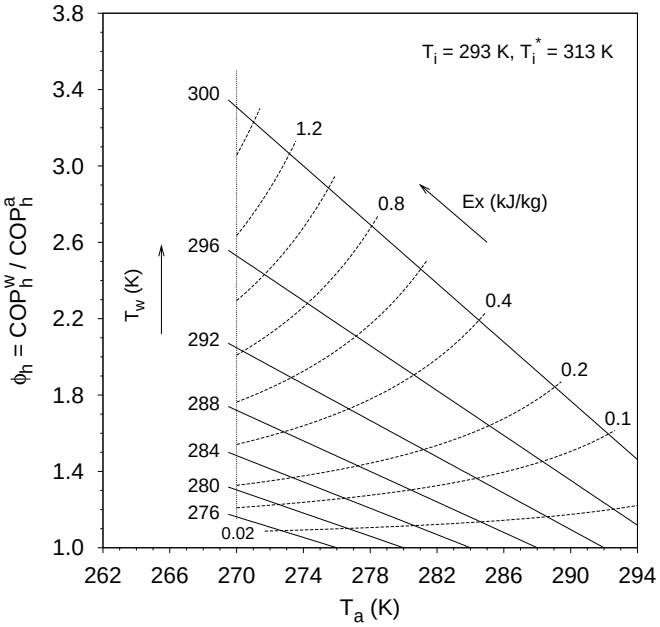

Fig. 4.2: Heating mode of operation: coefficient of performance ratio and exergy potential as function of air and ground temperatures.

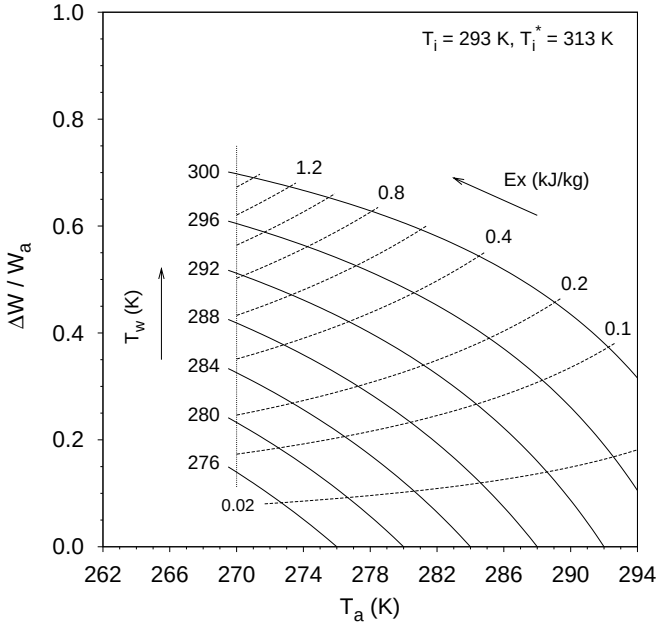

Fig. 4.3: Heating mode of operation: energy consumption reduction and exergy potential as function of air and ground temperatures.

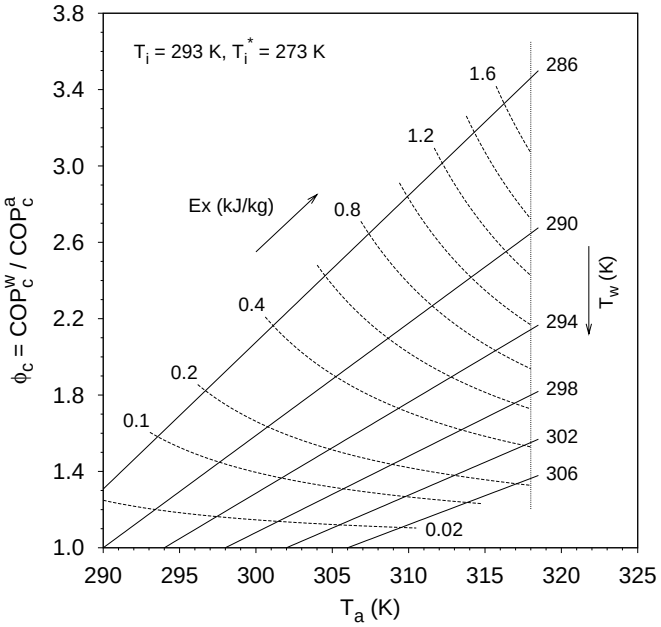

Fig. 4.4: Cooling mode of operation: coefficient of performance ratio and exergy potential as function of air and ground temperatures.

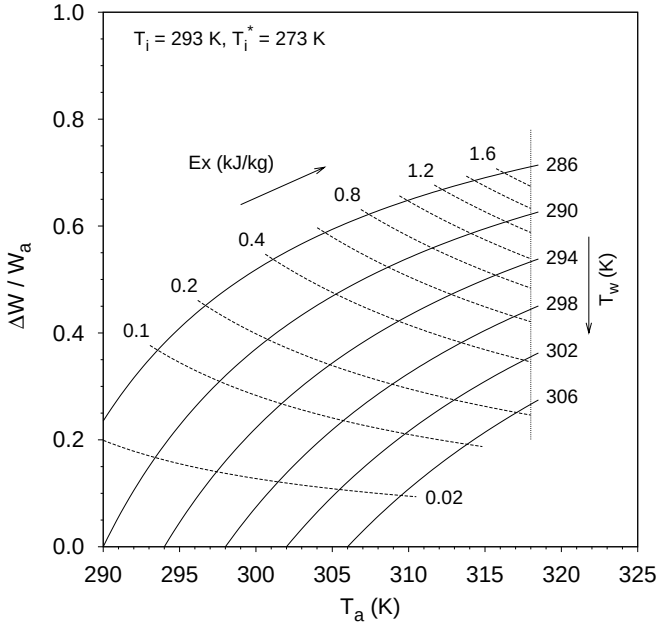

Fig. 4.5: Cooling mode of operation: energy consumption reduction and exergy potential as function of air and ground temperatures.

4.4 Use of the exergy potential for improving heat pump performance

The non-flow air-to-ground exergy potential was calculated from the values of air and ground temperatures, T_a and T_w respectively, with the help of Eq. (4.14). The values of temperature used in the calculations were hourly values averaged over each month, during a ten year period (1995–2004). The hourly values are themselves the average of six values measured with intervals of ten minutes at the Mitra meteorological station near the city of Évora. The air temperatures were taken in standard conditions, i.e. 1.5m above the ground level, and the ground temperatures are measured at 0.30 and 0.70m below ground level.

The hourly mean air temperature for typical winter, spring, summer and autumn days is shown in Fig. 4.6. The monthly averaged temperatures of air and ground are shown in Fig. 4.7. The monthly mean value of ground temperature was used because ground temperature is practically constant over the day. Fig. 4.8 shows the variation of the hourly exergy potential in a day period. Fig. 4.9 displays the coefficient of performance ratio with reference to the ground temperature at the depth of 0.70 m corresponding to the typical months referred above. For the monthly averaged temperatures at the depths of 0.30 and 0.70 m, Figs. 4.10 and 4.11 show the variation in the coefficient of performance and energy consumption, respectively.

In all cases considered, the maximum of the exergy potential occurs when either heating or cooling is most required. In fact, we can observe that in wintertime the minimum of the air temperature corresponds to a high exergy potential that can be used either for driving or improving the performances of passive or active heating devices. Conversely, during summertime the maximum of the exergy potential occurs when cooling is most needed. Therefore, the exergy potential is available either for driving or improving the performances of cooling devices or for ventilation, or else for water pumping for irrigation. The spring and autumn patterns are quite similar, though the exergy potential is a little higher in autumn.

4.4.1 Heating

The analysis of Figs. 4.2 and 4.3 indicates that exergy potentials of order $0.1\,\mathrm{kJ\,kg^{-1}}$ may increase heat pump performances up to 50%, while allowing energy savings of the same magnitude. From Fig. 4.8 we see that the exergy potential may go up to $0.1\,\mathrm{kJ\,kg^{-1}}$ that is just the order of its upper limit in the Évora region.

Taking into consideration the exergy potential available in the Évora region along the year we can see in Fig. 4.10 that the use of water reservoirs at temperature of the ground at the bare depth of 0.7 m may increase heat pump heating performances up to 20% in autumn (average 10%), with energy savings of the same magnitude (Fig. 4.11). The reference to 0.7 m is conservative and is due to the fact that we have

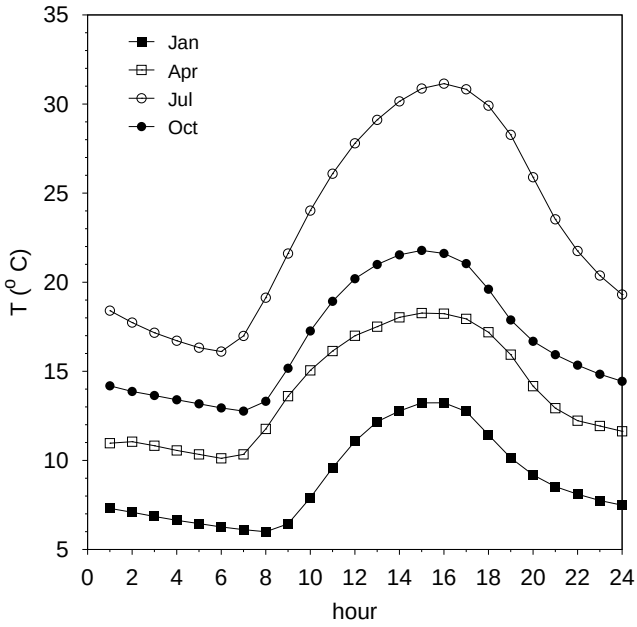

Fig. 4.6: Air temperature hourly averaged over typical months of winter, spring, summer and autumn.

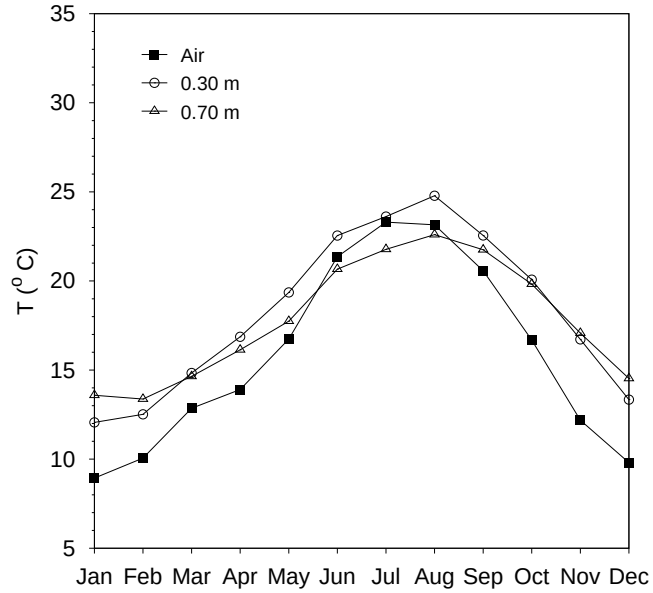

Fig. 4.7: Monthly averaged air and ground temperatures.

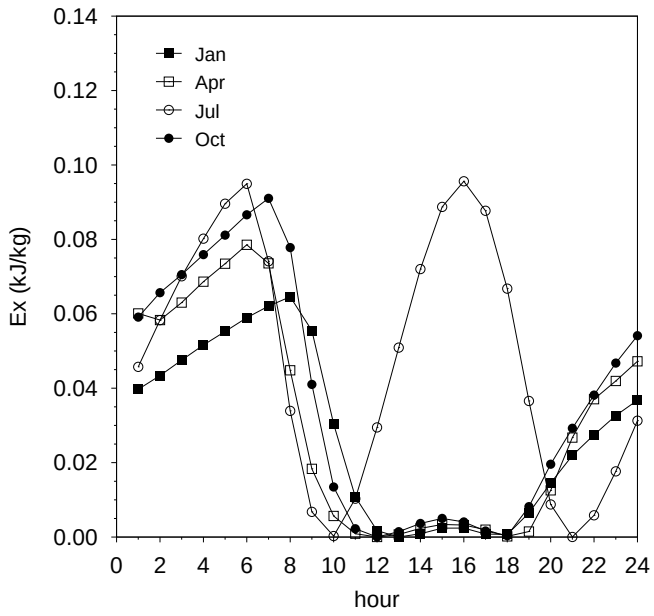

Fig. 4.8: Hourly averaged values of exergy potential for ground temperature at 0.70m depth.

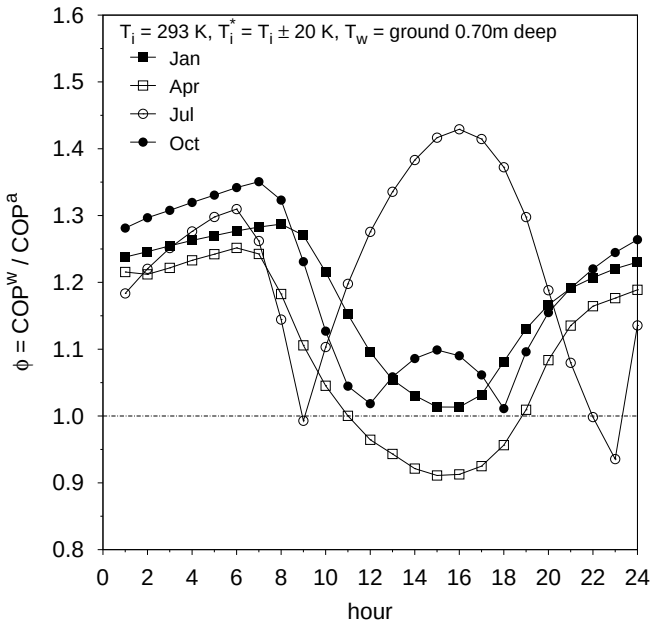

Fig. 4.9: Coefficient of performance ratio for ground temperature at 0.70 m depth.

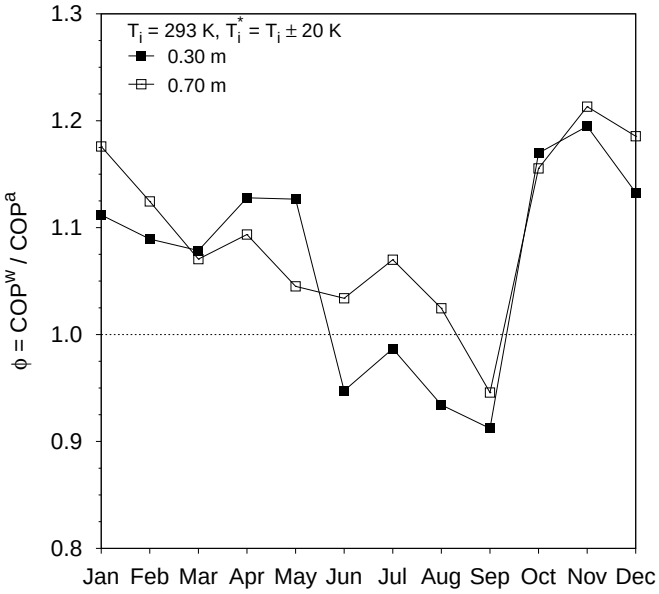

Fig. 4.10: Variation of the coefficient of performance ratio along the year.

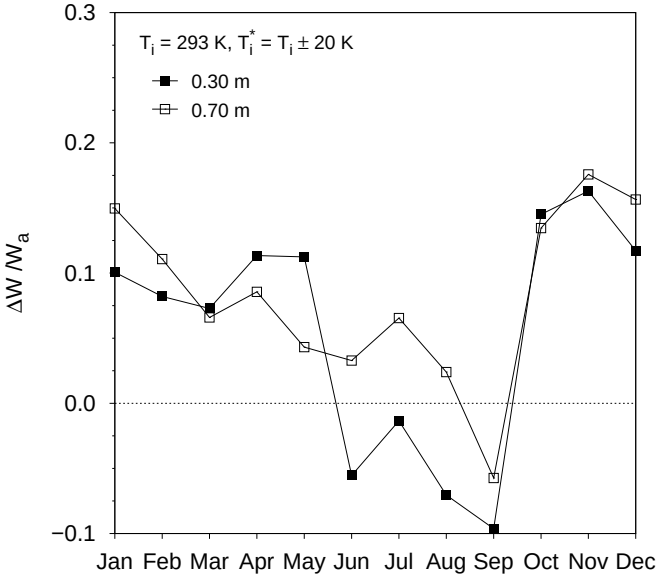

Fig. 4.11: Variation of the energy consumption reduction along the year.

used temperatures measured at this depth, because it is a reference for meteorological measurements. If temperatures corresponding to deeper levels (corresponding to most water-tables) were considered, heat pump heating performances would surpass 20% in autumn. In wintertime the exergy potential is somewhat lower than in autumn but the energy savings are still significant and of order 10%. If we consider the distribution of the exergy potential along the day, we may observe in Figure 4.8 that it is most significant during night-time, between 9 p.m. and 7 a.m., that matches the period in which heating is most necessary.

4.4.2 Cooling

As we can observe in Fig. 4.8, the use of the air-to-ground exergy potential of the Évora region for cooling purposes is less interesting than for heating. Nevertheless it can also lead to interesting energy savings as seen in Fig. 4.11. We note that with water reservoir temperature corresponding to ground temperature at a depth of 0.3 m, energy savings are not possible at all. However, energy savings become interesting for temperatures that match those of the ground at 0.7m depth. In this case, average energy savings in the order of 5% may be reached. Therefore, we may anticipate that if temperatures of deeper levels are used, energy savings will become more significant.

4.5 Conclusions

The use of air-to-ground exergy potential was considered in relation with improvement of heat pump performance. From thermodynamic considerations it was shown how this potential could be related to the coefficient of performance (COP) and to savings in the power consumed by the heat pump compressors. The analytic formulation was translated into thermodynamic charts that display these relationships in a wide range of temperatures, therefore, allowing examination of the use of the exergy potential in particular cases.

We investigated the use of air-to-ground exergy potential in the Evora region. The hourly averaged exergy potential were evaluated for the months of January, April, July and October as well as the monthly averaged values that were evaluated for every month. These data were analysed with the help of thermodynamic charts relating the exergy potential to COP and energy saving.

As a general conclusion we can say that, in the Évora region the use of the air--ground exergy potential should be considered of interest in energy saving strategies. Actually, energy savings are in the order of 10% in heating mode, though can rise to 20%, while in the order of 5% in cooling mode. Despite this analysis was focused on the Évora region, the method is general and of wide application.

References

[1] I. Dincer, M.A. Rosen, Thermal Energy Storage: Systems and Applications, Wiley, West Sussex, 2002.

[2] E.R.G. Eckert, The ground used as energy source, energy sink, or for energy storage, Energy 1 (1976) 315–323.

[3] Y. Ding, Q. Chai, G. Ma, Y. Jiang, Experimental study of an improved air source heat pump, Energy Conversion and Management 45 (2004) 2393–2403.

[4] Y. Bi, T. Guo, L. Zhang, L. Chen, Solar and ground source heat-pump system, Applied Energy 78 (2004) 231–245.

[5] P.S. Doherty, S. Al-Huthaili, S.B. Riffat, N. Abodahab, Ground source heat pump – description and preliminary results of the Eco House system, Applied Thermal Engineering 24 (2004) 2627–2641.

[6] J.C. Lam, W.W. Chan, Energy performance of air-to-water and water-to-water heat pumps in hotel applications. Energy conversion and Management 44 (2003) 1625–1631.

[7] L.W. Pratsch, Geothermal heat pumps benefit the consumer, utility, and nation, Geo-Heat Center Quarterly Bulletin 14 (1992) 1–6.

[8] B. Sanner, C. Karytsas, D. Mendrinos, L. Rybach, Current status of ground source heat pumps and underground thermal energy storage in Europe, Geothermics 32 (2003) 579–588.

[9] I. Dincer, The role of exergy in energy policy making, Energy Policy 30 (2002) 137–149.

[10] M.A. Rosen, I. Dincer, Exergy as the confluence of energy, environment and sustainable development, Exergy – Int. J. 11 (2001) 3–13.

[11] Z. Lian, S.-R. Park, H. Qi, Analysis on energy consumption of water-loop heat pump system in China, Appl. Thermal Engineering 25 (2005) 73–85.

[12] O. Ozgener, A. Hepbasli, Performance analysis of a solar-assisted ground-source heat pump system for greenhouse heating: an experimental study, Building and Environment 40 (2005) 1040–1050.

[13] W.M. Kays, M.E. Crawford, Convective Heat and Mass Transfer, McGraw-Hill, New York, 1993, pp. 429–431.

[14] S.A. Klein, Design considerations for refrigeration cycles, Int. J. Refrig. 15 (1992) 181–185.

Nomenclature

c_p	heat capacity ($\mathrm{kJ\,kg^{-1}\,K^{-1}}$)
$\dot{C}$	heat conductance ($\mathrm{kW\,K^{-1}}$)
COP	coefficient of performance
Ex	specific exergy ($\mathrm{kJ\,kg^{-1}}$)
$\dot{Q}$	heat transfer rate (kW)
K	overall heat conductance ($\mathrm{kW\,K^{-1}}$)
$\dot{m}$	mass flow rate ($\mathrm{kg\,s^{-1}}$)
T	temperature (K or ^{o}C)
W	work (kJ)
ε	heat exchanger efficiency
ϕ	coefficient of performance ratio

Subscripts

a	air
c	cooling
h	heating
H	hot end (condenser)
HC	hot end temperature
i	room temperature
L	cold end (evaporator)
LC	cold end temperature
w	groundwater

Superscripts

a	air
in	inlet
out	outlet
w	groundwater
$*$	equivalent temperature

Chapter 5

Performance analysis of an endoreversible heat pump system for optimal air-ground or water environmental exergy potential utilization[†]

Abstract

This paper reports the optimization of a ground or water source heat pump system for housing applications with respect to the best exergy performance and maximum environmental exergy potential use. The analysis presented also offers the opportunity of explore a new objective for the optimization of the use of exergy sources: "In any system powered by an external exergy source optimization is achieved when the exergy flux to the environment is minimum under the existing constraints". This corresponds to utilizing the supplied exergy to overcome the total irreversibilities of such a system only. The environmental exergy utilization and the exergy output to the environment are analyzed in connection with this objective.

Keywords: Ground source heat pump; Exergy analysis; Environmental exergy; Optimization.

5.1 Introduction

The use of air-source heat pump systems for indoor heating and cooling is nowadays widespread and represents a large parcel of the electric and primary energy consumption in buildings. In the year 2004 the total energy demand in buildings represented nearly 40% of the final energy consumption in the European Union [1]. The exergy input (work or heat) of those systems is directly or indirectly (through the electric energy generation in thermal power plants) produced from fossil fuels that burn at very high temperature. Therefore the overall exergy efficiency is very

[†]Paulo Canhoto[(1)], A. Heitor Reis[(1)], A.F. Miguel[(1)], Performance analysis of an endoreversible heat pump system for optimal air-ground or water environmental exergy potential utilization, *International Journal of Energy Research*, 33 (2009), 205–210.

[(1)] Physics Department and Geophysics Centre of Évora, University of Évora.

low because a high-exergy content fuel is used to produce low-exergy heating or cooling. The same is to say that most of the work that could be produced from the fossil fuels is wasted. Additionally, part of the work input to indoor air conditioning systems is directly 'lost' to the environment in the process. This means that high cost exergy produced from fossil fuels is being released directly to the environment. However, the efficiency of these systems can be improved if ground or water is used as heat source instead of environmental air.

Groundwater and water from lakes or rivers present an environmental exergy potential relatively to the atmospheric air, which varies with the diurnal and seasonal cycles [2 – 4][1]. In recent years, the interest on these systems was increased due to the rational energy utilization and environmental issues [5 – 7]. Such systems not only continue to use the exergy input corresponding to external work but also make use of the environmental potential.

In this paper the exergy analysis of a groundwater or water source heat pump system in housing applications is presented, offering the opportunity to pursue a new objective for optimization of the use of exergy sources: "In any system powered by an external exergy source optimization is achieved when the exergy flux to the environment is minimum under the existing constraints". This corresponds to utilizing the supplied exergy only to overcome the total irreversibilities of the system. The main exergy fluxes are quantified and analyzed from the point of view of the environmental exergy potential use and of minimum exergy output to the environment.

5.2 System description

Fig. 5.1 shows the flow diagram of a groundwater or water source heat pump system for housing cooling in summertime. Groundwater or water from lakes or rivers can be used as external fluid in the hot end heat exchanger, consisting in a heat reservoir with temperature T_H. As first approach this heat reservoir is considered to have a large capacity, which means that it is able to exchange heat without significant temperature variation. The temperature inside the house is to be maintained at T_L, and the environmental air temperature is T_0 ($T_L < T_H < T_0$). Heat conduction through the walls and windows, air infiltration and ventilation are responsible for the heat input, $\dot{Q}_i$, from the exterior into the house.

Atmospheric air conditions are used as the reference for the exergy calculation,

[1]The paper "Utilisation of air-groundwater exergy potential for improvement of the performance of heat pump systems", *Int. J. Exergy* 3 (2006) 1–15 by P. Canhoto, A.H. Reis, A.F. Miguel and R. Rosa [2] is included in this thesis in the Chapter 4.

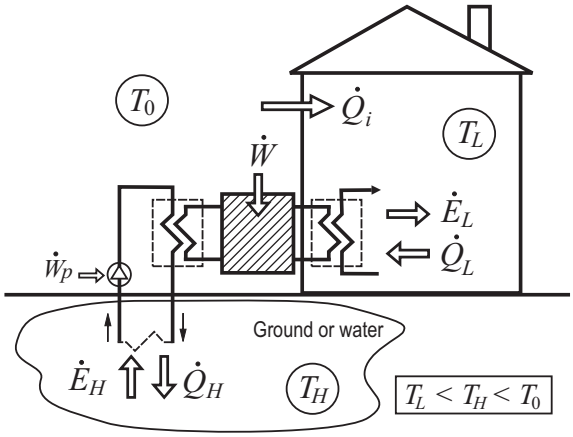

Fig. 5.1: Groundwater or water source heat pump system flow diagram for housing cooling in summertime.

because the indoor temperature will approach to those conditions if the system is turned off. In other words, as the system pumps exergy into the house, an exergy potential will be created and maintained in reference to the environmental conditions. The Carnot coefficient of performance of the groundwater or water source heat pump will be higher than that of a similar air-source system. In practice, the generation and maintenance of the indoor temperature requires less external exergy input rate (power) if a reservoir with an exergy potential closer to the desired indoor potential is used.

The exergy balance of the heat pump system reads

$$\dot{E}_H + \dot{W} = \dot{E}_L + \dot{I} \tag{5.1}$$

where $\dot{E}_H$, $\dot{E}_L$, $\dot{W}$ and $\dot{I}$ are, respectively, the exergy transfer rate at the hot end, the exergy transfer rate at the cold end, the power input and the irreversibility generation rate.

5.3 Exergy analysis and optimization

In the present work we refer to the situation when the system operates with optimal relation between the heat transfer rate at the cold end, $\dot{Q}_L$, and the coefficient of performance, ε, of an endoreversible heat pump working in cooling mode between the temperatures T_H and T_L [8]

$$\dot{Q}_L = K\left(T_L - \frac{T_H}{1+\varepsilon^{-1}}\right) \tag{5.2}$$

where

$$K = \frac{\alpha\beta}{\left[\alpha^{1/2} + \beta^{1/2}\right]^2} \tag{5.3}$$

α and β being the thermal conductance between the internal working fluid and the hot and cold ends heat reservoirs, respectively. As the optimal heat transfer rate decreases monotonically with the coefficient of performance, its maximum value is defined as

$$\dot{Q}_L^{\max} = KT_L \tag{5.4}$$

which is obtained by setting $\varepsilon = 0$ in Eq. (5.2). On the other hand, by setting the optimal heat transfer rate equal to zero as a limit condition, the equation reduces to the Carnot coefficient of performance

$$\varepsilon_c = T_L / \left(T_H - T_L\right) \tag{5.5}$$

The rate at which heat is released at the hot end is related to the absorbed heat rate and the coefficient of performance through

$$\dot{Q}_H = \left(1 + \varepsilon^{-1}\right) \dot{Q}_L \tag{5.6}$$

According to Fig. 5.1 we can define the net exergy output as

$$\dot{E} = \dot{E}_L - \dot{E}_H = \dot{W} - \dot{I} \tag{5.7}$$

which represent the net exergy flow at the heat exchangers or, alternatively, the difference between power input and irreversibility generation rate. Therefore, the net exergy output takes the following form

$$\dot{E} = \dot{Q}_L \left(\frac{T_0}{T_L} - 1\right) - \dot{Q}_H \left(\frac{T_0}{T_H} - 1\right) \tag{5.8}$$

where all the quantities in the right hand side of Eq. (5.8) were assumed as positive.

By combining Eqs. (5.2) to (5.6) and (5.8) the dimensionless rate of exergy output reads

$$\frac{\dot{E}}{\dot{Q}_L^{max}} = \frac{\varepsilon^{-1} - \varepsilon_c^{-1}}{1 + \varepsilon^{-1}} \left[\varepsilon^{-1} - \left(\varepsilon^{-1} - \varepsilon_c^{-1}\right) \frac{T_0}{T_H}\right] \tag{5.9}$$

Yan and Chen [9] obtained and applied a similar expression for an endoreversible refrigerator with lower values of T_L. Fig. 5.2 shows the normalized curves of the net exergy output rate for three different values of T_H, with $T_0 = 310\,\mathrm{K}$ and $T_L = 290\,\mathrm{K}$.

The net exergy output presents a maximum value at

$$\varepsilon_A = \left[\sqrt{\left(1 + \varepsilon_c^{-1}\right)\left(1 + \frac{\varepsilon_c^{-1}}{1 - T_H/T_0}\right)} - 1\right]^{-1} \tag{5.10}$$

which corresponds to the following heat transfer rate

$$\dot{Q}_L^A = \dot{Q}_L^{max} \left(1 - \sqrt{\frac{1 + \varepsilon_c^{-1}}{1 + \varepsilon_c^{-1} / \left(1 - T_H/T_0\right)}}\right) \tag{5.11}$$

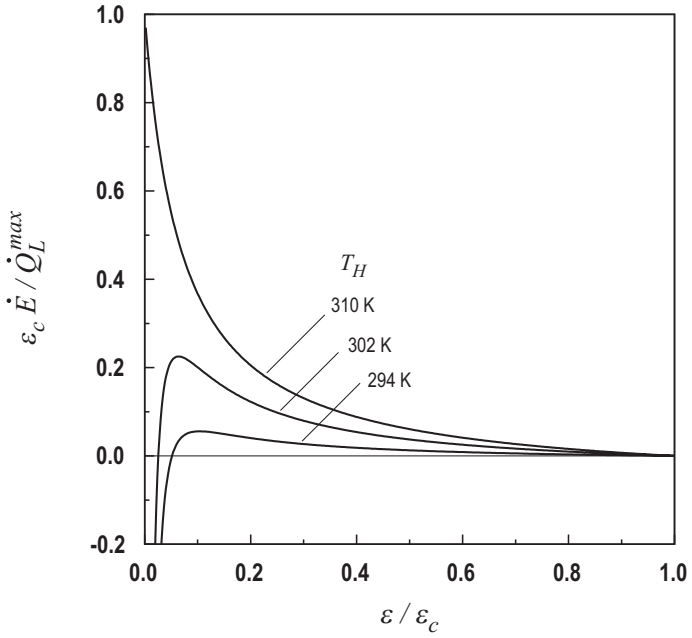

Fig. 5.2: Net exergy output as function of the coefficient of performance for various hot end reservoir temperatures.

In the case of a null exergy output, the coefficient of performance is given by

$$\varepsilon_0 = (1 - T_H/T_0)\,\varepsilon_c \tag{5.12}$$

and the corresponding heat transfer rate reads

$$\dot{Q}_L^0 = \dot{Q}_L^{\max}\left(1 - \frac{1+\varepsilon_c^{-1}}{1+\varepsilon_c^{-1}/\,(1-T_H/T_0)}\right) \tag{5.13}$$

This situation corresponds to the case when the irreversibility generation rate of the heat pump system balances the power input. This means that an amount of exergy input equal to the supplied power is consumed for overcoming the internal irreversibilities, i.e., the exergy pumped into the house equals the exergy taken out from the hot end reservoir. Furthermore, if the net exergy output becomes negative, some amount of exergy from the high-temperature reservoir is also destroyed. This occurs only when the temperature T_H is lower than the environmental temperature T_0. If these temperatures are equal the curve does not intercept the x-axis and the maximum occurs for the limit condition $\varepsilon = 0$.

In order to investigate the optimal use of the environmental exergy potential, we can define the following quantities:

$$\phi_W = \frac{\dot{E}}{\dot{W}} \tag{5.14}$$

and

$$\phi_H = \frac{\dot{E}}{\dot{E}_H} \tag{5.15}$$

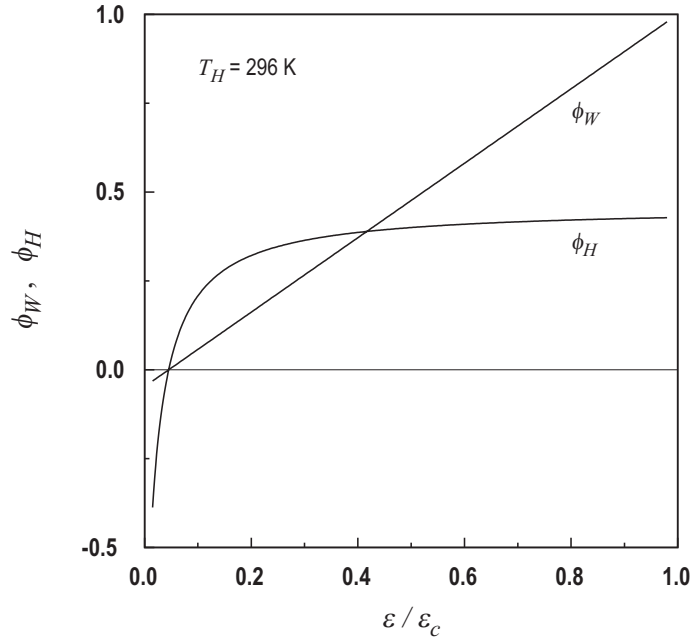

Fig. 5.3: Variation of ϕ_W and ϕ_H with the coefficient of performance.

which can be considered as representative of the net exergy output efficiencies from the power input perspective and from the environmental exergy perspective, respectively. The first equation may also be seen as the ratio between $\dot{W} - \dot{I}$ and the power input $\dot{W}$, and therefore representing a measure of the fraction of power that is released into the house when $\varepsilon > \varepsilon_0$. Eqs. (5.14) and (5.15) are represented in the Fig. 5.3 as function of the coefficient of performance, for $T_H = 296\,\mathrm{K}$ and for $\alpha = \beta = 1.96\,\mathrm{kW\,K^{-1}}$. Both functions intercept the x-axis at ε_0, and increase with ε. The first one increases linearly and the second one increases asymptotically to a maximum value that depends on T_H. Another remark to this function is that $\phi_H \to \infty$ when $T_H \to T_0$.

We can also define the following empirical function:

$$\phi = \phi_H - \phi_W = \dot{E}\left(\frac{1}{\dot{E}_H} - \frac{1}{\dot{W}}\right) \tag{5.16}$$

to compare the contribution of the exergy input from the hot end reservoir and of the power to the net exergy output. The objective is to investigate a way of maximizing the environmental exergy use and to reduce the fraction of power that is ultimately released to the environment. Using Eqs. (5.2) to (5.8) the empirical function reads

$$\phi = \left[\frac{(T_0/T_L - 1)\,\varepsilon}{(T_0/T_H - 1)\,(\varepsilon + 1)} - 1\right]\left[1 - (\varepsilon + 1)\left(\frac{T_0}{T_H} - 1\right)\right] \tag{5.17}$$

This function is plotted in Fig. 5.4 for various values of T_H, and we can clearly see the existence of maximum points of ϕ for the hot end reservoir temperatures shown.

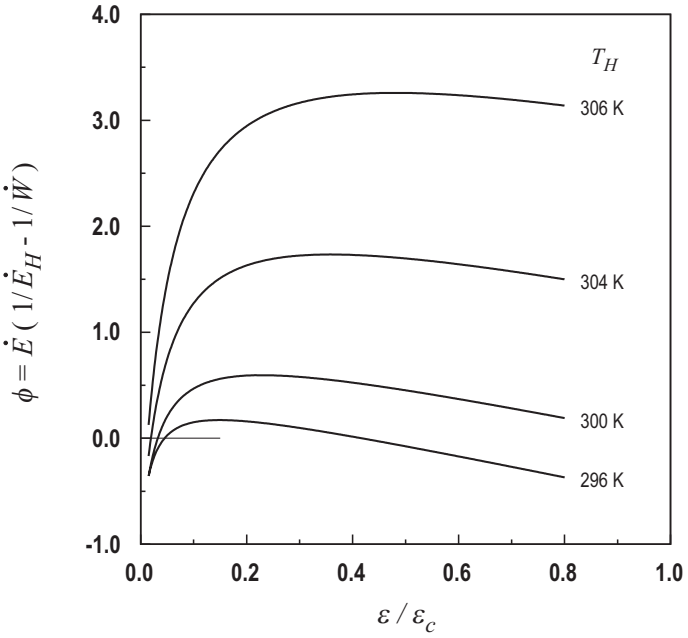

Fig. 5.4: Variation of ϕ with the coefficient of performance for various hot end reservoir temperatures.

Setting the condition $\partial\phi/\partial\varepsilon = 0$, we find the coefficient of performance ε_B that maximizes ϕ, in the following form

$$\varepsilon_B = \sqrt{\frac{T_0/T_L - 1}{(T_0/T_H - 1)\,(T_0/T_L - T_0/T_H)}} - 1 \tag{5.18}$$

This coefficient of performance tends to infinity as T_H tends to T_0. Therefore, the previous condition and Eq. (5.18) are only valid for values of T_H lower than a limiting value corresponding to $\varepsilon_B = \varepsilon_c$, which also matches the case of $\dot{Q}_L = 0$. For higher values of T_H the groundwater or water source heat pump system is not competitive in the perspective of function ϕ, while the heat transfer rate becomes numerically negative and the previous analysis and the ϕ definition do not hold anymore.

We compare the previous results with the so-called ecological function [9, 10] defined as

$$Ec = \dot{E} - \dot{I} \tag{5.19}$$

where the irreversibility rate is given by

$$\dot{I} = T_0 \left(\frac{\dot{Q}_H}{T_H} - \frac{\dot{Q}_L}{T_L} \right) \tag{5.20}$$

By using Eqs. (5.2) to (5.8) again, and applying the condition $\partial Ec/\partial\varepsilon = 0$, we find the optimal coefficient of performance that maximizes the ecological function in the

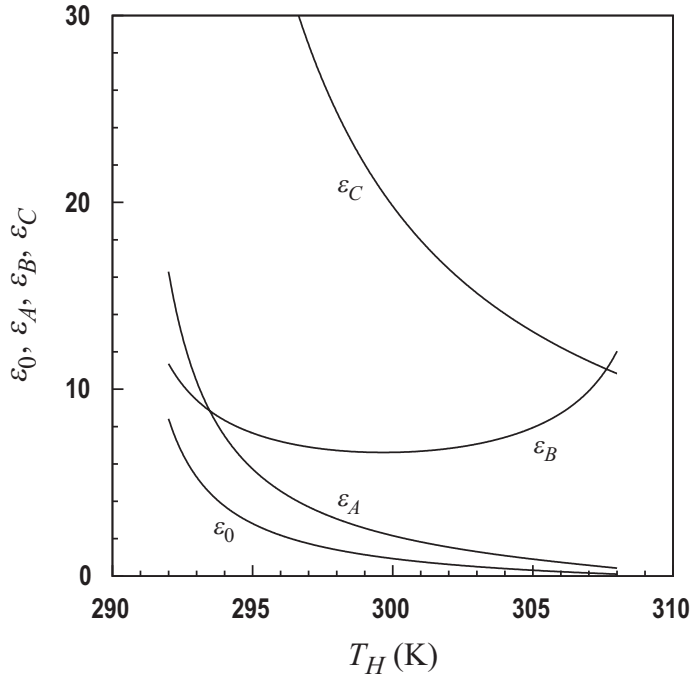

Fig. 5.5: Coefficients of performance ε_0, ε_A, ε_B and ε_C, as function of the hot end reservoir temperature.

form

$$\varepsilon_C = \left[\sqrt{(1+\varepsilon_c^{-1}) \left(1 + \frac{\varepsilon_c^{-1}}{1 - T_H/(2T_0)} \right)} - 1 \right]^{-1} \tag{5.21}$$

Fig. 5.5 shows the various coefficients of performance $\varepsilon_0, \varepsilon_A, \varepsilon_B$ and ε_C, (Eqs. (5.10), (5.12), (5.18) and (5.21)) as function of the hot end reservoir temperature. All the coefficients of performance tend to infinity as T_H approach to T_L, as well the Carnot coefficient does.

The coefficients ε_0 and ε_A decrease and approach 0 as T_H tend to T_0 and the coefficient of performance that arises from the optimization of the ecological function presents higher values. The coefficient of performance obtained from Eq. (5.18) shows mid-range values in the admissible range of T_H. This last curve crosses the other ones and therefore, depending of the value of T_H, it corresponds either to an optimization for null exergy output to the environment (ε_0), to an optimization for maximum net exergy output (ε_A), or to an optimization based in the ecological function (ε_C).

5.4 Conclusions

This paper presents the exergy analysis of a ground or water source heat pump system for indoor air cooling. With this analysis we identified the operating conditions for null net exergy output to the environment and for maximum net exergy

output. The optimization of the system based on the ecological function criterion was also presented and compared. The dependence of the net exergy output both on power input and on exergy input from the groundwater or water heat reservoir was also studied. A coefficient of performance was obtained to identify the maximum environmental exergy potential use together with the minimum exergy release to the environment. It was found that, depending on the hot end heat reservoir temperature the system optimization through this function corresponds to an optimization for null net exergy output function (hot end reservoir temperature close to indoor temperature), or as an 'ecological function' optimization (hot end reservoir temperature close to the environmental air temperature).

References

[1] European Commission. *Energy and transport: Report 2000-2004*. Office for Official Publications of the European Communities 2004, Luxemburg, ISBN 92-894-7457-2.

[2] P. Canhoto, A.H. Reis, A.F. Miguel, R. Rosa, Utilisation of air-groundwater exergy potential for improvement of the performance of heat pump systems, Int. J. Exergy 3 (2006) 1–15.

[3] O. Buyukalaca, F. Ekinci, T. Yilmaz, Experimental investigation of Seyhan River and dam lake as heat source-sink for heat pump, Energy 28 (2003) 157–169.

[4] O. Zogou, A. Stamatelos, Effect of climatic conditions on the design optimisation of heat pump systems for space heating and cooling, Energy Conversion and Management 39(1998) 609–622.

[5] O. Ozgener, A. Hepbasli, Modeling and performance evaluation of ground source (geothermal) heat pump systems, Energy and Buildings 39 (2007) 66–75.

[6] A. Hepbasli, O. Akdemir, Energy and exergy analysis of a ground source (geothermal) heat pump system, Energy Conversion and Management 45 (2004) 737–753.

[7] B. Sanner, C. Karytsas, D. Mendrinos, L. Rybach, Current status of ground source heat pumps and underground thermal energy storage in Europe, Geothermics 32 (2003) 579–588.

[8] Z. Yan, J. Chen, A class of irreversible Carnot refrigeration cycles with a general heat transfer law, J. Phys. D: Appl. Phys. 23 (1990) 136–141.

[9] Z. Yan, L. Chen, Optimization of the rate of exergy output for an endorreversible Carnot refrigerator, J. Phys. D: Appl. Phys. 29 (1996) 3017–3021.

[10] L. Chen, S.X. Sun, C. Wu, Ecological optimization for generalized irreversible Carnot refrigerators, J. Phys. D: Appl. Phys. 38 (2005) 113–118.

Nomenclature

$\dot{E}$	exergy transfer rate or net exergy output (W)
Ec	ecological function – Eq. (5.19) (W)
$\dot{I}$	irreversibility generation rate (W)
K	composite thermal conductance – Eq. (5.3) ($\mathrm{W\,K^{-1}}$)
$\dot{Q}$	heat transfer rate (W)
T	temperature (K)
$\dot{W}$	work (W)

Greek symbols

α	thermal conductance at hot end ($\mathrm{W\,K^{-1}}$)
β	thermal conductance at cold end ($\mathrm{W\,K^{-1}}$)
ε	coefficient of performance
ε_c	Carnot coefficient of performance, $\equiv T_L/\left(T_H - T_L\right)$
ϕ	empirical function for performance evaluation – Eq. (5.14) to (5.16)

Subscripts

0	reference or null net exergy output
H	hot end
L	cold end

Superscripts

0	null net exergy output
max	maximum

Chapter 6

Conclusions

In this thesis, the performance improvement of forced convection heat sinks and heat pumps was addressed through two distinct approaches:

(i) optimization of fluid flow and internal geometric structure of compact heat sinks based on energy analysis using both intersection-of-asymptotes and numerical methods;

(ii) optimization of either groundwater or water source heat pump systems based on exergy analysis for the best utilization of the environmental exergy potential, i.e. the non-flow exergy potential due the natural temperature differences that exists between ground/groundwater or water from lakes and rivers and the atmospheric air.

The main conclusions are referred in the following.

6.1 Optimization of forced convection heat sinks

Heat sinks composed of parallel circular or non-circular ducts were considered, subjected to three distinct constraints: (i) fixed pressure drop; (ii) fixed pumping power; and (iii) fixed heat transfer rate. Optimization was carried out by considering that heat sink substrate (solid matrix) is composed of a high thermal conductivity material, and thus assuming that for practical purposes the walls of ducts may be considered isothermal. In fact, if the Biot number – which weights the thermal resistance by conduction in the solid against the convective resistance in the wall – is much smaller than 1, the assumption of a uniform temperature distribution is acceptable [1]. This is in line with recent works on optimization of multi-channel heat sinks, (e.g. see Refs [2 – 4]). Further explanations about the validity and limitations of this assumption were already presented and discussed in Section 2.2. On the other hand, we can also regard this temperature (uniform) as the scale of surface temperature, which is distinct from the inlet temperature of the fluid [5, 6]. Additionally, the flow was assumed to be laminar, steady and equally distributed among

the ducts, together with constant fluid properties. The overall dimensions and the porosity (ε) of the stack are set (fixed) by the design in face of the available space and other construction constraints.

Heat transfer rate was maximized at fixed pumping power for circular, parallel plates, rectangular 1:4, square and equilateral triangular ducts. This is equivalent to improving heat sink performance since the amount of heat that is extracted per unit of energy that is consumed is also maximized. An asymptotic analysis was carried out for small and large ducts using the dimensionless thermal length (x_*) as primary optimization variable, which proved to be advantageous because it allows to directly see if the fluid is efficiently used for the cooling purpose. Similar analysis was also carried out using the ratio of hydraulic diameter to duct length (D_h/L) as the main design parameter, and a simple expression for determining the optimum D_h/L ratio was disclosed thus allowing the estimation of the optimal internal structure of the heat sink.

Additionally, it is verified that the maximum heat transfer rate per unit of volume that is effectively occupied by the fluid scales with the group $\mathrm{Pr}^{2/3}\left(P_N^*/\varepsilon\right)^{1/3}$, while the optimum ratio of hydraulic diameter to duct length scales with the group $\mathrm{Pr}^{-1/3}\left(P_N^*/\varepsilon\right)^{-1/6}$, where P_N^*/ε stand for pumping power per unit of volume bathed by the fluid. As a conclusion, in the case that plenum losses are neglected, the optimum hydraulic diameter is nearly insensitive to porosity (ε) and to pumping power (P_N^*), while the optimum dimensionless thermal length is independent of ε and P_N^*, and the maximum heat transfer rate varies both with $\varepsilon^{2/3}$ and $P_N^{*1/3}$.

Numerical optimization was also carried out at the same conditions as above, and for various values of Prandtl number and for all duct geometries under consideration. The numerical results were correlated through simple equations for determining the optimum hydraulic diameter and maximum heat transfer density in the range $0.1 < \mathrm{Pr} < 100$. By comparing these values with the results of scale analysis obtained before, it was verified that the estimate of optimum hydraulic diameter reproduces the numerical results with an error within -8.6% to 13.5% in the range $0.1 < \mathrm{Pr} < 10$ for all the duct geometries, except for the case of parallel plates in which the lower limit of the relative error is 23%. It was also verified that a heat sink composed of parallel plates presents the highest heat transfer density, followed in descending order by the rectangular 1:4, circular, square and equilateral triangular ducts, for fixed values of pumping power and porosity and in the range $0.1 < \mathrm{Pr} < 100$.

The influence of local pressure losses at the inlet and outlet plenums were studied using the numerical method by varying the porosity and it was concluded that the optimum x_* varies contrariwise to porosity, while the maximum heat transfer rate and optimum hydraulic diameter vary likewise the same quantity. This is explained by the increasingly higher values of local pressure drop as ε decreases, leading to

lower values of maximum heat transfer density. As compared to the case in which the local pressure losses are neglected the observed variations in optimal hydraulic diameter and maximum heat transfer density are less than 1.5% and 3.0%, respectively.

Results were extended for the case of pumping power minimization with fixed heat transfer density and a simple equation for determining the optimum D_h/L ratio was also presented. It was concluded that the optimum hydraulic diameter is nearly constant for $\mathrm{Pr} > 0.7$. Therefore, a fairly accurate method follows: the heat sinks can be simply optimized geometrically for the required heat transfer density and then operated according to the fluid in use for achieving minimum pumping power requirement. This aspect of heat sinks optimization was not explicitly addressed before in previous works (as e.g. [2 – 6]), and it is useful in the cases in which both heat transfer demand and nominal or maximum operating temperature are known, and the objective is minimization of the energy consumption of fluid pumping.

Optimization of a heat sink composed of parallel tubes was carried out for three distinct sets of objectives and constraints: (i) maximization of heat transfer rate at fixed pressure drop; (ii) maximization of heat transfer rate at fixed pumping power; and (iii) fluid flow optimization at fixed heat transfer rate. If the maximization of heat transfer rate is considered, it was shown that the optimum values of dimensionless thermal length predicted by the method of intersecting the asymptotes are nearly independent of the imposed fluid flow constraint, either fixed pressure drop or fixed pumping power, in the range $0.1 < \mathrm{Pr} < 100$. These optimum values decrease with Pr and converge to the same value in both cases, being slightly higher in the case of fixed pressure drop as compared to the values found for fixed pumping power for lower values of Pr.

It was also shown that the values of optimum x_* obtained through maximization of heat transfer rate at either fixed pumping power or fixed pressure drop are the same that are obtained respectively through minimization of pumping power or minimization of pressure drop at fixed heat transfer rate. Furthermore, the values of optimum D_h/L ratio predicted through the method of intersecting the asymptotes are independent of the Prandtl number and of the optimization objective, either it is minimization of Δp^* or minimization of P_N^*.

These results were further investigated by developing a new approach of the method of intersecting the asymptotes, which comprise two optimization variables: one of geometric nature that is represented by ratio of diameter to tube length; and the other relative to fluid flow conditions, represented by the Reynolds number. It was verified that for a fixed heat transfer rate, the optimum dimensionless thermal length that arises from this method is very close to that corresponding to the joint minimization of pressure drop and pumping power. A simple theoretical

expression for determining the optimum diameter was presented together with the corresponding values of pressure drop and pumping power which in average were found to surpass the respective minima obtained numerically by only 4% and 9%.

As a conclusion, the optimal design that emerges from the intersection-of-asymptotes method for a given heat transfer rate and inlet fluid-to-wall temperature difference match very closely the criterion of joint minimization of 'fluid flow driving potential' (pressure drop) and 'fluid flow energy rate' (pumping power). In the same way, if either pressure drop or pumping power are set fixed, this method allows predicting the maximum 'heat transfer rate' at a given 'heat transfer driving potential' (inlet fluid-to-wall temperature difference). Now we are able to notice that this duality or competition between 'driving potential' and 'energy rate' is also present in the basis of the intersection-of-asymptotes method. In fact, we can recognize the fully developed flow limit as corresponding to a configuration of maximum heat transfer rate (not the configuration for the overall maximum but the configuration in which no more heat can be extracted), and the developing flow limit as corresponding to a configuration of maximum heat transfer driving potential in which the temperature difference between the wall and the fluid in the core flow is maximum.

The correctness and validity of the approximation made in the method of asymptotes was also demonstrated, by showing that the Nusselt number obtained by the use of the similarity solutions of heat transfer and fluid flow over a flat plate is very close to the data for thermally developing flow in a circular tube with uniform wall temperature. The condition for using this similarity solution is that the mean gradient of the fluid velocity near a flat plate surface must be equal to the velocity gradient at the wall of the tube. A theoretical expression for the mean Nusselt number was deduced, which is very similar to Lévêque's solution and that shows an error lower than 3.04% in the range $10^{-4} < \mathrm{Pr} < 10^{-2}$ if tested against data. This contributed not only to validate the optimization method, but also constitutes a new result *per se*.

The theoretical results were validated and complemented through numerical simulations of entire temperature and flow fields for the various sets of objectives and constraints, and readily usable data for heat sink optimization are provided either through simple expressions as in table form.

6.2 Optimization of groundwater or water source heat pump systems

In this work, the coefficient of performance of a groundwater or water source heat pump system was related to the environmental air-to-groundwater exergy potential for both cooling and heating modes of operation. Simple expressions were deduced and charts were presented for a wide range of air and groundwater (or surface water)

temperatures, thus providing an easy way of estimating the exergy potential, the improvement on performance and the savings in energy consumption compared to air-to-air systems. It was shown that the reduction in the energy required to drive the heat pump depends on the square root of the exergy potential.

An assessment of the exergy potential at the Évora region (Portugal) was carried out based on the hourly averaged values of air temperature and ground temperature at a deep of 0.70 m for the months of January, April, July and October. The same assessment was also carried out using the monthly averaged values for every month. This allowed estimating the improvement in coefficient of performance and savings in energy consumption of a groundwater source heat pump in this region. It was concluded that the use of the natural exergy potential can provide energy savings up to 10% in the heating mode, while energy savings in the order of 5% are achieved in the cooling mode. This shows that the use of natural exergy potential should be considered in the improvement of energy efficiency and in strategies for the rational use of energy.

Distinct conditions of operation were identified through exergy analysis of an endoreversible heat pump system connected to a groundwater or water heat reservoir, in cooling mode of operation. First, the coefficient of performance together with the heat transfer rate at the evaporator were obtained as function of the temperature of the hot end reservoir for maximum net exergy output (exergy released into the cooled space minus exergy extracted from the hot end reservoir), as well as for null net exergy output. This last situation also corresponds to the case where power input balances the irreversibility generation rate. An empirical expression was put forward to compare the contribution to the net exergy output of both exergy input from the hot end reservoir and of power input. From the sake of maximization of this expression, a coefficient of performance was obtained corresponding to the combined maximization of exergy extracted from the hot reservoir together with minimization of power input. These distinct operation conditions were represented in terms of coefficient of performance as function of the temperature of the hot end heat reservoir.

References

[1] F.P. Incropera, D.P. DeWitt, Fundamentals of Heat and Mass Transfer, Wiley, New York, 1985.

[2] Y. Muzychka, Constructal design of forced convection cooled microchannel heat sinks and heat exchangers, Int. J. Heat Mass Transfer 48 (2005) 3119–3127.

[3] T. Wen, F. Xu, T.J. Lu, Structural optimization of two-dimensional cellular metals cooled by forced convection, Int. J. Heat Mass Transfer 50 (2007) 2590–2604.

[4] A. Yilmaz, O. Buyukalaca, T. Yilmaz, Optimum shape and dimensions of ducts for convective heat transfer in laminar flow at constant wall temperature, Int. J. Heat Mass Transfer 43 (2000) 767–775.

[5] A. Bejan, E. Sciubba, The optimal spacing of parallel plates cooled by forced convection, Int. J. Heat Mass Transfer 35 (1992) 3259–3264.

[6] S. Mereu, E. Sciubba, A. Bejan, The optimal cooling of a stack of heat generating boards with fixed pressure drop, flowrate or pumping power, Int. J. Heat Mass Transfer 36 (1993) 3677-3686.

Contactos:

Universidade de Évora

Instituto de Investigação e Formação Avançada - IIFA

Palácio do Vimioso | Largo Marquês de Marialva, Apart. 94

7002-554 Évora | Portugal

Tel: (+351) 266 706 581